



BOOSTER SYNCHROTRON

Booster Staff

E. L. Hubbard, Editor

January 1973

	Page
A. Introduction	1
B. Lattice and Orbits	8
1. Lattice	8
2. Apertures	10
3. Space Charge	11
C. Magnet System	18
1. Introduction	18
2. Combined Function Synchrotron Magnets	18
3. Alignment	25
D. Magnet Power System	35
1. Resonant Circuit	35
2. Power Supply	36
3. Monitoring	38
4. Magnet Current Regulator	39
E. Correction Magnets	52
1. Introduction	52
2. Dipoles	52
3. Quadrupoles	53
4. Skew Quadrupoles	53
5. Mechanical Design	54
6. Power Supply	55
7. Sextupoles	55
8. Higher-Order Corrections	56
F. Vacuum System	59

G.	Beam-Position Monitors	Page 66
H.	RF Acceleration System	71
	1. Introduction	71
	2. RF Cavities	73
	3. Ferrite Tuners	73
	4. RF Power Amplifiers	74
	5. Booster Low-Level RF System	76
	6. Synchronization with Main Ring	79
I.	200-MeV Beam Transfer System	96
	1. Introduction	96
	2. Chopper	97
	3. Linac Beam Analysis System	99
	4. Transport to the Booster	101
	5. Space Charge Effects	103
	6. Injection into the Booster	104
J.	Extraction	115
K.	Staff	120

BOOSTER SYNCHROTRON

A. Introduction

At NAL, the proton beam is accelerated to the final energy in three stages. The first stage is a 203-MeV linac. The second is an 8-GeV, fast cycling, booster synchrotron. The final stage is the 2000-m diameter main synchrotron. The entire system was described in the NAL Design Report.^{A1} However, the booster design has been changed substantially since publication of the Design Report. This report has been compiled to provide a description of the booster which was actually built.

The booster is an alternating gradient synchrotron with a radius of 75.5 m. The magnet ring contains 96 10 foot long combined-function magnets, which both focus the beam and bend it around the circular orbit. The magnet lattice is divided into 24 identical periods. Each period contains four of the combined-function magnets, and a 6-m long straight section. The 16-rf cavity resonators used to accelerate the beam are located in eight of the 6-m straight sections. Two of the 6-m straight sections are used for injection, and two are used for the extraction system.

The magnets are excited with a 15-Hz biased sine wave. The beam from the 200-MeV linac is injected into the booster when the magnetic field is near its minimum value of approximately 500 gauss and is extracted near the maximum field of approximately 7000 gauss. The basic parameters of the booster are summarized in Table A-1.

During the 33-msec period of rising magnetic field, the beam goes around the booster ring about 16,000 times and is accelerated to 8 GeV by the 16-rf cavity resonators. At 8 GeV, where $\beta \approx 1$, the frequency of the booster accelerating system is made equal to the 53 MHz frequency of the main ring acceleration system in order to permit synchronous transfer of the booster beam bunches into the rf buckets in the main ring.

Since $\beta = 0.57$ at the injection energy of 200 MeV, the frequency of the accelerating cavities must be lowered to 30 MHz at injection and must track the increasing velocity of the protons as they are accelerated. The cavities are tuned to the correct resonant frequency by changing the current in bus bars linking ferrite-loaded tuners which are part of the resonant structure.

The beam from the linac is bunched at 200 MHz. However, the momentum spread is large enough that it debunches in approximately one turn around the booster. The beam is then adiabatically rebunched at 30 MHz and captured in the 30 MHz rf buckets by turning on the booster rf voltage in 16 steps over a period of 150 μ sec.

The 8-GeV beam is extracted from the booster with a fast kicker magnet system which produces a beam pulse whose length is equal to the circumference of the booster. However, the circumference of the main ring is 13.25 times larger. To fill the main ring with beam, the magnetic guide field in the main ring is held constant at the injection field strength for 0.8 sec. at the beginning of each main ring cycle. During this interval, up to

13 pulses of beam from successive cycles of the booster are stacked end to end in the main ring.

To reach the design intensity of 5×10^{13} protons per pulse in the main synchrotron, the booster must inject 13 pulses of 3.8×10^{12} protons each at the beginning of each cycle of the main ring. This corresponds to a beam current of 390 mA in the booster at 8 GeV.

At the injection energy of 200 MeV, the beam current required in the booster is 230 mA. Although beam currents of 230 mA are within reach of present-day linac technology, operating the linac at a lower intensity may prove more satisfactory. To reduce the peak current demand in the linac, provision has been made for multiturn injection. Beam injected during successive turns is stacked side by side in the booster aperture. Allowing for some beam loss during injection and rf capture, the nominal peak beam current required from the linac is reduced to 75 mA.

The booster magnet ring is located in a concrete tunnel 8 ft. high and 10 ft. wide, which is covered with 15 ft. of earth shielding. The booster tunnel is on the same level as the main ring tunnel, and there is a tunnel connecting the booster tunnel to the transfer hall where the beam is both injected into the main ring and extracted from it. Provision is made for steering the 8-GeV beam into a beam dump located beneath the floor of this tunnel thus allowing operation of the booster while workmen are in the main ring enclosure.

As shown in the layout of the injector complex in Fig. A-1, the beam from the linac is injected into the booster at a point

180° around the ring from the extraction point. The level of the linac tunnel is 13-1/2 ft. higher than the booster tunnel. Beam travels down into the booster tunnel from the linac tunnel through a 2-1/2 x 3 ft. duct.

The magnets in the booster ring are mounted on 25-ft. long box girders. Each girder supports two of the combined function magnets as well as the vacuum pumps and the chokes and capacitors for the magnet power circuit. As seen in Fig. A-2, the magnets are located against the inner wall of the tunnel with the utility distribution systems behind them.

Two equipment galleries are located above and to the inside of the tunnel. The galleries are above the parts of the tunnel which house rf cavities or injection or extraction components. The power supplies for the rf systems, power supplies for auxiliary magnets, rough vacuum pumps, and many of the control system components are located in these galleries. There is sufficient shielding between the tunnel and the galleries that maintenance work can be carried out in the galleries while the booster is operating.

A utility yard outside each gallery provides space for high voltage transformers and switch gear, the power supplies for the ring magnet, and the 25-kV dc power supplies for the rf system.

Reference

A1. Design Report, National Accelerator Laboratory (1968).

Table A-1

BOOSTER PARAMETERS

Injection Energy	200 MeV
Extraction Energy	8 GeV
Average Radius	75.47 meters
Circumference Factor	1.7 meters
Peak Intensity	4×10^{12} proton/pulse
Cycling Rate	15 Hz
Injection Field	488 gauss
Extraction Field	6.7 kilogauss
Average Vacuum	5×10^{-7} Torr

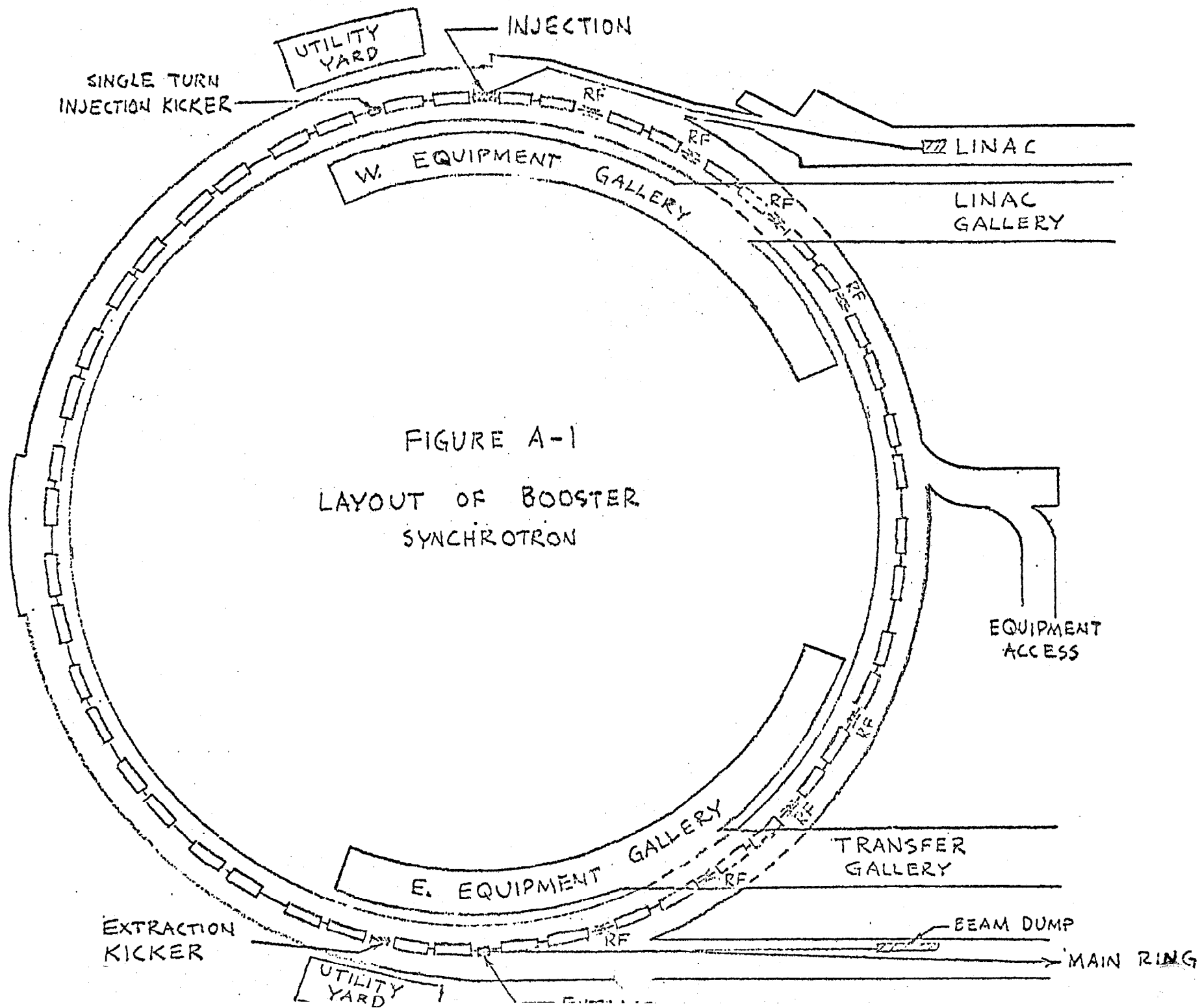


FIGURE A-1
LAYOUT OF BOOSTER
SYNCHROTRON

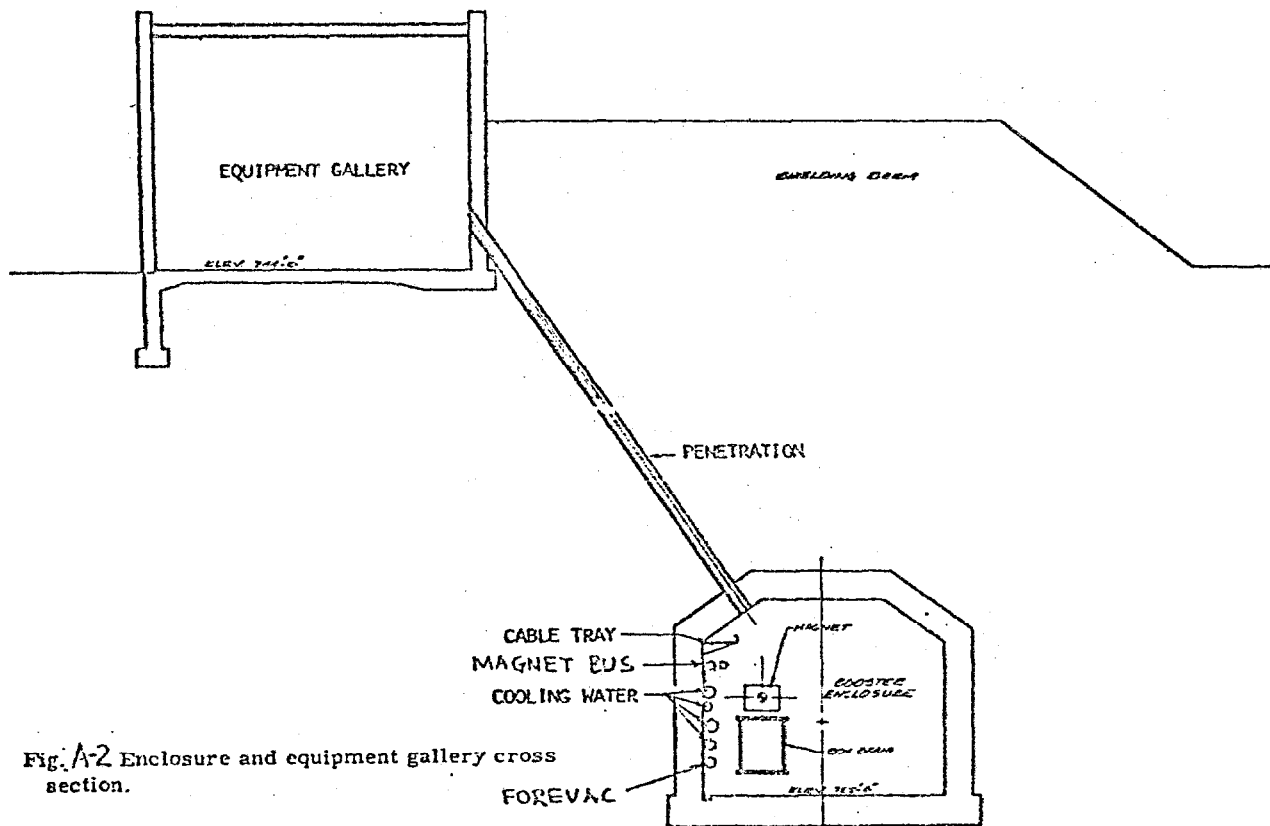


Fig. A-2 Enclosure and equipment gallery cross section.

B. Lattice and Orbits

1. Lattice

The lattice for the 96 combined function magnets in the booster ring is divided into 24 identical periods. Each period contains two horizontally focusing (F) magnets and two horizontally defocusing (D) magnets. The arrangement of these magnets in one period of the lattice is shown in Figure B-1. There is no superperiod structure in the booster. The injection and extraction equipment and the rf accelerating cavities fit into the 6-m long straight sections between the D magnets. Beam detectors and orbit correcting magnets are located at the downstream end of each of the 6-m long mid-D straight sections and each of the 1.2-m long mid-F straight sections. Connections to the high vacuum pumps are made in the 0.5-m straight sections separating the F and D magnets.

The nominal betatron frequencies in the horizontal and vertical planes are $\nu_x = 6.7$ and $\nu_y = 6.8$, respectively. Thus, there are no second or third-order structure resonances adjacent to the working diamond. There is a fourth-order structure resonance on the integral boundary at $\nu = 6$, but no fourth-order structure resonance within the diamond. The vertical and horizontal betatron frequencies are made slightly different to prevent coupling between the radial and vertical oscillations. Multiple-turn injection makes the horizontal emittance of the beam in the booster larger than the vertical emittance, and coupling could cause the vertical amplitude to grow larger than the vertical aperture.

The transition energy occurs at $\gamma_t = 5.446$. This is far enough below the extraction energy that the large momentum spread and small synchrotron frequency at transition should not interfere with synchronous bunch transfer to the main ring. The synchrotron frequency $\nu_s = 0.075$ at injection is low enough that coupling between the betatron and synchrotron oscillations is not expected to be a problem.

The steel part of the magnets is made by stacking thin laminations shaped as shown in Figure B-2. The major part of the focussing is provided by the wedge shape of the gap between the poles. The laminations are stacked in such a way that magnets have the curvature of the beam path. However, all the laminations are parallel so that there is a small amount of edge angle focussing at each end of a magnet.

To produce the desired tunes, normalized field gradients $k = \frac{1}{B_0} \frac{dB}{dx}$ of 2.20 m^{-1} and -2.76 m^{-1} are required in the F and D magnets, respectively. In addition, a small sextupole-field component was included in order to reduce the dependence of the betatron frequencies on momentum.^{B1} The pole tips were contoured to produce field gradients on the median plane within 1% of the design fields over the specified "good field width" with the poles as narrow as possible.^{B2} Measured normalized gradients are shown in Figure B-3.

After the final pole profiles had been chosen, it became evident that there were residual errors in the field shape sufficient to cause radial and vertical tune shifts in excess

of ± 0.1 over the momentum width of the aperture. In order to correct for this deficiency, special end shapes were constructed to reduce the momentum dependence of the tune to less than ± 0.1 . The resultant effective gradient lengths for the F- and the D-magnets are shown in Figures B-4 and B-5, respectively. Table B-II summarizes the results obtained from the field measurements.

2. Apertures

The betatron amplitude and the dispersion function throughout a period of the lattice are tabulated in Table B-I and are plotted in Figure B-1. The apertures in the F and D magnets are different in order to accommodate the different beam dimensions in the two kinds of magnets. The vertical aperture is 1.64 in. in the center of an F magnet and 2.25 in. in a D magnet. Horizontally, the design value of the "good field width" is 4.3 in. in an F magnet and 3 in. in a D magnet.

The acceptance of the booster for a beam which fills the design horizontal "good field width" and the vertical magnet aperture is 90π mm-mrad horizontally and 40π mm-mrad vertically. The emittance of the 203-MeV beam from the linac is approximately 10π mm-mrad. Ideally the emittance should damp according to p^{-1} and reach 0.725π mm-mrad at 8 GeV. The horizontal emittance is larger when multiturn injection is used. To increase the beam accepted by the booster to 3 or 4 times the linac beam current, the full 90π mm-mrad horizontal acceptance is required. The corresponding emittance at 8 GeV is 6.5π mm-mrad.

The width and height of the beam are nearly equal in the 6-m long straight sections since the small value of β_x nearly compensates for the larger horizontal emittance from multiturn injection. The fast kicker magnets and the rf accelerating cavities, which are located in the 6-m straight sections, have a circular aperture 2-1/4 inches in diameter. The circular aperture reduces the horizontal acceptance below 90π mm-mrad for particles which are not centered vertically.

The limiting aperture in the mid-F straight sections is a circular pipe 4-1/2 inches in diameter.

3. Space Charge

If the 40π vertical acceptance of the booster were filled with beam, the booster should accommodate 8×10^{12} particles before incoherent space charge effects depress the vertical betatron frequency by $\Delta\nu = 1/4$. The beam is injected into the booster with a vertical emittance of 10π mm-mrad, but at high intensities, it is expected that space charge will blow up the vertical emittance until it more nearly fills the available vertical aperture.

Space is available in the unused 6-m long straight sections for a coherent oscillation damping system if it proves necessary. If space charge proves to be a problem at transition, it is planned to jump the tune with pulsed quadrupoles in the 1.2-m straight sections.^{B3}

References

- B1. S.C. Snowdon, NAL Report, FN-192 (1969).
- B2. S.C. Snowdon, NAL Report, FN-180 (1969).
- B3. L.C. Teng, NAL Report, FN-207 (1970).

Table B.-I.

BOOSTER LATTICE TUNE INCLUDING EDGE FOCUSING 2/16/70

[illegible]

BEIJING FUNCTIONS THROUGH BUU.

CYCLE	S	NAME	PS17/2P1	BETAX	ALPHAX	REQ	DXEQ	MX $\sqrt{P_x}$	PS17/2P1	BETAT	ALPHAT	TEQ	DTEQ	MT $\sqrt{P_x}$
1	0.0	00	0.0	33.66233	0.00000	3.18908	0.00000	5.80192	0.0	5.27346	0.00000	0.0	0.0	2.29
2	0.30000	00	0.00142	33.66593	-0.00091	3.18908	0.00000	5.80215	0.00904	5.29053	-0.00689	0.0	0.0	2.30
3	0.60000	EF	0.00284	33.67102	-0.00182	3.18908	0.00000	5.80285	0.01803	5.34173	-0.011378	0.0	0.0	2.31
4	0.90000	F	0.00426	33.67302	-0.00470	3.18908	0.00276	5.80285	0.01803	5.34173	-0.01915	0.0	0.0	2.31
5	1.32240	F	0.00628	32.80055	1.24278	3.15193	0.10537	5.72720	0.01893	5.75479	-0.46803	0.0	0.0	2.39
6	2.06441	F	0.00992	30.14996	2.39172	3.03757	0.21049	5.49090	0.05754	6.71950	-0.88018	0.0	0.0	2.59
7	2.76721	F	0.01400	26.02082	3.26953	2.84927	0.30950	5.10106	0.07299	8.34702	-1.39131	0.0	0.0	2.68
8	3.48961	EF	0.01891	20.88146	3.77677	2.59239	0.39988	4.56962	0.08516	10.82233	-2.05644	0.0	0.0	3.28
9	3.48961	U	0.01891	20.88146	3.75868	2.59239	0.39751	4.56962	0.08516	10.82233	-2.05644	0.0	0.0	3.28
10	3.73461	U	0.02091	19.04743	3.77756	2.49298	0.39751	4.36433	0.08867	11.88052	-2.17681	0.0	0.0	3.44
11	3.98461	EQ	0.02310	17.30389	3.79685	2.39357	0.39753	4.15979	0.09187	12.99912	-2.29757	0.0	0.0	3.60
12	3.98461	U	0.02310	17.30389	3.78551	2.39357	0.39613	4.15979	0.09187	12.99912	-2.28943	0.0	0.0	3.60
13	4.71202	D	0.03074	13.21627	2.32992	2.14720	0.28763	3.63542	0.09978	16.10139	-1.96176	0.0	0.0	4.71
14	5.41442	D	0.04059	10.43932	1.55367	1.97622	0.18733	3.23095	0.10640	18.55471	-1.40014	0.0	0.0	4.71
15	6.15682	D	0.05277	6.63678	0.96592	1.87527	0.09285	2.93884	0.11233	20.06651	-0.67159	0.0	0.0	4.71
16	6.87922	EQ	0.06706	7.59194	0.45401	1.86140	0.00115	2.75535	0.11798	20.45649	0.13714	0.0	0.0	4.72
17	6.87922	UU	0.06706	7.59194	0.49005	1.86140	0.00000	2.75535	0.11798	20.45649	0.14995	0.0	0.0	4.72
18	9.37922	UU	0.10133	6.48931	0.24503	1.86140	0.00000	2.54741	0.12976	20.11911	0.07498	0.0	0.0	4.73
19	9.87922	UU	0.13950	6.12177	-0.00000	1.86140	0.00000	2.47422	0.14167	20.00664	-0.30000	0.0	0.0	4.74
20	11.37922	U	0.17782	6.48931	-0.24503	1.86140	0.00000	2.54741	0.15355	20.11911	-0.07498	0.0	0.0	4.75
21	12.87922	EQ	0.21210	7.59194	-0.49005	1.86140	0.00000	2.75535	0.16516	20.45649	-0.14995	0.0	0.0	4.76
22	12.87922	U	0.21210	7.59194	-0.49481	1.86140	0.00115	2.75535	0.16516	20.45649	-0.13714	0.0	0.0	4.76
23	13.60163	D	0.22639	6.63678	0.96592	1.87527	0.09285	2.93884	0.17100	20.06651	0.67159	0.0	0.0	4.77
24	14.32403	D	0.23057	10.43932	-1.55367	1.97622	0.18733	3.23095	0.17693	18.55471	1.40014	0.0	0.0	4.78
25	15.04643	D	0.24084	13.21627	-2.32992	2.14720	0.28763	3.63542	0.18055	16.10139	1.96176	0.0	0.0	4.78
26	15.76254	EQ	0.25606	17.30389	-3.78561	2.39357	0.39613	4.15979	0.19146	12.99912	2.28943	0.0	0.0	3.60
27	15.76254	U	0.25606	17.30389	-3.75655	2.39357	0.39763	4.15979	0.19146	12.99912	2.29757	0.0	0.0	3.60
28	16.01584	U	0.25825	19.04743	-3.77756	2.49298	0.39763	4.36433	0.19468	11.88052	-2.17681	0.0	0.0	3.44
29	16.26884	EF	0.26024	20.88146	-3.75868	2.59239	0.39763	4.56962	0.19818	10.82233	2.05644	0.0	0.0	3.28
30	16.26884	F	0.26024	20.88146	-3.77677	2.59239	0.39988	4.56962	0.19818	10.82233	2.05644	0.0	0.0	3.28
31	16.99124	F	0.26515	26.02082	3.26953	2.84927	0.30950	5.10106	0.21036	8.34702	1.39131	0.0	0.0	2.68
32	17.71364	F	0.26924	30.14996	-2.39172	3.03757	0.21049	5.49090	0.22579	6.71950	-0.88018	0.0	0.0	2.59
33	18.43605	F	0.27283	32.80055	-1.24278	3.15193	0.10537	5.72720	0.24441	5.75479	0.46803	0.0	0.0	2.39
34	19.15845	EF	0.27714	33.67102	0.00470	3.18908	0.00276	5.80285	0.26530	5.34173	0.01915	0.0	0.0	2.31
35	19.15845	UU	0.27632	33.67302	0.01782	3.18908	0.00000	5.80285	0.26530	5.34173	0.011378	0.0	0.0	2.31
36	19.45645	UU	0.27774	33.66593	0.00891	3.18908	0.00000	5.80215	0.27429	5.29053	0.00689	0.0	0.0	2.30
37	19.75265	UU	0.27916	33.66233	0.00000	3.18908	0.00000	5.80192	0.28333	5.27346	-0.00000	0.0	0.0	2.29

TKMS = 0.0

TRANSITION GAMMA = 5.445833

FILE # 1151, LINE # 4508, UNIFIED STORAGE # 7417.

Table B-II

	<u>$k(m^{-1})$</u>	<u>$L_B(m)$</u>	<u>$\rho(m)$</u>	<u>$L_G(m)$</u>
F	2.204	2.917	41.211	2.904
D	2.767	2.916	48.488	2.942

$L_B \rightarrow$ effective dipole length at 8 GeV

$L_G \rightarrow$ effective gradient length at 8 GeV

$\rho \rightarrow$ radius of curvature of beam trajectory at 8 GeV

$k =$ average normalized gradient $\frac{1}{B_0} \frac{dB}{dx}$ from 4 GeV to 8 GeV

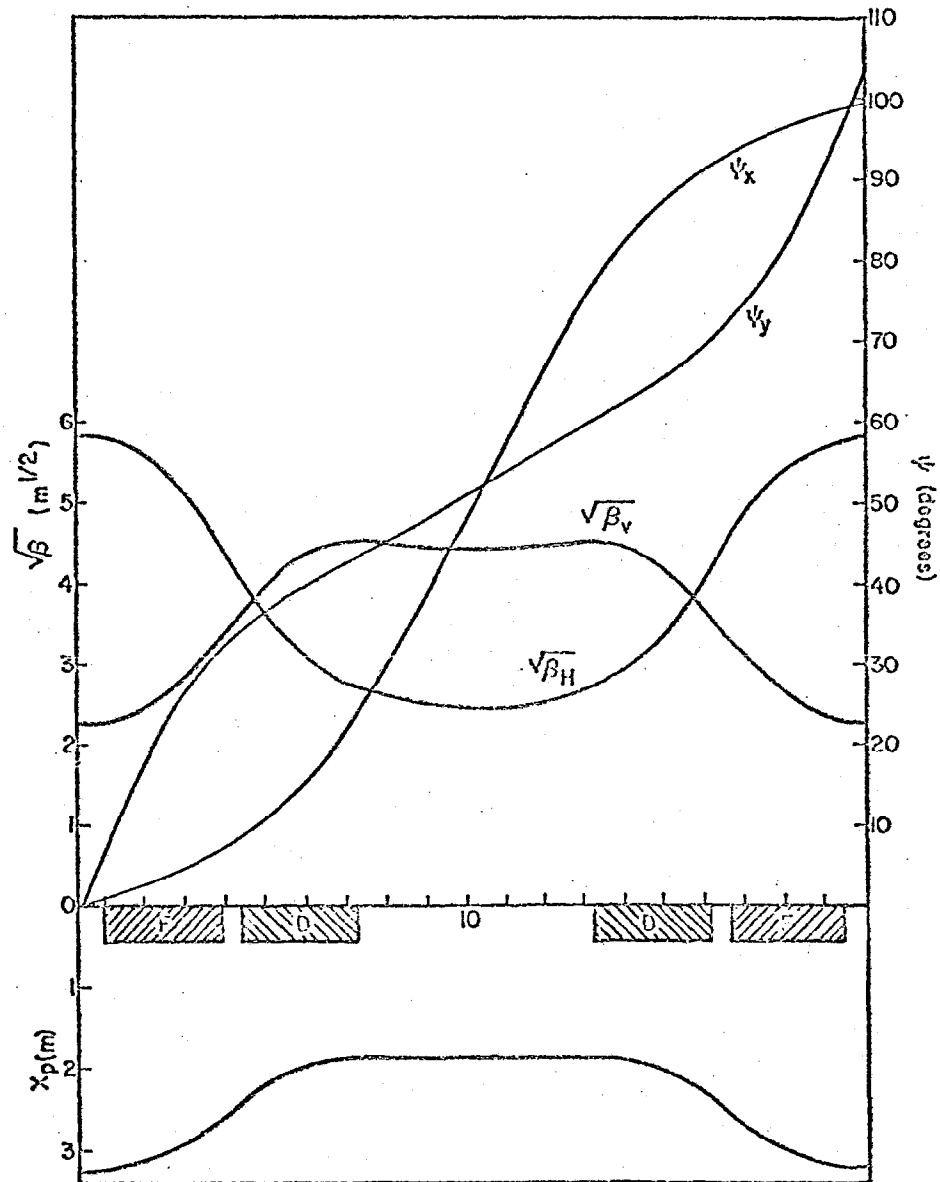


Figure B-1 Booster-Lattice Orbit Functions

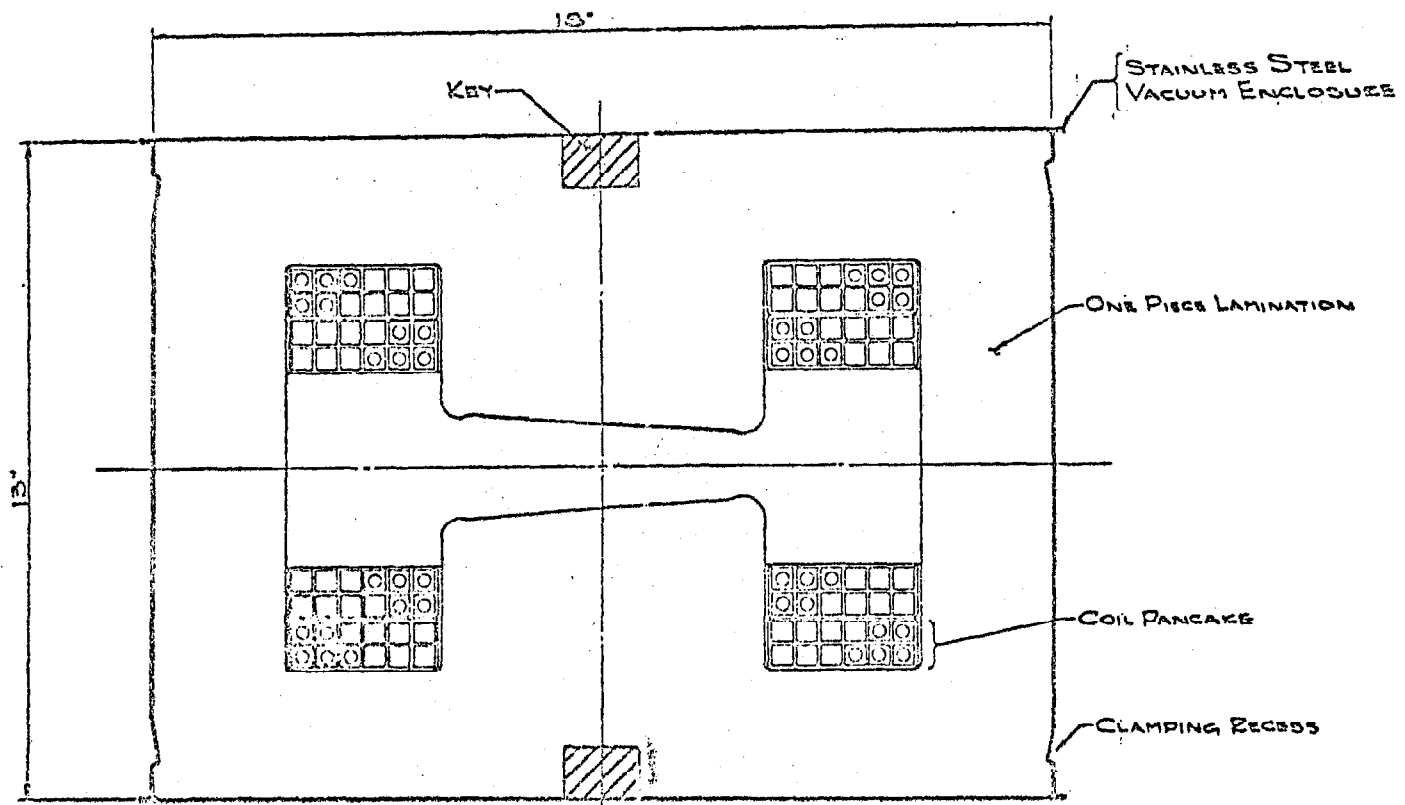


Fig. B-2 Magnet cross section. (F)

MEASURED NORMALIZED GRADIENTS (PETERS)

$$k_1(F) = 2.2006 \text{ m}^{-1}$$

$$k_1(D) = -2.7627 \text{ m}^{-1}$$

$$B_0(F) = 7259 \text{ G}$$

$$B_0(D) = 6152 \text{ G}$$

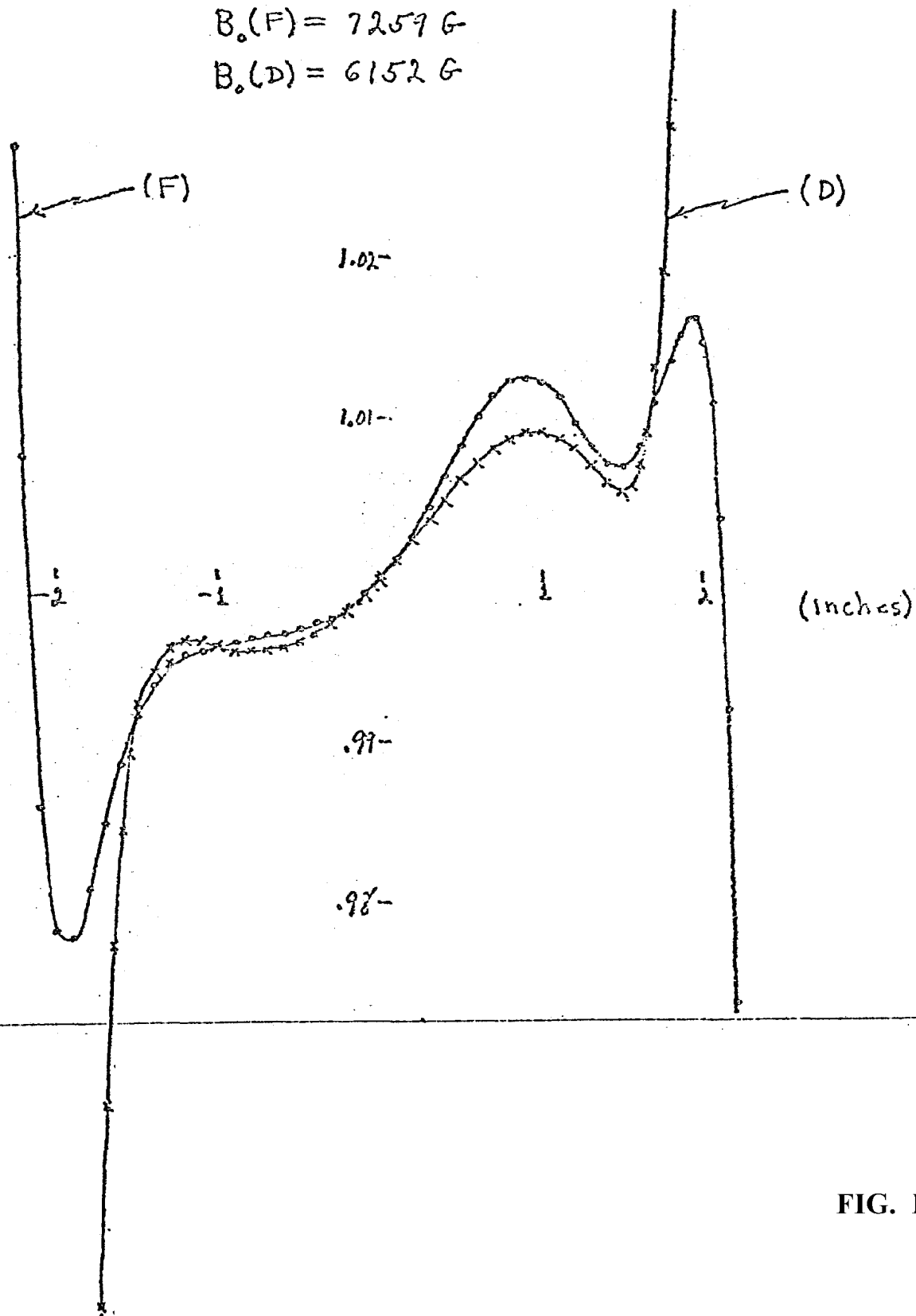


FIG. B-3

D.

$$L_G(0) = 115.83$$

$$L_G(X) - L_G(0)$$

(INCH)

-2.0

-1.0

1.0

2.0

X (IN.)

-1.0

-2.0

FIG. B-5

$$L_G(0) = 114.34$$

$$L_G(X) - L_G(0)$$

(INCH)

F

-2.0

-1.0

1.0

2.0

X (IN.)

-1.0

-2.0

FIG. B-4

C. Magnet System

1. Introduction

The booster synchrotron magnet system consists of 48 complete modules. Each of these modules (Figure C-1) consists of a support girder which carries a pair of 10-ft. long magnets (one focussing and one defocussing), a choke, a bank of capacitors, a high-vacuum ion pump, a concentric set of correction magnets, and a beam position and intensity detector. This whole system of components was preassembled, connected for power, cooling and vacuum, and completely tested out as a working unit prior to installation in the synchrotron ring. Two of these modules (which are mirror images of each other), together with a 6-meter long straight section form one period of the lattice. The complete synchrotron ring consists of 24 such periods.

There are three supports for the two girders in each period. One of the supports is located under the mid-F straight section in the center of a period. The mid-F ends of both girders are pinned to this central support (A in Figure C-4). Another support is located under the other end of each girder. Each support is mounted on two jacks, which are used for vertical alignment of the girders, and each support has an adjusting screw for radial alignment.

2. Combined Function Synchrotron Magnets

Magnet Requirements. Each pair of magnets is placed in series with a choke, across which is a capacitor bank. The total volume

and cost of these latter components is proportional to the peak energy stored in the synchrotron magnet. In order to achieve the compact modular design described above, it was necessary to keep the magnet apertures to an absolute minimum consistent with the design intensity requirements. Consequently, it was decided to eliminate the inner vacuum chamber and enclose the gradient magnets in a stainless steel skin. This concept, first used by R. R. Wilson at Cornell,^{C1} has now been developed to permit closer tolerances to be achieved and considerably better radiation resistance and vacuum properties.^{C2}

To avoid excessive eddy currents in the magnets they are assembled from .025"-thick transformer steel laminations. They are bonded together with epoxy resin. Heat-cured epoxy resin casting compounds were found to be satisfactory, both from the point of view of low outgassing and high radiation stability. However, the heating cycle required to cure these compounds increases the danger of mechanical distortion occurring.

The accuracy requirements of the magnet are that trueness in the horizontal plane be within .005" overall and local deviations less than .001"/ft., and in the azimuthal direction the dimensions must be maintained within .010". The vacuum requirement is 5×10^{-7} Torr average pressure with a pumping speed of 600 l/sec for each pair of magnets. This implies an average outgassing rate of less than 3×10^{-9} Torr liter/cm²/sec. The required stacking factor is 96% minimum; however, in practice about 98.5% was obtained. This makes for better magnetic characteristics, more structural rigidity,

and less epoxy fill, thus less outgassing and less potential problems from radiation damage.

Mechanical Design. The magnet is designed to form a rigid, void-free monolithic structure that requires no outer structural support beyond that provided by a thin stainless steel container. The magnets are 13" x 18" in cross-section and 10' long. They are laminated using .025" thick M-22 silicon transformer steel, which has an insulating phosphate coating on both surfaces. The stampings have H-shaped apertures with the dimensions shown in Fig. C-2. The coils are made of flat pancakes, which are located off the midplane and thus are shielded from excessive radiation. Each magnet is "canned" in a stainless steel skin which has a multiple function. First, it is used as a vacuum impregnation container; second, it becomes an efficient structural "box" to support the magnet rigidly; and finally, it provides a reliable vacuum seal in the event of a crack in the epoxy insulation system or a breakdown in the epoxy due to radiation damage.

The magnet consists of about 4400 laminations stacked on the mean radius of curvature of the beam path. At each end, 90 laminations are shaped to produce the proper magnetic gradient length across the aperture. Outside the end-shaped laminations is a 1"-thick stainless steel end frame at each end. These hold the magnet together mechanically by means of two stainless steel keys which run the length of the magnet and are welded to the end frames. The keys are tight-fitting in the laminations for mechanical support of the laminations and for electrical grounding. The laminations

are not welded but are held in place by the epoxy bonding in addition to the end frame. Beyond the end frames are "poleless" laminations to simply fill the volume around the coil ends. The outer skins are 1/16" stainless steel top and bottom, which are spot welded to the end frames. The sidewalls are 1/8" thick and are seam welded to the top and bottom skins and plug welded to the end frames. The ends of the magnet enclosure are 1/32" covers welded to the top, bottom, and sidewalls. One end incorporates a bellows and both have thin disc flanges which are welded and are reweldable in the event of disassembly.

The coil conductors for each of the four pancakes pass through ceramic/copper vacuum feed-throughts brazed to a stainless steel plate so that the remaining electrical and water connections are made on the outside of the magnet. All four water circuits are connected in parallel. To reduce the peak voltage to ground, the four coil pancakes are connected electrically in a crossed series/parallel arrangement, which avoids the possibility of unbalanced flux linkage.

Choice of Materials. The stainless steel, the stacked steel epoxy composite, and the copper coils have similar coefficients of thermal expansion to minimize the possibility of bond failures during the thermal cycles which occur both during fabrication and operation. The coils are prestressed over the magnet pole tips to further reduce this possibility. The stainless steel components are grit blasted to improve bond strength.

Radiation resistance studies revealed that Nadic methyl anhydride epoxy has superior radiation resistance.^{C3} Vacuum

studies and its use in the vacuum chamber of the Princeton Penn Accelerator proved NMA to have excellent vacuum characteristics.^{C4} Other desirable characteristics are its good bond strength to copper, steel, and stainless steel, its long working time for impregnation, and its relatively low cure temperature.

All voids inside the magnet are filled with tightly packed fiberglass or with precast pieces made from a filled NMA epoxy. Fillers are used to avoid resin-rich regions which could develop cracks. Large corner blocks at the ends of the coils are precast using tiny glass beads as the filler making possible an exceptionally high filler-to-epoxy ratio of 4:1 providing low outgassing and high radiation resistance. During the final stage of impregnation alumina powder is added to the epoxy to fill any remaining voids.

To achieve the requirements of accuracy and high vacuum, the fixture and fabrication technique have been designed to minimize the amount of exposed epoxy on the inner vacuum side of the magnet, eliminate the possibility of trapped volumes of gas, minimize the heat loss during the curing cycle and keep the remaining heat loss uniform to minimize distortion of the magnet. The magnets are produced in a production line consisting of five stages:^{C5,C6}

1. Coil fabrication
2. Magnet stacking
3. Welding of skins and installation of coils
4. Vacuum impregnation
5. Clean up, inspection, vacuum bake-out and testing

The coil is wound from .460" square copper conductor with a .250" round hole. The F magnet has 12 turns per pancake (two layers) and the D has 14 turns. Each magnet contains four pancakes which are located two above and two below the midplane. This permits installation of the coils through the magnet gap. The turn insulation is a mica-glass epoxy system .014" thick. The layers are separated by .025" of epoxy-glass laminate and the ground wrap is three layers of half-lapped .010" glass tape. (See Fig. C-3.) The turn insulation is cured after winding, whereas impregnation of the glass cloth is accomplished as part of the final impregnation of the complete magnet. The copper conductor is obtained in lengths up to 156' so that each pancake contains only one joint.

The magnets are stacked in accurate fixtures which apply a pressure of 50 psi on the lamination surface. The outside of the magnet is painted with room cure epoxy to hold the magnet during movement to the next stage.

The magnet is then moved to allow the addition of the top and bottom stainless-steel skins. Following this the four pancake coils are installed and held in position. The end skins and feedthrough plate are then added and the whole external skin welded and vacuum tested. To minimize distortion and provide good heat transfer the magnet assembly is supported by tightly clamped heater platens. The entire assembly is enclosed in a rectangular vacuum tank which serves as effective insulation. An inflatable silicone rubber bag is installed in the magnet gap to prevent the epoxy from coating the edges of the laminations.

The magnet is evacuated to 20 microns and heated to 45° to 55° C for outgassing for 24 hours. Following this, preheated NMA epoxy resin is introduced under vacuum with the silicone bag still deflated. Once the epoxy-resin completely fills the magnet, the bag is then pressurized to 30 psi above atmospheric pressure. This serves to force resin between the laminations and into all voids. After being held under pressure long enough to accomplish this, the epoxy pressure is relieved and the bag is forced tightly against the inner vacuum surfaces. This technique has been found to leave the pole faces of the magnet completely free of resin.

The resin is then partially cured by gradually raising the temperature of the magnet to 75° to 85° C and maintaining this for four hours. This causes the epoxy to gel. The heat required for this phase is provided by passing a dc current through the coil. The temperature of the coil exceeds that of the magnet by 5° to 8° C, thus preparing it for prestressing. The coil temperature is controlled and monitored at this time by running water slowly through the coils. The temperature of the magnet and coil is then elevated to the cure temperature of 100 to 110° C by added heat from the heater platens. It has been found that the coil-to-magnet differential is maintained when doing this. The magnet assembly is then allowed to cool slowly after which the silicone bag is removed.

The final stage consists of pumping the magnet at an elevated temperature for two weeks to drive out any excess water vapor or other volatile residues.

3. Alignment of the NAL Booster Gradient Magnets

The booster alignment was done in three steps:

1. Establish vertical- and radial-position monuments in the booster tunnel.
2. Align magnets vertically, and radially with respect to girder.
3. Move girders into correct radial position by surveying from the monuments.
4. Use beam position measurements to refine the alignment.

Vertical Monuments. There are 24 vertical monuments equally spaced around the booster tunnel, one at the center of each long straight section. Each monument, which is anchored to the wall, locates an optical tooling scale which reads vertically. All vertical sightings were done with a WILD N-3 precision level. A typical circuit of the booster ring, consisting of 48 sightings (two on each monument) closed with an error of .010 inch. Shifts as great as .050 inch in relative vertical positions of the monuments occurred over periods of several months. Monument #1, near the injection point, is always taken as fixed.

Radial Monuments. 24 radial monuments, one at each long straight section center, form a 24-sided regular polygon of accurately known dimensions. Each monument, which is anchored to the wall, consists of a mounting base for the KERNS DKM-2A Theodolite. The reproducibility of locating the DKM-2A or an optical target on a monument is better than .001 inch. Monuments are all at the same height within 1/2 inch. They were set in place radially using the DKM-2A and a Keuffel & Esser precision

LOVAR tape. The angle at each vertex of the 24-sided polygon was measured to ± 1 second of arc and the length of each side to $\pm .005$ inch. A typical circuit of the 24 vertex angles (48 sightings) closed with an error of 5 seconds of arc.

Alignment of Magnets on the Girder. Each magnet has four precisely located reference holes (see Fig. C-4). The median plane of the magnet is established from the bottom of these holes. First the girder is leveled and set to the correct height. Then the magnets are set vertically. Most magnets are not flat. The amount of twist is typically .020 inch or .030 inch from side to side. Each magnet is aligned to give zero average roll.

As shown in Fig. C-4, there are two reference points on each girder, points A and B. The magnets are set longitudinally by measuring from point A with an accurately calibrated metal tube. A typical error in magnet length is .025 inch. A magnet is always set longitudinally with the center in the design position. A stretched wire is used for the radial positioning of magnets relative to the girder. The wire is located with respect to points A and B. A precisely calibrated fixture employing a micrometer head is used to position the magnet reference holes relative to the wire. Precision in this adjustment is .001 inch. There is some interaction between vertical and radial movements of a magnet so several iterations of both alignment procedures is required.

Moving the Girders into Position. After the magnets are aligned vertically and radially relative to the girder, the girders are

moved into the correct radial position. A sight line is established between 2 wall monuments (Figure C-5) with the DKM-2A. Offsets from this line to the magnet reference holes are measured using an optical tooling scale and an optical micrometer attachment on the DKM-2A. These offsets are set to the design value and the alignment is complete. The girders are moved radially with negligible effect on the vertical alignment.

At high field the optical alignment resulted in rms deviations of the closed orbit from the center of the magnet apertures by 6.4 mm radially and more than 3.2 mm vertically. The original closed-orbit error at each of the beam detectors is shown in Figure C-6 and Figure C-7.

Closed-Orbit Correction. The closed orbit errors have been subsequently reduced by realignment of the magnets. The realignment was accomplished by computing a set of magnet displacements that would reduce the largest closed orbit errors in one plane. The magnets were then moved by the computed amount. The closed-orbit errors were remeasured, a new set of magnet displacements was computed, and the magnets were moved again. After repeating this process several times in each plane, the closed orbit deviations were reduced to 2.0 mm radially and 1.6 mm vertically. The remaining closed orbit errors at points around the ring are shown in Figures C-6 and C-7.

References

- C1. R.R. Wilson, The 10 to 20 GeV Cornell Electron Synchrotron Lab. of Nuclear Studies, Cornell Univ. Report CS-33 (1967).
- C2. R. Billinge, W. Hanson, and P. Reardon, International Symposium on Magnet Technology, DESY, Hamburg (1970).
- C3. Effects of High Energy Radiation on Mechanical Properties of Epoxy Resin Systems Used for Particle Accelerator Construction, R. Sheldon, G. Stapleton, RHEL/R152, Rutherford Laboratory Report, January, 1968.
- C4. Vacuum Characteristics of Some Epoxy Resins, U.I. Patel, NAL Technical Memo, TM-228 (1970).
- C5. NAL Specification--Booster Gradient Magnet, December 1, 1969, Specification No. 0321-ES-2540.
- C6. NAL Specification--Procedure and Check List for the Fabrication of Booster Gradient Magnet Spares, Specification No. 0321-ES-2546.

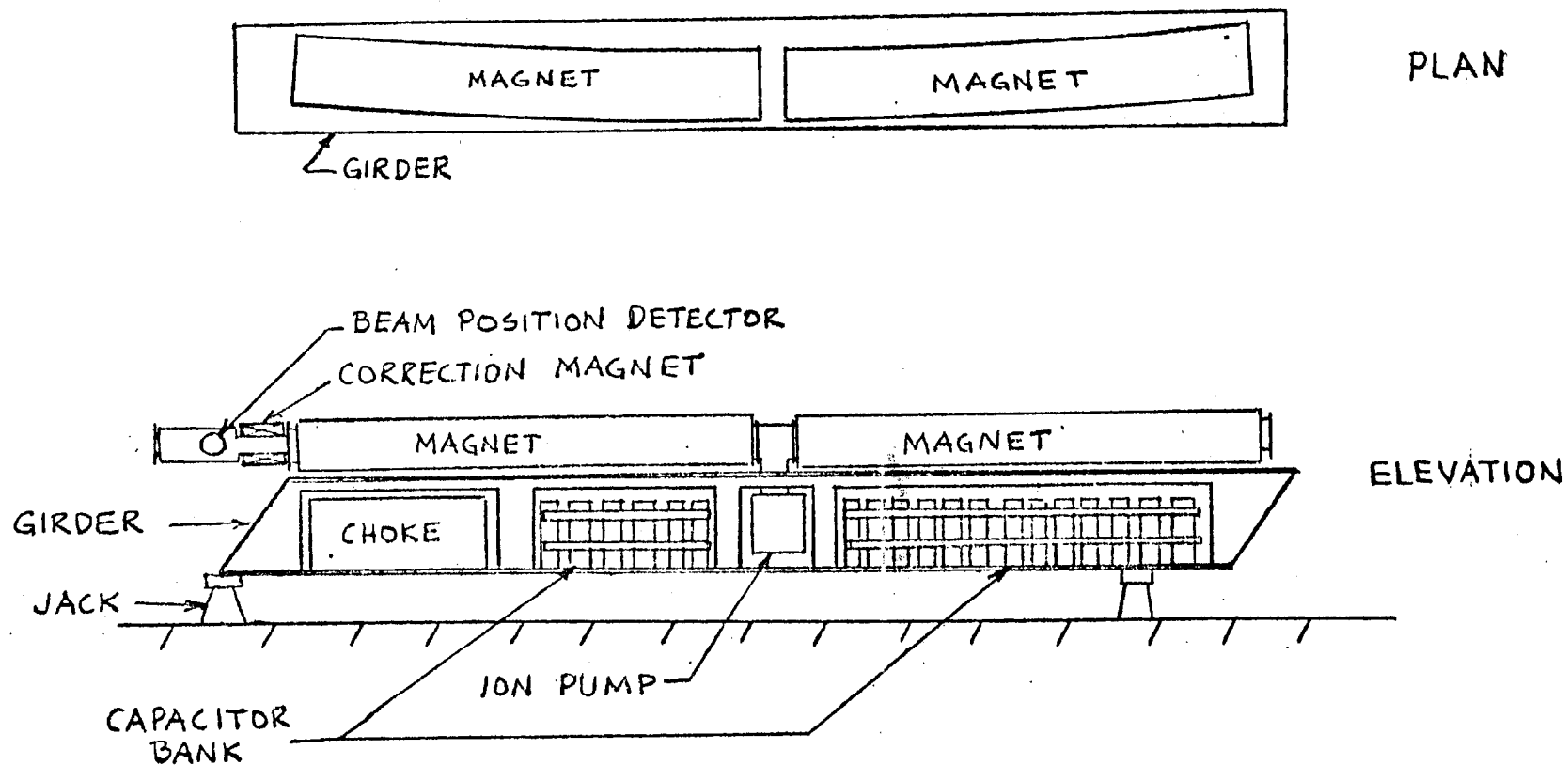


FIGURE C-1
MAGNET GIRDER
ASSEMBLY

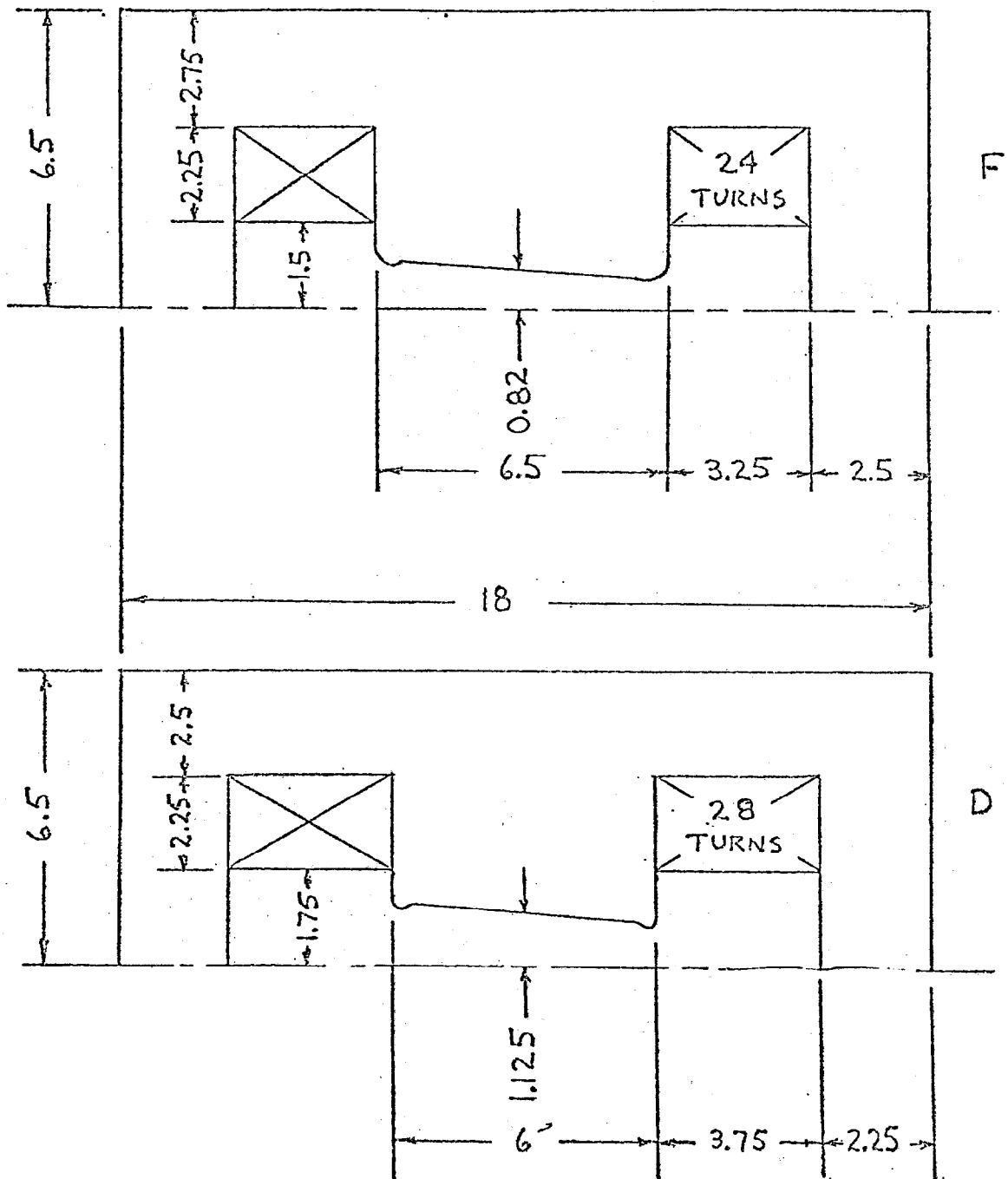


FIGURE C-2
MAGNET CROSS SECTION
DIMENSIONS (INCH)

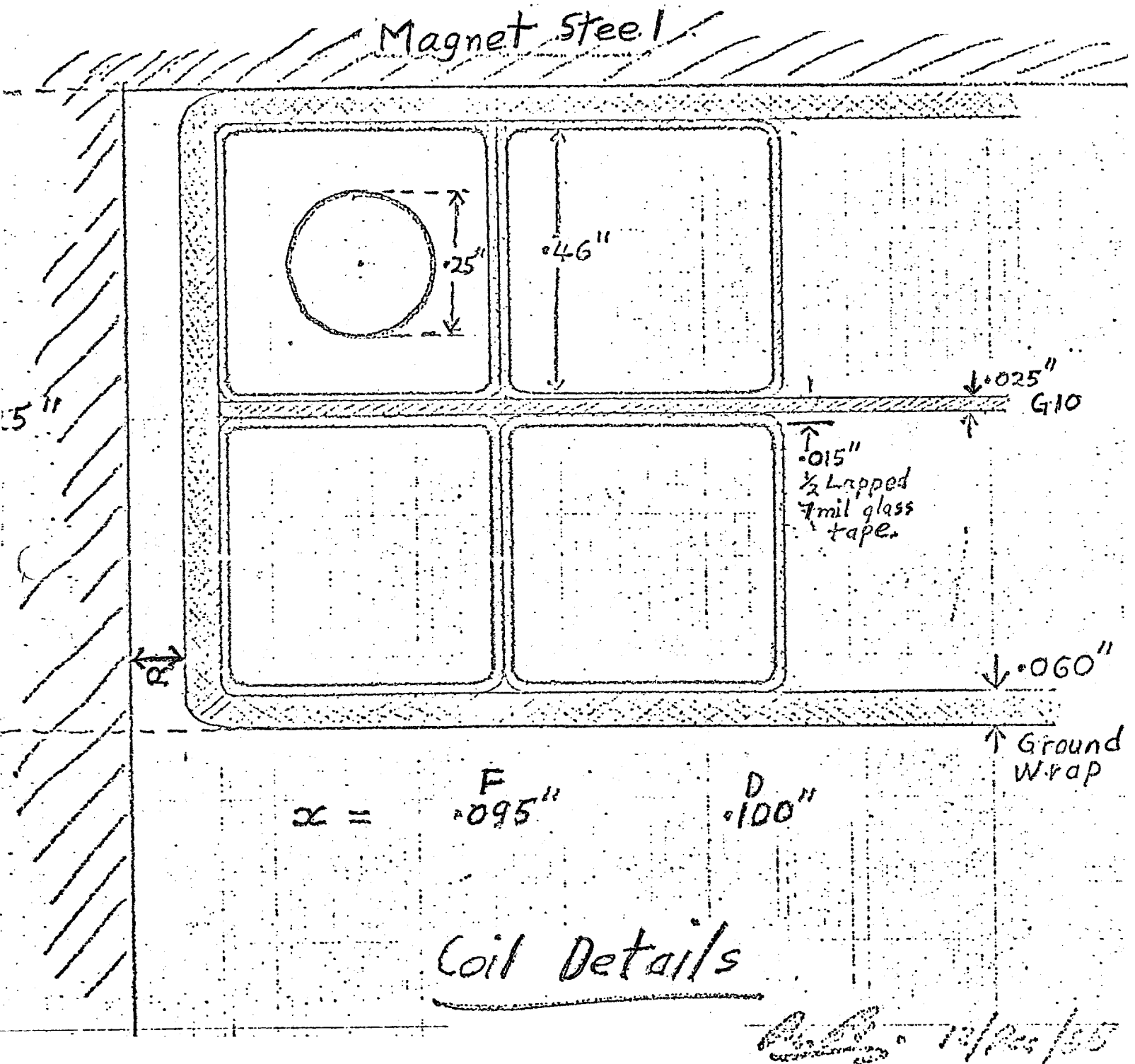


FIGURE 3-C

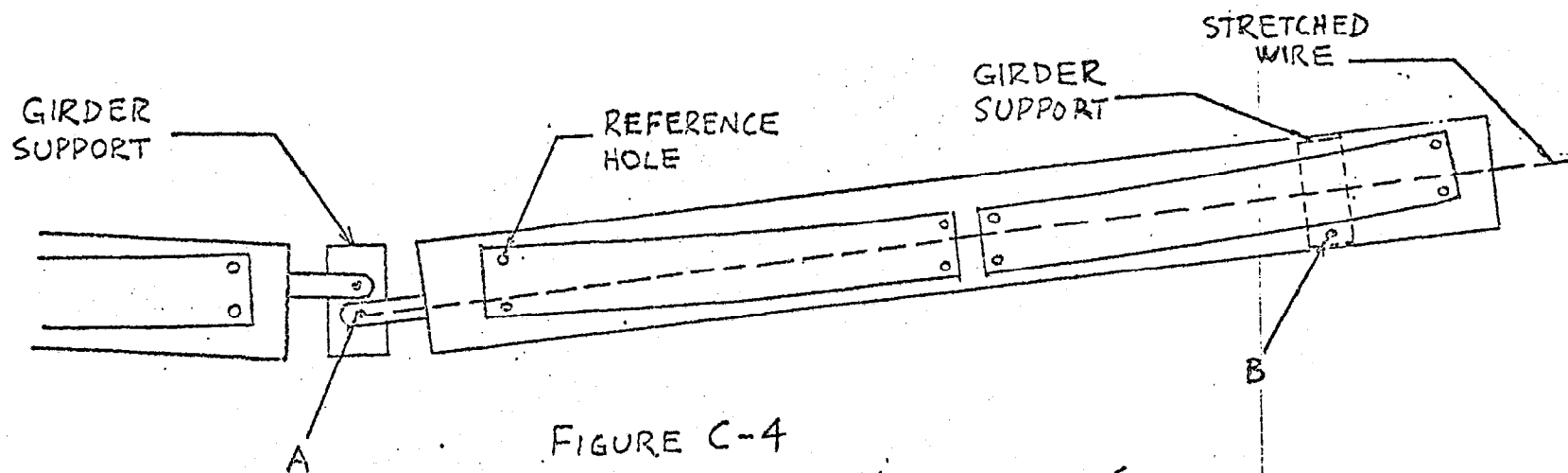


FIGURE C-4

ALIGNMENT OF MAGNETS ON GIRDER

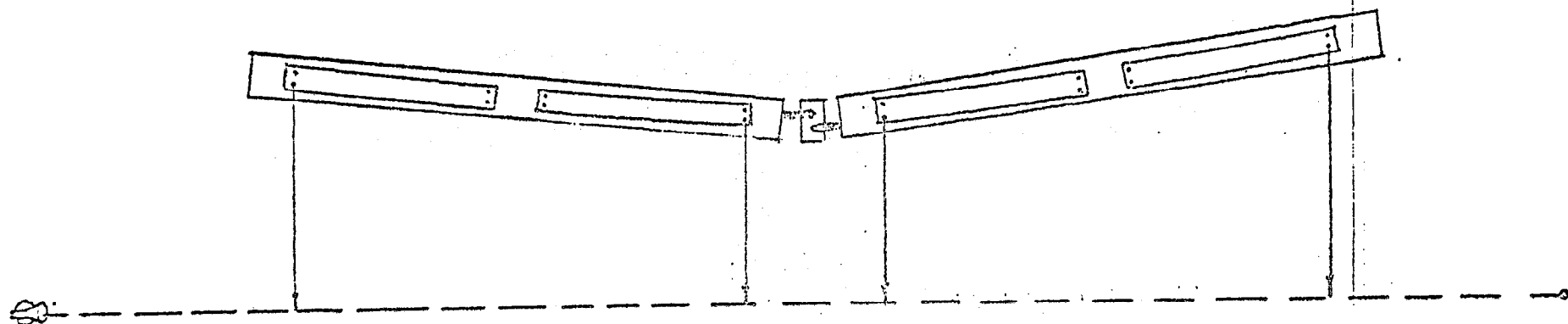
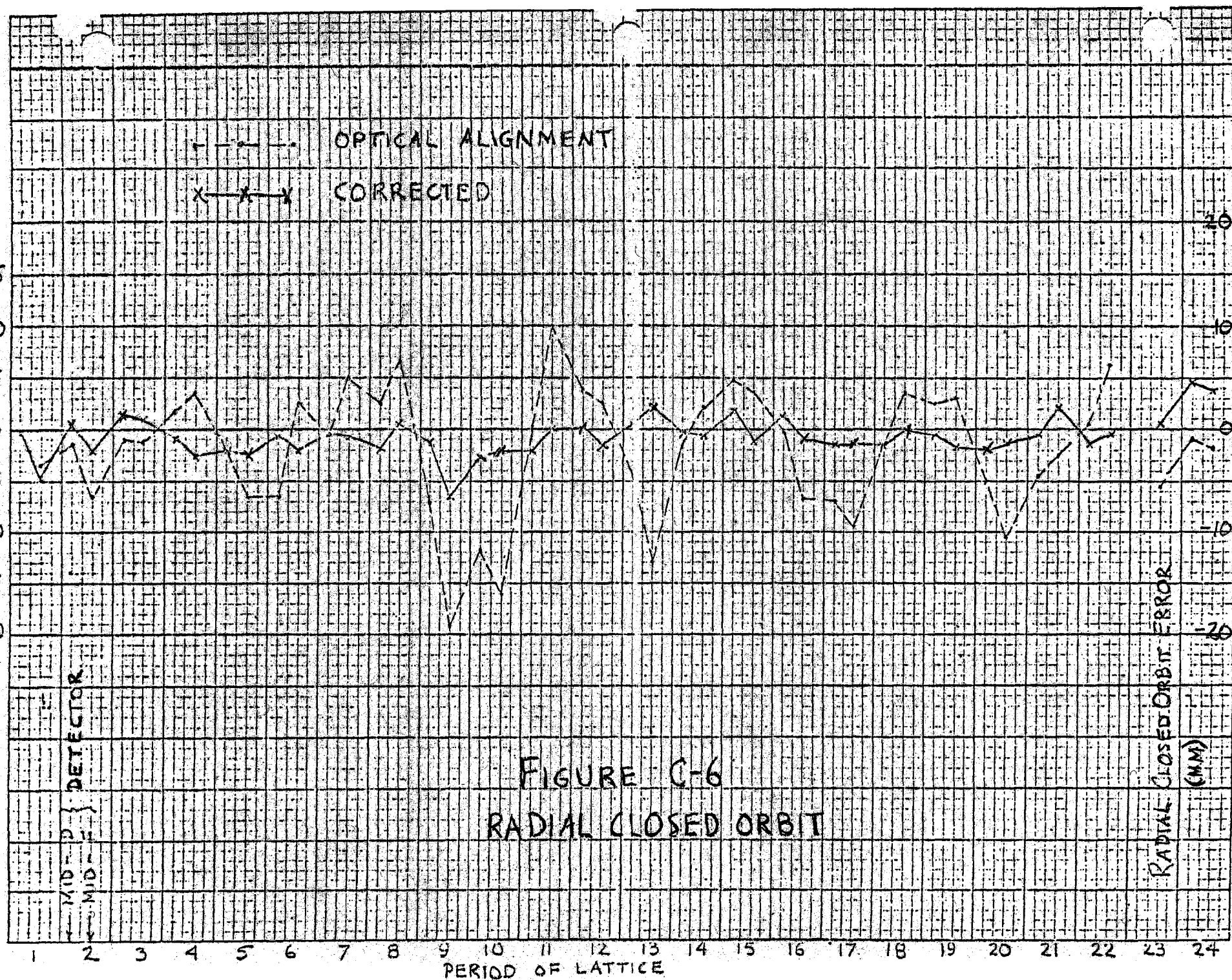


FIGURE C-5

RADIAL ALIGNMENT OF GIRDERS

RADIAL CLOSED ORBIT ERROR (MM)



VERTICAL CLOSED ORBIT ERROR (MM)

--- OPTICAL ALIGNMENT
 x-x-x CORRECTED

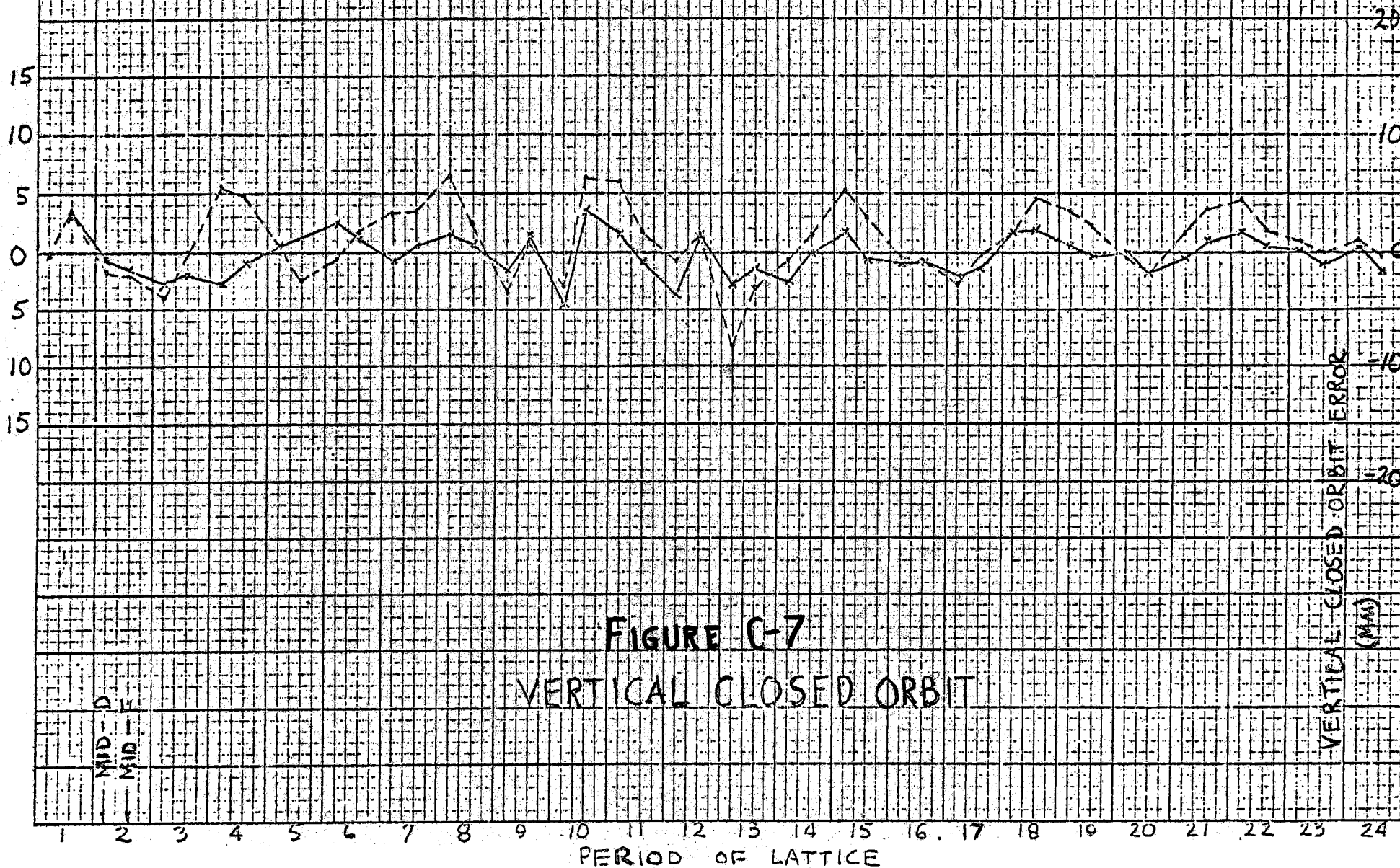


FIGURE C-7

VERTICAL CLOSED ORBIT

VERTICAL CLOSED ORBIT ERROR (MM)

D. Magnet Power System

1. Resonant Circuit

The magnetic field, used to maintain the equilibrium orbit of the booster synchrotron has the form:

$$B(t) = B_{dc} - B_{ac} \cos 2\pi ft$$

Aside from saturation effects in the magnets, the flux density may be considered as a linear function of the magnet current. With this assumption, the magnet power supply has to generate a current of the form:

$$I(t) = I_{dc} - I_{ac} \cos 2\pi ft$$

For reasons of economy, a resonant system was chosen, in which the synchrotron magnets resonate with a distributed capacitor bank. A distributed choke system is used for dc current bypass around the capacitor and for coupling between the different resonant cells. There are a total of 48 resonant cells, each cell consisting of an F and a D magnet, a choke and a capacitor bank. The basic resonant circuit is shown in Figure D-1. All cell components are physically mounted so that they form a module together with their support structure.

The choice of 48 series-connected resonant cells limits the peak voltage to ground to 700 volts. This is important since the coils are in high vacuum and the magnet terminals have to be brought out through vacuum feed-throughs. The magnet parameters are given in Table D-I, and the resonant cell parameters are listed in Table D-II. Each cell has a trimmer capacitor that is used to tune it to resonance. The measured resonance curve is

shown in Figure D-2. The chokes have secondary windings, which are coupled to the primary windings as in a transformer. The choke secondaries are all connected in parallel in order to equalize the ac voltages across the cells.

The main system parameters are listed in Table D-III. The voltage, current and stored energy wave shapes are shown in Figure D-3.

The resonant system elements with their stray capacitors to ground form a transmission line. Power supply output ripple, or other disturbances of the resonant system, may drive delay line resonant modes. In order to reduce the transmission line mode excitation, the power supplies have been designed as 12-phase supplies with a basic ripple frequency of 720 Hz. The lowest mode is suppressed by connecting one point of the magnet ring to ground through a 5000 Ω resistor instead of grounding it directly. The resistance of 5000 Ω is large compared to the characteristic impedance of the ring.

2. Power Supply

The biased sine wave for the booster synchrotron magnets is generated by programmed solid state power supplies. In contrast, the earlier rapid cycling machines, such as the NINA, DESY, CEA, Princeton Penn and Cornell machines, used two separate power supplies to generate the dc and ac components for the magnet excitation.

A total of four power supplies are connected in series with the complete booster synchrotron resonant circuit as shown in Figure D-1. Each power supply has to power twelve resonant cells

in series. Distributing the power supplies around the ring reduces the dc voltage to ground.

Two power supplies are located in each of the utility yards near the booster galleries. They operate directly off the 13-kV line. Each power supply consists of two 3-phase thyristor rectifier bridges connected in series as shown in the schematic circuit in Figure D-4. Each 13-kV transformer has two secondary windings which supply voltage to the two bridge circuits which are displaced in phase by 30° . Thus the ripple on the dc output has a frequency of 720 Hz. The ripple is further reduced by an L-C filter network on the output of each power supply. Free-wheeling diodes across the power supply output provide a discharge path for magnet circuit energy when power is turned off.

The firing circuits control the firing angle of the thyristors in such a way that the output voltage is proportional to the 0 to 5 volt input signal provided by the magnet regulator. The regulator output, which controls the firing circuits, is a 15-Hz biased trapezoidal wave which is synchronized to the 60-Hz power line.

Since the dc impedance of the magnet circuit is lower than the ac impedance, the voltage would swing negatively at the current minimum if the relation between the magnet current and the voltage were linear. However, if a sine wave is applied to the firing circuits, the free-wheeling diodes distort the voltage wave form as shown in Figure D-5, and the minimum magnetic field cannot be controlled accurately by the thyristor firing circuits. With the trapezoidal waveform, the firing circuits maintain sufficient control of the minimum current, and the Q of the magnet circuit

is high enough that the magnet current follows a sine wave.

3. Monitoring

Since there is no room for magnetic field monitoring apparatus in the aperture of the synchrotron magnets, a special magnet located in the equipment gallery has been provided for this purpose. The coil of the reference magnet is connected in series with the synchrotron magnets so that its magnetic field tracks the magnetic field in the ring.

The rate of change of the magnetic field, \dot{B} , is detected with a search coil located in the gap of the reference magnet. As shown in Figure D-6, the integrated emf generated by the \dot{B} coil is sampled at the maximum and minimum of the magnetic field cycle, held, and read with digital voltmeters.

To eliminate the effect of drift in the integrator, it is zeroed once every cycle of the magnet with a clamp circuit. The integrator is unclamped at precisely the same field every cycle by the signal from a peaking strip mounted in the gap of the reference magnet. The peaking strip is a strip of high permeability metal surrounded by a coil which generates a pulse when the magnetic field goes through zero. Since the synchrotron magnets are biased above zero field throughout the cycle, a special dc bias winding has been added to the reference magnet. The dc bias is set to make the field in the reference magnet go through zero and produce a pulse from the peaking strip approximately 2 msec before the minimum magnetic field. A dc offset voltage from a series resistor in the bias circuit is summed with the output of the integrator to provide the proper-biased sine wave

to the sample and hold circuits. The waveforms associated with the monitoring circuits are shown in Figure D-7.

The maximum and minimum values of the integrator output were also used by the original magnet current regulator. However, this regulator has been replaced by one which monitors the magnet current with a transducer.

4. Magnet Current Regulator

The maximum and minimum values of the magnet current are set by digital commands from the control room. A 15-Hz square wave is generated by switching between these two levels. The square wave is then filtered to produce the biased trapezoidal wave input to the thyristor firing circuits for the four power supplies. The switching is controlled by the booster clock which is synchronized with the 60-Hz power line.

The magnet regulator contains two loops: a loop to correct for slow changes such as temperature variations in the magnets and a loop to compensate fast changes such as fluctuations in the line voltage.^{D1} The fluctuations in the maximum current from cycle to cycle must be held below $\Delta I/I = 10^{-4}$ to keep the momentum of the beam steady enough for rf capture in the main ring.^{H5} The tolerance on the minimum current is $\Delta I/I \approx 2 \times 10^{-4}$.

Figure D-8 is a schematic of the regulator circuit. The error signals for slow regulation are derived by comparing the command voltage settings for the maximum and minimum currents with output of a transducer which measures the current in the magnet. The transducer output is sampled and held at both the maximum and minimum currents which are determined when the emf

generated by the B coil crosses through zero. The held levels are subtracted from the corresponding commands to derive error signals for the maximum and minimum currents. The error signals are then summed with the corresponding command voltages to produce the two input levels to the 15-Hz switch.

For fast regulation, a signal proportional to the sum of the output voltages of the four power supplies is summed with the 15-Hz trapezoidal wave output of the current regulator, and the combined signal is used to control the firing of the thyristors in the main power supplies.

Reference

- D1. A.R. Donaldson and R.A. Winje, Proceedings 1973 Particle Accelerator Conf., San Francisco.

Table D-I

MAGNET PARAMETERS

Excitation	$i = 548 - 475 \cos 2\pi 15t$
Magnet current at extraction	1023 A
Magnet current at injection	74 A
Peak current density in magnet conductor	3148 A/sq in

	<u>D Magnet</u>	<u>F Magnet</u>
Peak ampere turns	28631	24541
Number of turns	28	24
Inductance at peak field	10.2 mH	10.2 mH
dc resistance	15.9 m Ω	13.6 m Ω
Maximum ac voltage	455 V	455 V
dc voltage	8.7 V	7.5 V
Peak stored energy	5.34 kJ	5.34 kJ
dc power loss	4.8 kW	4.1 kW
ac power loss	3.6 kW	3.2 kW

Table D-II

RESONANT CELL PARAMETERS

Number of resonant cells	48
Number of magnets per resonant cell	1F, 1D
Number of chokes per resonant cell	1
Number of capacitor banks per resonant cell	1
Magnet inductance per cell	20.4 mH
Choke inductance per cell	40 mH
Capacitance per cell	8341 μ F
Magnet dc resistance per cell	29.5 m Ω
Choke dc resistance per cell	25 m Ω
Magnet effective ac resistance per cell	60.3 m Ω
Choke effective ac resistance per cell	94 m Ω
Choke Q	40
Peak voltage per cell	926 V
Maximum voltage to ground	710 V
Magnet peak stored energy	10.68 kJ
Choke peak stored energy	12.5 kJ
Capacitor peak stored energy	3.6 kJ
Magnet ac power loss	6.8 kW
Choke ac power loss	2.75 kW
Capacitor ac power loss	1.0 kW
Magnet dc power loss	8.9 kW
Choke dc power loss	7.5 kW

Table D-III

TOTAL SYSTEM PARAMETERS

Total magnet stored energy	512 kJ
Total choke stored energy	600 kJ
Total capacitor stored energy	173 kJ
ac power losses	510 kW
dc power losses	790 kW
Number of distributed power supplies	4
Power supply peak voltage	890 V
Power supply peak current	1023 amps
Total dc resistance of ring	2.6 Ω
Power supply filter	
Capacitance (5 x 480 μ F)	2400 μ F
Inductance	1 mH

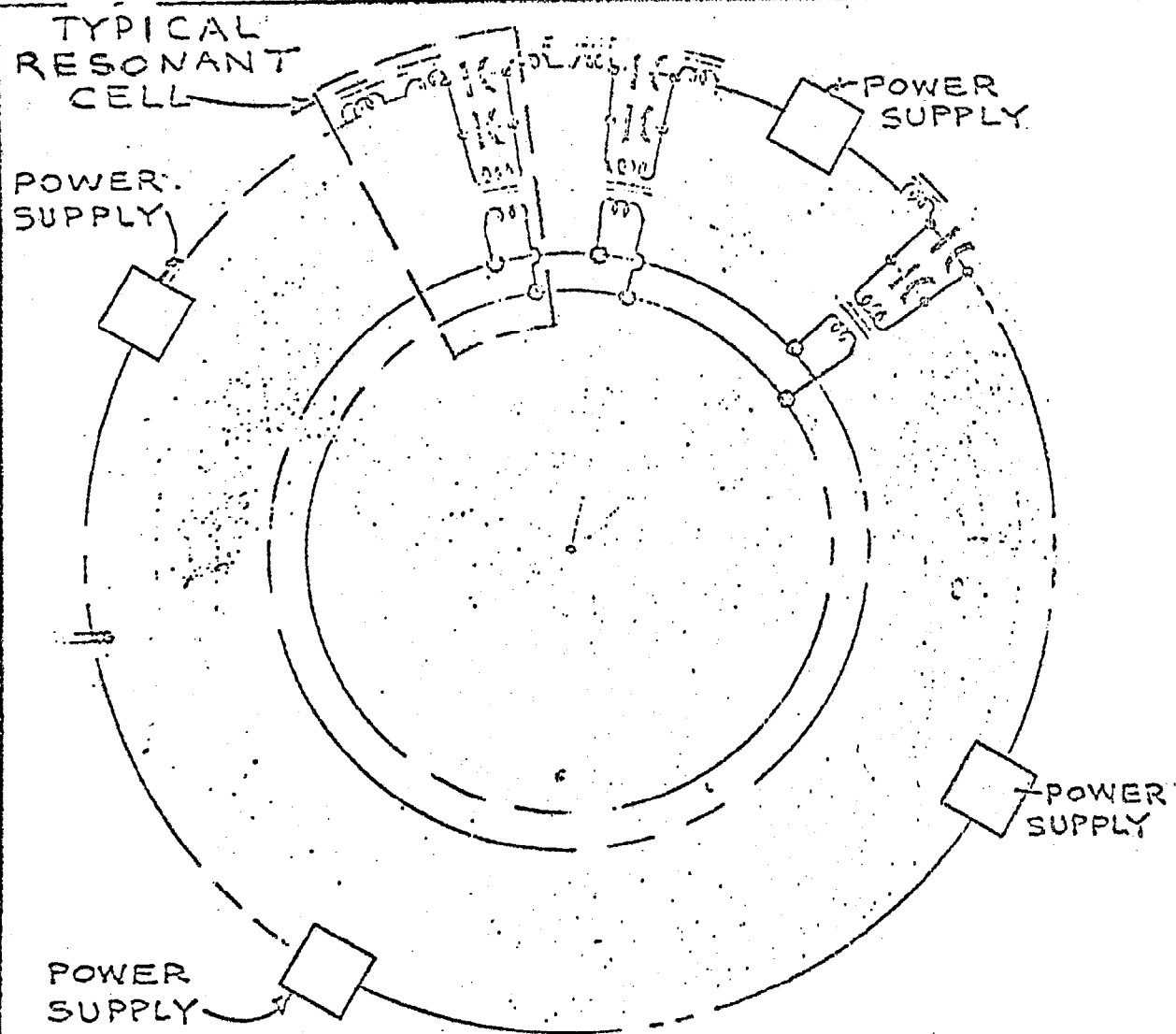



FIGURE D-1

 THIS DRAWING IS THE PROPERTY OF THE NATIONAL ACCELERATOR LABORATORY			
TITLE BOOSTER SYNCHROTRON MAGNET CIRCUIT			
SCALE	SHEET	DRAWING No.	REV.
7/	OF	0323-EA-220	

PERIOD OF TRANSDUCER CURRENT (MSEC)

FIGURE D-2

8 GeV magnet resonance curve

2.4

2.0

1.6

1.2

.8

.4

0

Non
linear

0.1%

$\Delta P = 1.64 \text{ msec}$

$Q = 40.6$

$Q = 43.6$

$\Delta P = 1.53$

107 I MAX

Period of Transducer current (m sec)

70

70

63

64

65

66

67

68

69

64

65

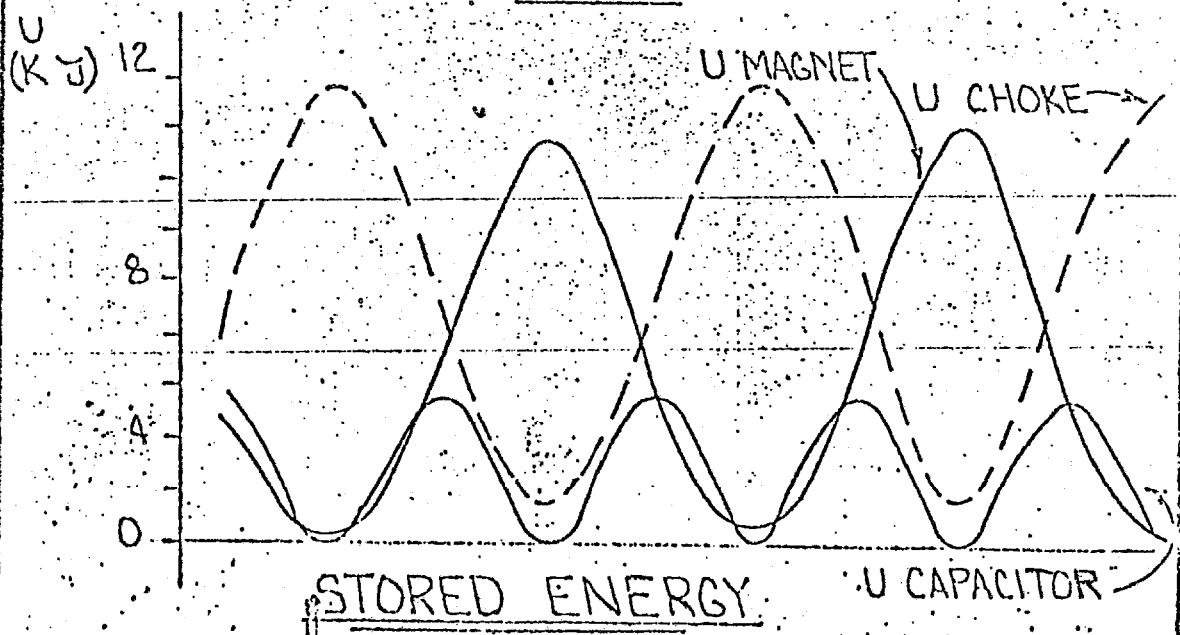
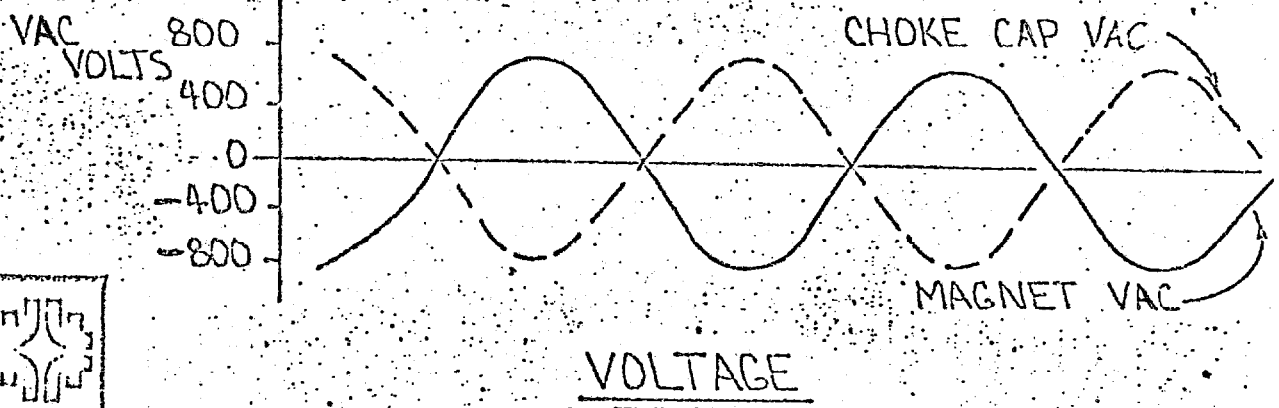
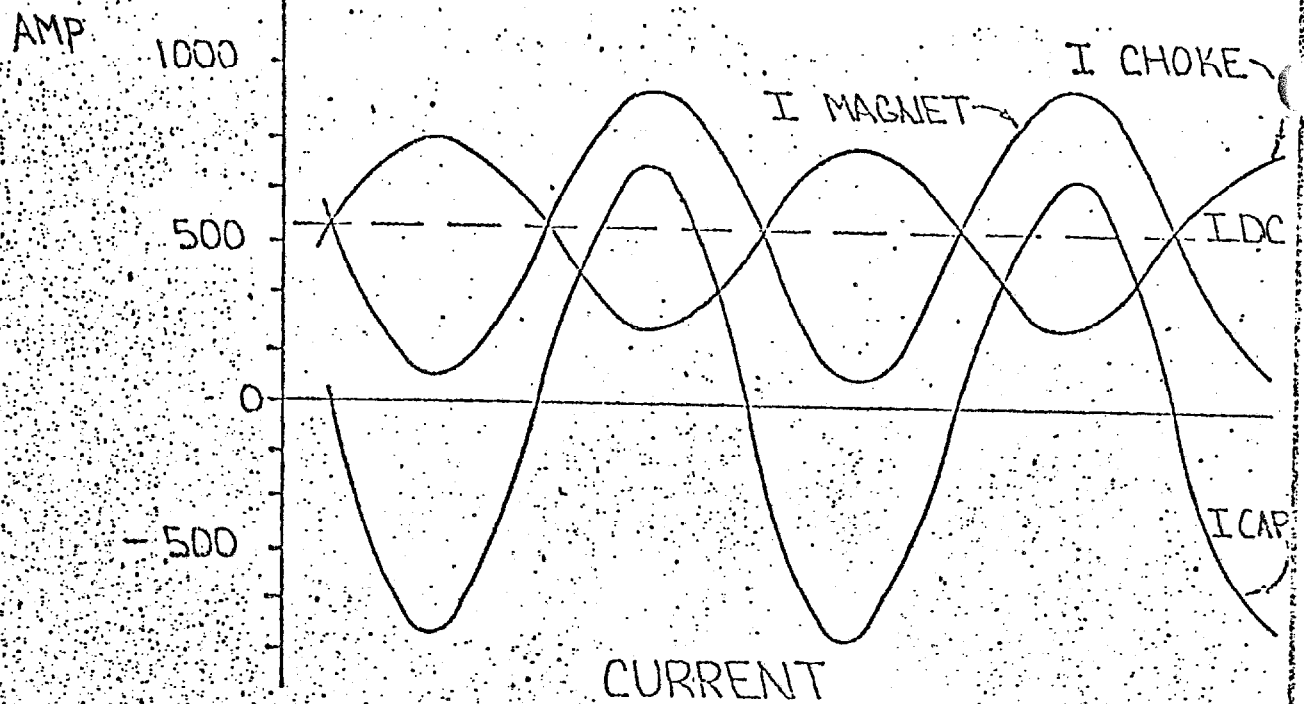
66

67

68

69

63



THIS DRAWING IS THE PROPERTY OF THE
NATIONAL ACCELERATOR LABORATORY

TITLE
VOLTAGE-CURRENT-STORED ENERGY
TIME FUNCTIONS

SCALE
SHEET
DRAWING NO.
0323-EA-2409
REV.

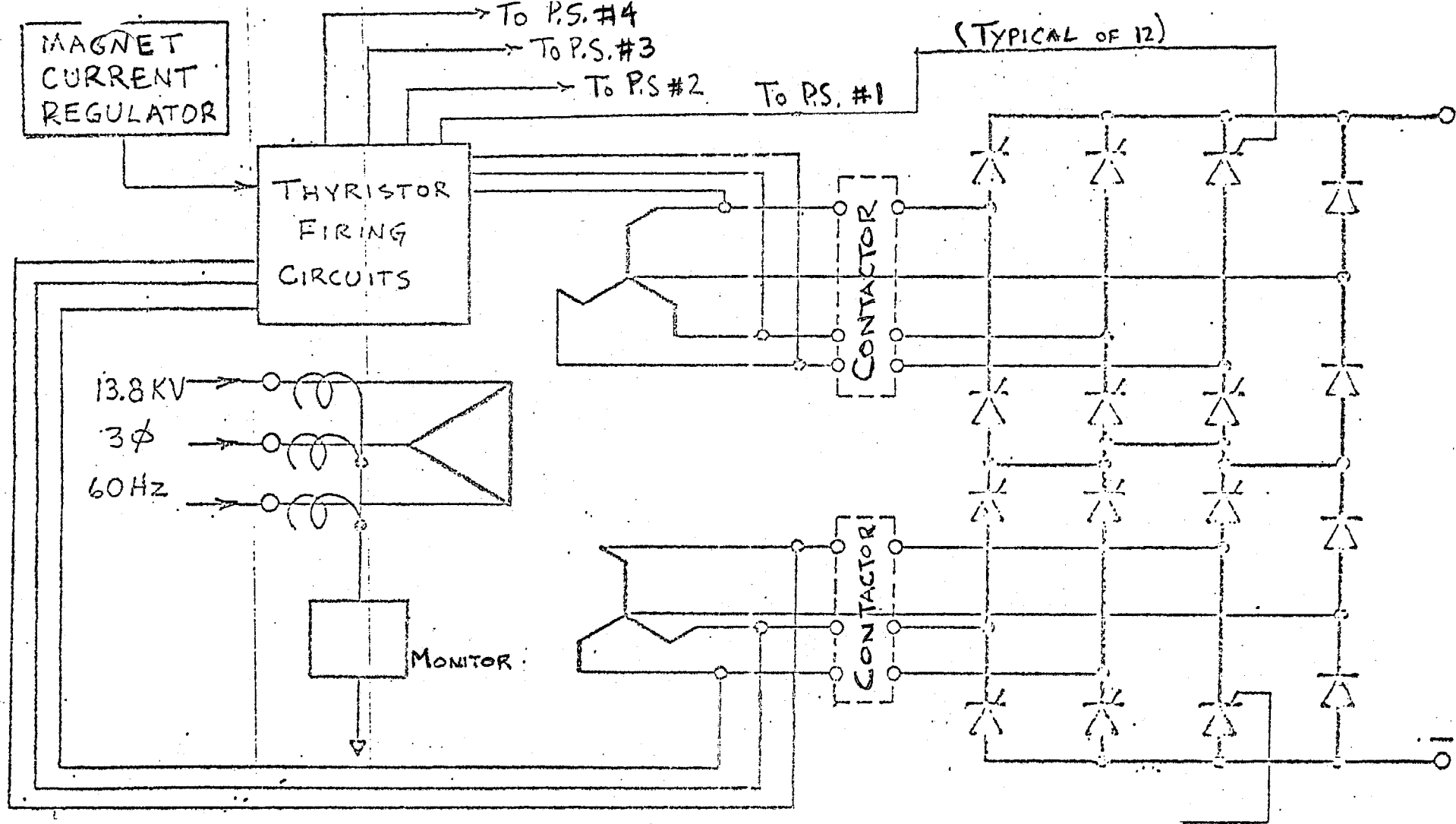


FIG. D-4

REVISIONS 1/1/64 04, ONT		THIS DRAWING IS THE PROPERTY OF THE NATIONAL ACCELERATOR LABORATORY		
		TITLE BOOSTER SYNCHROTRON- TYPICAL POWER SUPPLY CIRCUIT		
A	SCALE 1" = 1"	SHEET OF	DRAWING NO. 00000-01-2200	REV. A

Current and Voltage Wave Shapes

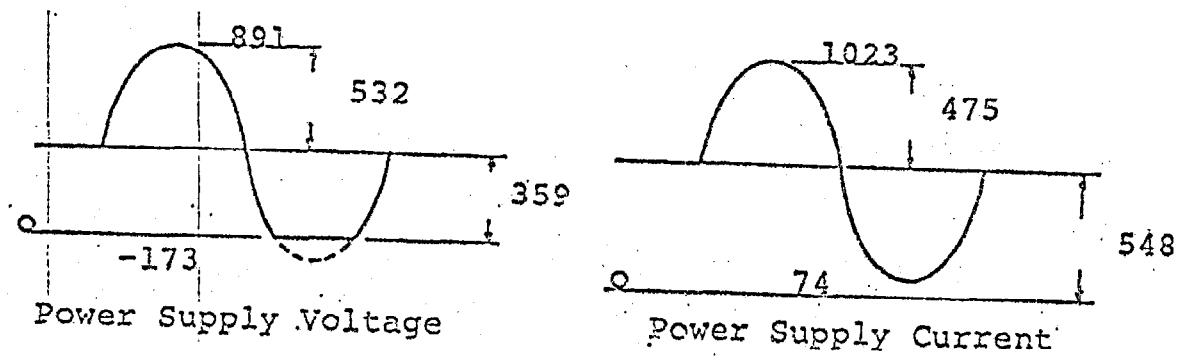


FIG. D-5

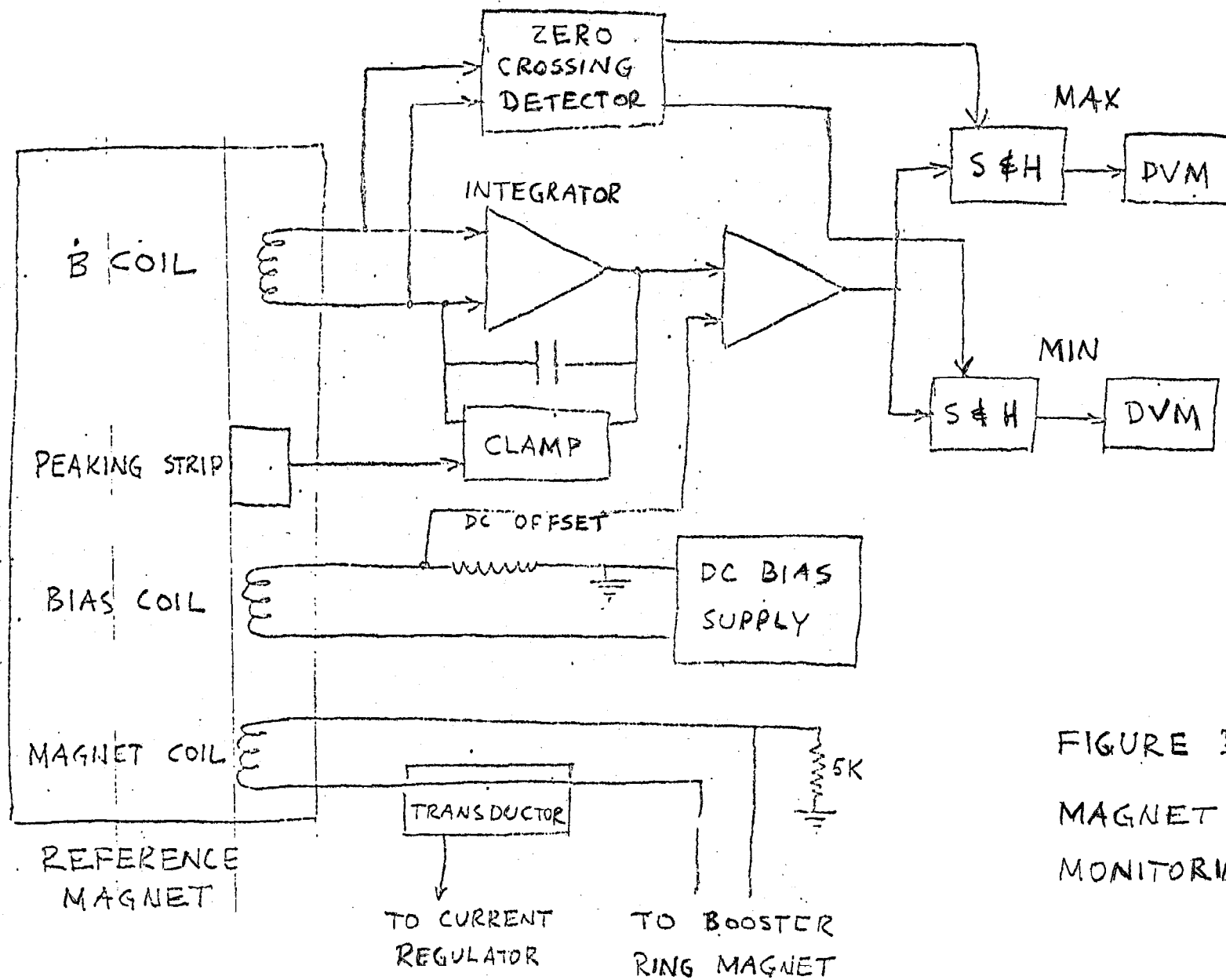


FIGURE D-6
MAGNET
MONITORING

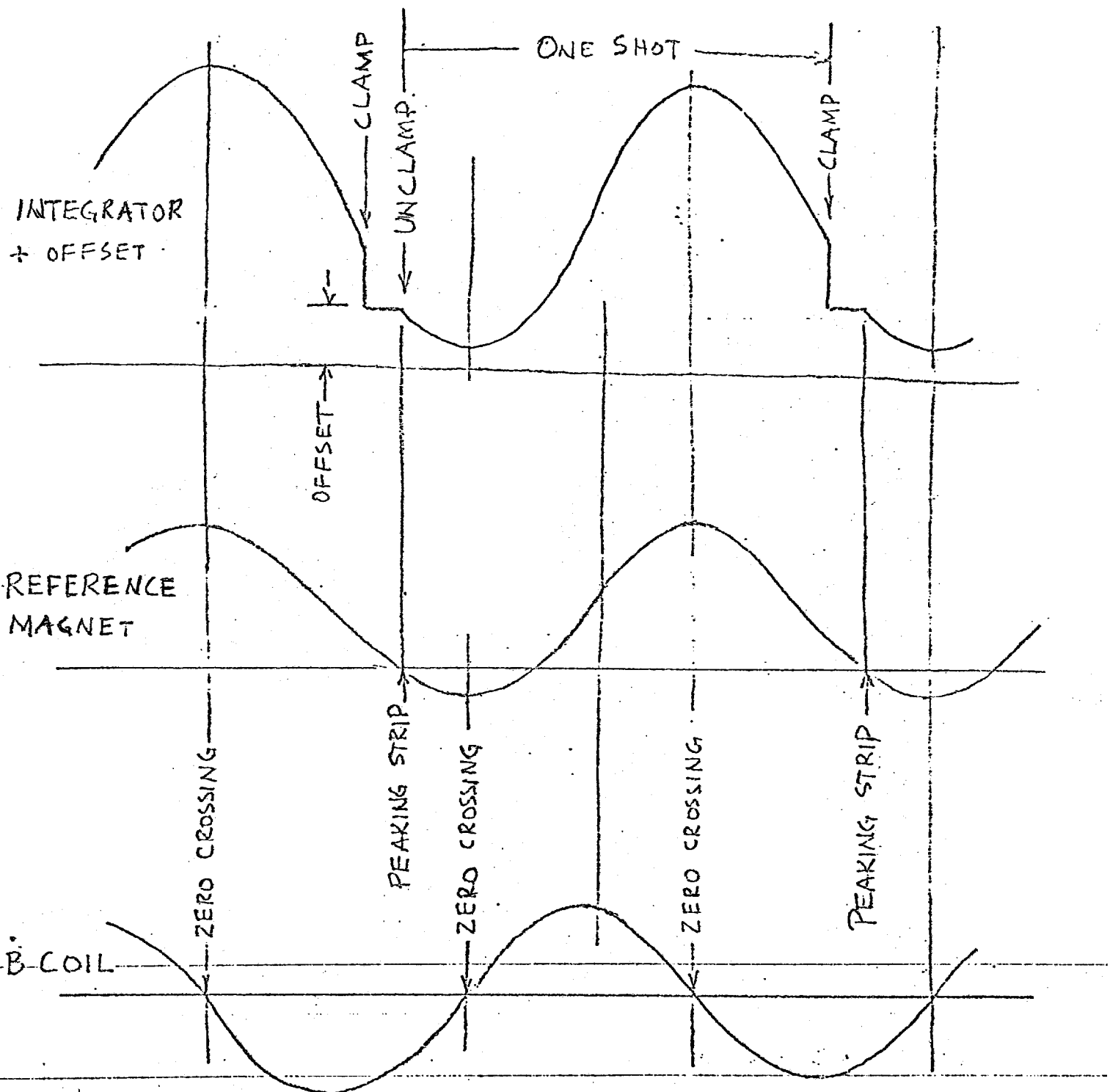


FIGURE D-7

MONITORING WAVEFORMS

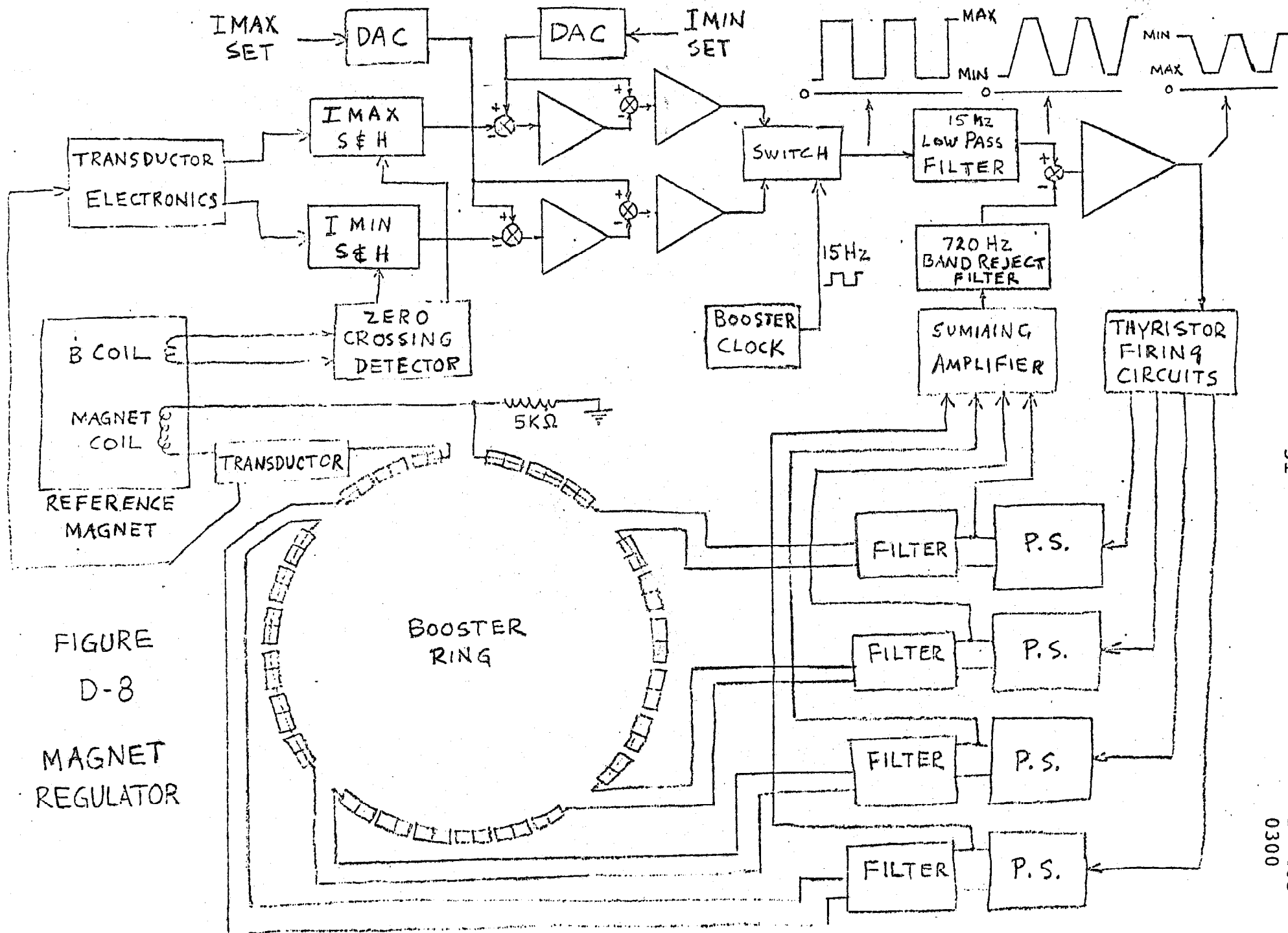


FIGURE
D-8
MAGNET
REGULATOR

E. Correction Magnets

1. Introduction

The errors in the magnet structure can be divided into two categories. These are dc errors, such as remanent field effects and stray fields which remain constant during the cycle, and ac errors which can be assumed to be proportional to the proton beam momentum. The second category results from variations in effective length, magnet tilts and misalignments, etc. The ac errors will be corrected by realignment of the magnets.

For closed-orbit corrections, tuning at injection, and suppression of horizontal-vertical coupling, a correction-magnet assembly consisting of a horizontal and a vertical dipole, a quadrupole, and a skew quadrupole is placed in each short and each long straight section. The correction elements provide dc compensation for the low-field errors. An air core design has been used in order to preserve the future possibility of pulsing them to higher field level.

2. Dipoles for Closed-Orbit Correction

The dipoles are designed to introduce a bend of 1.4 cm in 10 m (the distance separating successive trim magnets) at injection. This requires a bending length of 3000 gauss-cm. The dipoles are individually controlled. The low field closed orbit can be corrected with localized orbit displacements produced by dipoles in three successive mid-D straight sections or three successive mid-F straight sections. The currents in

the three correcting dipole magnets are set in the proper ratio to produce the localized orbit displacement by the control computer, and the amplitude of the bump is controlled by a single knob.

3. Quadrupoles for Tuning at Injection

The design requirement here is to provide for tune shifts of .6 at injection. This amount of shift can be obtained by a gradient of 8.9 g/cm ($\int B'dl = 220$ gauss) in the quadrupoles in the long straight sections and 5.6 g/cm ($\int B'dl = 138$ gauss) in the quadrupoles in the short straight sections.

For multiturn injection it is desirable to lower the radial tune as close as possible to the stopband at $\nu_x = 6.5$. There is a possibility of beam deterioration from space charge effects, since the vertical tune may be reduced below 6.5 at injection and the half integral stop band at $\nu_y = 6.5$ crossed later during the cycle. Therefore, removing the thirteenth azimuthal harmonic of gradient errors may become important. Separate control of all 48 trim quadrupoles provides the greatest flexibility in producing any harmonic and phase that might be desired.

4. Skew Quadrupoles

Twisting of the magnetic median plane, stray fields, and azimuthal fields lead to coupling of the horizontal and vertical oscillations. The coupled motion will be unstable if

$\nu_x + \nu_y = \text{integer}$ (sum resonance). As mentioned earlier, both the horizontal and the vertical tune may be in the vicinity of 6.5 at injection, in which case $\nu_x + \nu_y = 13$.

The horizontal field component which is present in a twisted magnet can be compensated for by skew quadrupoles so that there is no net horizontal field component present when averaged around the ring. It would require 24 skew quadrupoles (33 cm long) with a gradient of 2.4 g/cm to cancel the effect of all the F and D magnets being rotated 5 mrad assuming that the horizontal fields thus produced were in the same sense. This rather adverse situation is unlikely, of course, but it becomes somewhat impractical to construct quadrupoles with gradients much smaller than this. The thirteenth azimuthal harmonic should, in fact, be provided by the skew quadrupoles with variable phase to cancel this coupling resonance.

The difference resonance which occurs when $\nu_x = \nu_y$ does not produce an unstable orbit, but when there is magnet twist present, the vertical and horizontal oscillations will none the less be coupled. This has been observed to lead to some disturbing effects when trying to tune the beam at other installations. To correct this, the zeroth harmonic is all that is necessary in the skew quadrupoles.

5. Mechanical Design

Each correction magnet assembly consists of a horizontal dipole, a vertical dipole, a quadrupole, and a skew quadrupole.^{E1} The magnets are all air core. The coils for all four magnets are nested concentrically around a 4-1/2-inch beam pipe as shown in Figure E-1. The parameters for the correcting magnets are listed in Table E-1.

In manufacturing the magnets, oval-shaped coils of insulated wire were wound in flat layers. The layers were then rolled to the proper radius and bonded together with radiation-resistant epoxy. Individual coils (four for each quadrupole and two for each dipole) were mounted on the vacuum pipe after the pipe was installed in the tunnel and vacuum-tested. The coil assemblies are supported by brackets attached to the ring magnet support girders.

6. Power Supplies

A power supply for half the correcting magnets in the booster is located in each of the equipment galleries. The current to each individual magnet is controlled by a separate regulator. Thus the current in the magnets can be controlled individually, or the control computer can be used to control them in any grouping desired and maintain any desired ratio of currents between the magnets in a group.

7. Sextupoles

Sextupole-correcting magnets were not included in the original design. Recently, however, twelve air-core sextupole magnets of the type used in the main ring have been installed to eliminate beam losses which were observed to occur just before transition when the intensity is above 1.5×10^{11} particles/pulse.^{E2} A group of four sextupole magnets is located in each of three 6-m long straight sections, which are located symmetrically in the lattice. They are operated dc, and the maximum strength of each magnet is

$\int B'' dl = 9.15 \text{ kG/m}$. All twelve magnets can change the chromaticity $\rho = \frac{\Delta v_x/v}{\Delta p/p}$ by 1.4 at 200 MeV, but half this much is sufficient.

The sextupoles are all connected in series and are driven from a single dc power supply.

8. Higher-Order Corrections

Resonances of order ≥ 5 can generally be ignored. Fourth-order sum resonances could give trouble under certain conditions although no such resonance has been pinpointed to date in the existing machines as causing trouble. There is a fourth-order sum resonance right through the booster operating point. This would be driven by the 24th azimuthal harmonic error. The correction for such an effect would be obtained by octupole magnets. As has been the case at other installations, this and other nearby high-order resonances are not expected to appear with any serious consequences, however, there is space available in long straight sections should they be necessary.

References

- E1. R. Juhala, International Symposium on Magnet Technology, Brookhaven National Laboratory (1972).
- E2. E.L. Hubbard, R.E. Peters, and A.G. Ruggiero, 1973 Particle Accelerator Conf., San Francisco.

Table E-1
CORRECTING MAGNETS

Magnet	Inner Radius cm	Outer Radius cm	Wire Size	Turns/ Section	Total Resistance Ω	Current A	$\int B dl$ or $\int B' dl$
Quadrupole	5.87	6.22	18 RD	259	14.1	1.01	220 g
Skew Quadrupole	7.14	7.40	20 RD	118	11.1	.27a	24 g
Inner Dipole	7.62	10.0	13 SQ	496	4.03	3.24a	3000 g-cm
Outer Dipole	10.16	12.57	11 SQ	455	2.32	5.6 a	3000 g-cm
Sextupole	7.0				0.1	40	15 kG/m

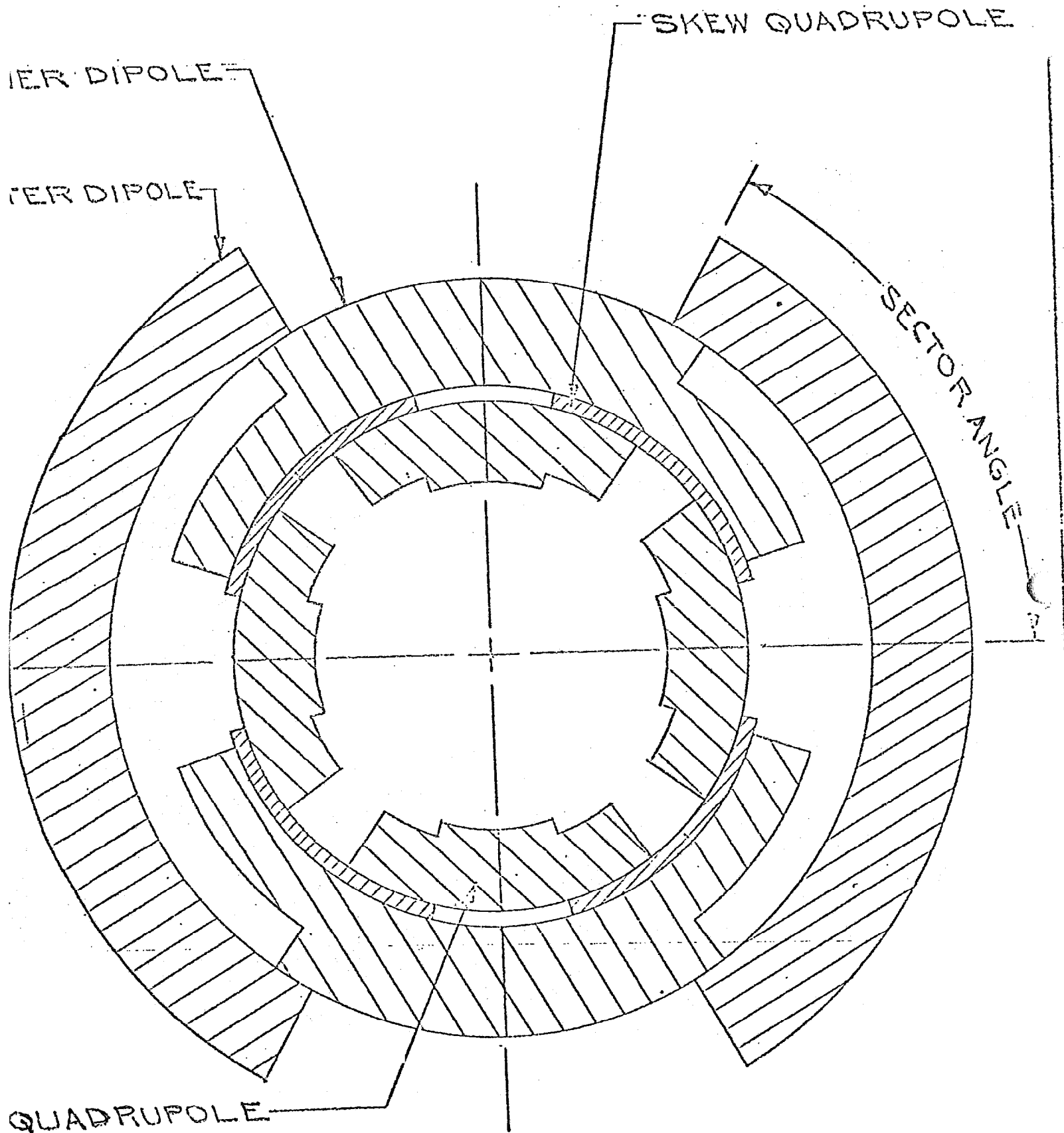


FIGURE E-1

Cross-sectional view of a typical assembly of four trim magnets.

F. Vacuum System

1. Introduction

Gas scattering should not be significant in the booster for pressures below 2×10^{-6} Torr, and there has been no difficulty in operating the booster at 10^{11} protons/pulse with pressures as high as 5×10^{-6} Torr at several places in the ring. However, sufficient pumping speed has been provided to reach 5×10^{-7} Torr in order to avoid coherent beam oscillation phenomena at high intensities. This pressure is reached by pumping each pair of magnets with a 600 l/sec sputter-ion pump. A 160 l/sec turbo-molecular pump is used to rough the four magnets in each period to 5×10^{-6} Torr before starting the ion pumps.

2. Magnet Vacuum Chamber

The magnets in the booster synchrotron are excited with a biased fifteen-cycle alternating current. If a continuous metal vacuum chamber were mounted in the magnet aperture, eddy currents would limit the wall thickness to about 0.005 inch. A metal chamber with walls this thin would require ribs or some other supporting mechanism to prevent it from collapsing. Ceramic vacuum chambers would have been very expensive and detracted considerably from the beam aperture. These considerations led to the design of a magnet that does not require a separate vacuum chamber.^{C2} Leaving out the internal vacuum chamber appreciably reduced the energy stored in the magnetic field and led to substantial savings in the cost of the plant and the resonant power supply system.

The coils and steel laminations for the H-frame booster magnets are enclosed inside a vacuum tight, stainless steel skin similar to the one used at Cornell.^{C1} At NAL, the entire assembly is bonded together into a single monolithic structure by vacuum impregnation of the magnet using the stainless steel skin as the impregnation "fixture." After impregnation, the edges of the laminations, the bonding epoxy, and the coils together form the effective walls of the vacuum chamber. The outer stainless envelope provides protection against leaks through the stack of laminations.

The interior surfaces of the magnets are painted with a conductive coating of graphite to remove any charged particles that might accumulate. After impregnation and painting, the magnets were outgassed by baking them under vacuum at about 150° F for nearly two weeks, before integrating them into the final vacuum system.

3. Vacuum Joints

As the system will be in the high radiation environment, welded joints have been used wherever possible. Sheet-metal disc type flanges which can be cut and rewelded several times are used at the magnet ends. A semi-automatic cutting tool has been developed for a quick, chip-free cutting operation of the flanges. The more frequently opened joints, such as on top of pumps and near gate valves, are of quick-disconnect type. Indium coated metal C-rings are used in all demountable joints close to the beam lines. However, for seals considerable distance away from

beam lines, and for initial temporary operation, polyurethane O-rings, which are interchangeable with the C-rings, are extensively used. Polyurethane is expected to withstand 10^9 rads before being damaged by radiation.

4. Vacuum Pumping System

The entire booster vacuum chamber is divided into eight sectors, separated by bellows-sealed gate valves. Any sector can be evacuated or let to air pressure independent of the rest of the booster ring.

The booster system is further subdivided into 24 periods, each consisting of 4 magnets mounted in pairs on two support girders. A schematic diagram of the vacuum system for one period is shown in Figure F-1. Each period is provided with one turbomolecular pump located in the space between the two girders. A sputter-ion pump is located centrally on each girder between the two magnets. Additional ion pumps are located in straight sections containing rf, injection, or extraction equipment.

High vacuum pumping is provided by the sputter-ion pumps which have a nominal pumping speed of 600 l/sec at the normal voltage of 4.75 kV. Half of the pump elements are differential elements with one tantalum cathode for stable pumping of inert gases. Each pump has an independent power supply capable of dual rated voltage operation at 4.75 kV and 8 kV. This feature permits enhancement of the pumping speed by about 30% at 1×10^{-6} Torr. A provision is made in the construction of the pump for insertion of a water-cooled sublimation pump at a later date for short-term enhancement of the pumping speed. However, this has not been necessary.

Intermediate stage pumping is accomplished by 160 l/sec Welch turbomolecular pumps. The system is pumped down from 200 μ to about 5×10^{-5} Torr with the turbos before starting the ion pumps. Besides intermediate pumping, the turbomolecular pumps also provide additional high-vacuum pumping when needed. The turbomolecular pumps can be isolated from the magnet vacuum system with 3" bellows-sealed gate valves when they are not in use. The turbo mount is designed to swing out for a quick removal of the pump to facilitate its maintenance in radiation environment. A 55° F LCW water facility in the booster is used to cool the turbos. All of the turbomolecular pumps in each sector are connected to a common 2-inch forevacuum line. The forevacuum line for each sector is connected to one of the four roughing stations located permanently at each corner of the two equipment galleries above the magnet enclosure.

Each roughing station consists of a 157-CFM Roots blower, backed by an 88-CFM oil-sealed rotary mechanical pump. The Roots blower is interlocked to start automatically when the system is pumped down to about 2 Torr by the mechanical pump. The roughing pumps up in the galleries can be connected either directly to the high vacuum chamber down in the tunnel by 3-inch diameter pipes or to the forelines. Dry N_2 is introduced through the roughing pipes to bleed up any sector of the magnet system or a sector of foreline. The system roughs a sector of the magnet system down to about 200 μ in approximately 15 minutes.

5. Performance Data

The booster vacuum system has been in operation with the entire accelerator under vacuum since December 20, 1970. After 1-1/2

months of operation, many sectors reached an average pressure of less than 1.2×10^{-6} Torr with 6 to 8×10^{-7} Torr in some regions. During the initial operation, various sectors of the vacuum system, inevitably, had to be let up to dry N_2 frequently to install or troubleshoot some machine components. After a year of operation, the average pressure around the ring was 5×10^{-7} Torr. The above-mentioned pressure has been obtained with the sputter-ion pump power supplies operating at a nominal 4.75 kV.

The pump-down time has considerably improved since the system was initially put into operation. After the system had been in operation for 1-1/2 months, any sector could be pumped down from atmosphere (after exposing to dry N_2 for 15 minutes) to a maximum operating pressure of 1×10^{-5} Torr in about 5 hours. A typical pump-down time of a sector is plotted in Figure 2. After a year of operation, a pressure of 5×10^{-6} Torr could be reached in 2 to 3 hours. It takes substantially longer if the system has been open for a day or more.

Reference

- F1. E.L. Hubbard, W.B. Hanson, and U. Patel, IEEE Trans. on Nuclear Sci., Vol. NS-18, No. 3, p. 654 (1971).

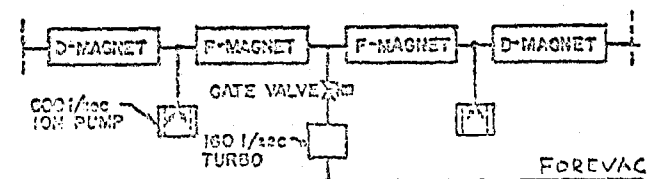


Fig. F-3 Booster vacuum module.

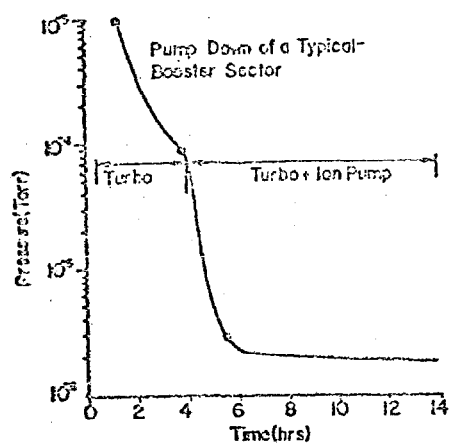


Figure F-2

G. Beam-Position Monitors

A beam-position monitor is located in each 6-inch long straight section and each 1.2 m straight section in the booster ring. The monitors are rectangular ferrite core transformers with windings on each of the sides as shown in Figure G-1. They have a frequency response of from 4 kHz to >100 MHz with a sensitivity of 100 $\mu\text{V}/\text{mA}$. The beam aperture in the cores in the 6-m long mid-D straight sections is 3 x 3 inches, and the aperture in the cores in the mid-F straight sections is 2 x 5 inches. Interaction between horizontal and vertical position measurements is negligible over the aperture of the booster. The low frequency response required to give good fidelity on coasting beam requires 10-turn windings. In order to achieve a flat response through 100 MHz, each winding is bifilar and center tapped to give a balanced system. Currents through opposite pairs of windings are monitored both in phase and differentially as shown in Figure G-2 to provide a SUM output, a horizontal difference output, and a vertical difference output. The detectors are mounted inside the vacuum chamber, and the signals are brought through vacuum-tight feedthrough insulators.

Each output is connected with a relay to one of three cables which run around the ring and up to the gallery to amplifiers. Any output signal can be selected by closing its relay and monitored with an amplifier to provide video information. The beam-position transformers can also be used with the detector circuit shown in Figure G-3 which provides dc voltages proportional to sum, vertical difference, and horizontal difference. This system looks at a gap in the beam and thus operates at the revolution frequency of the

booster. The dc signals are digitized and read by the control computer. In the computer, the difference signals are normalized by dividing them by the sum signal in order to give position data which is independent of the beam current. The calibration of the normalized position outputs is given in Table G-I. The computer can automatically select each detector in sequence and display the position of the closed orbit vs. the location in the ring.

Table G-I

CALIBRATION OF NORMALIZED POSITION SIGNALS

	<u>ΔV</u>	<u>ΔH</u>	<u>Aperture (in. x in.)</u>
6m Long St.	32% Sum/in.	28% Sum/in.	3 x 3
1.2m Short St.	30% Sum/in.	23% Sum/in.	2 x 5

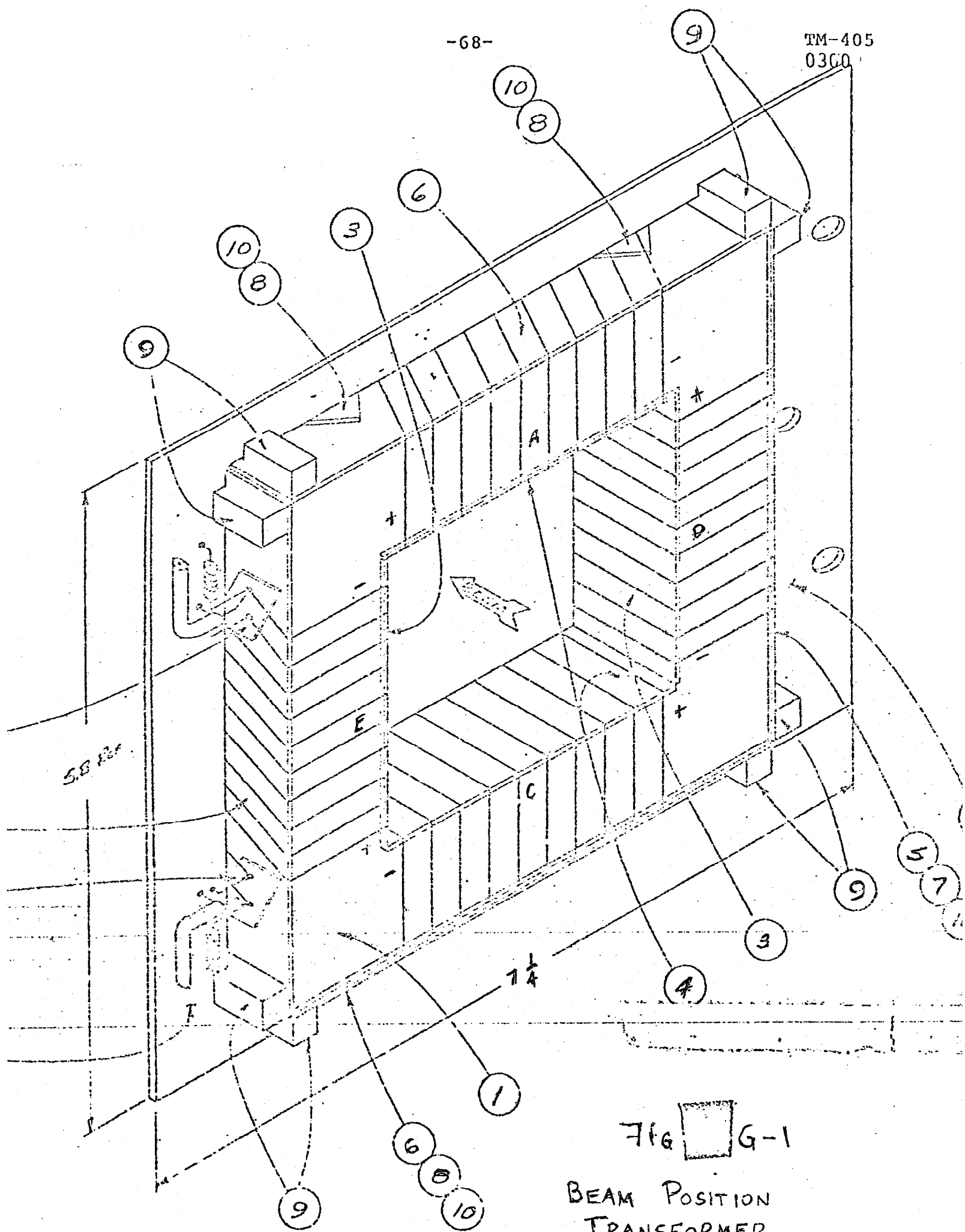
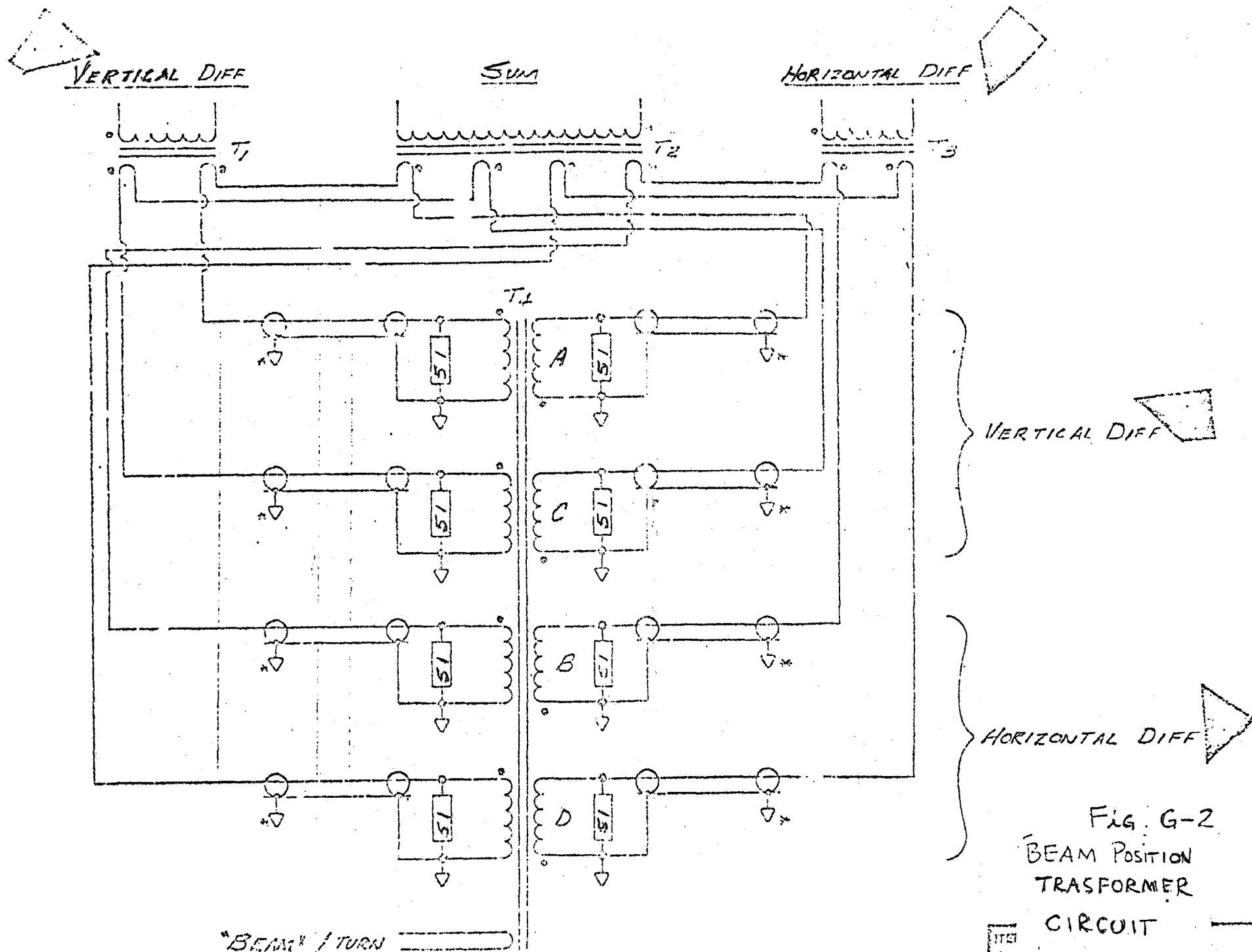


Fig. G-1

BEAM POSITION
TRANSFORMER



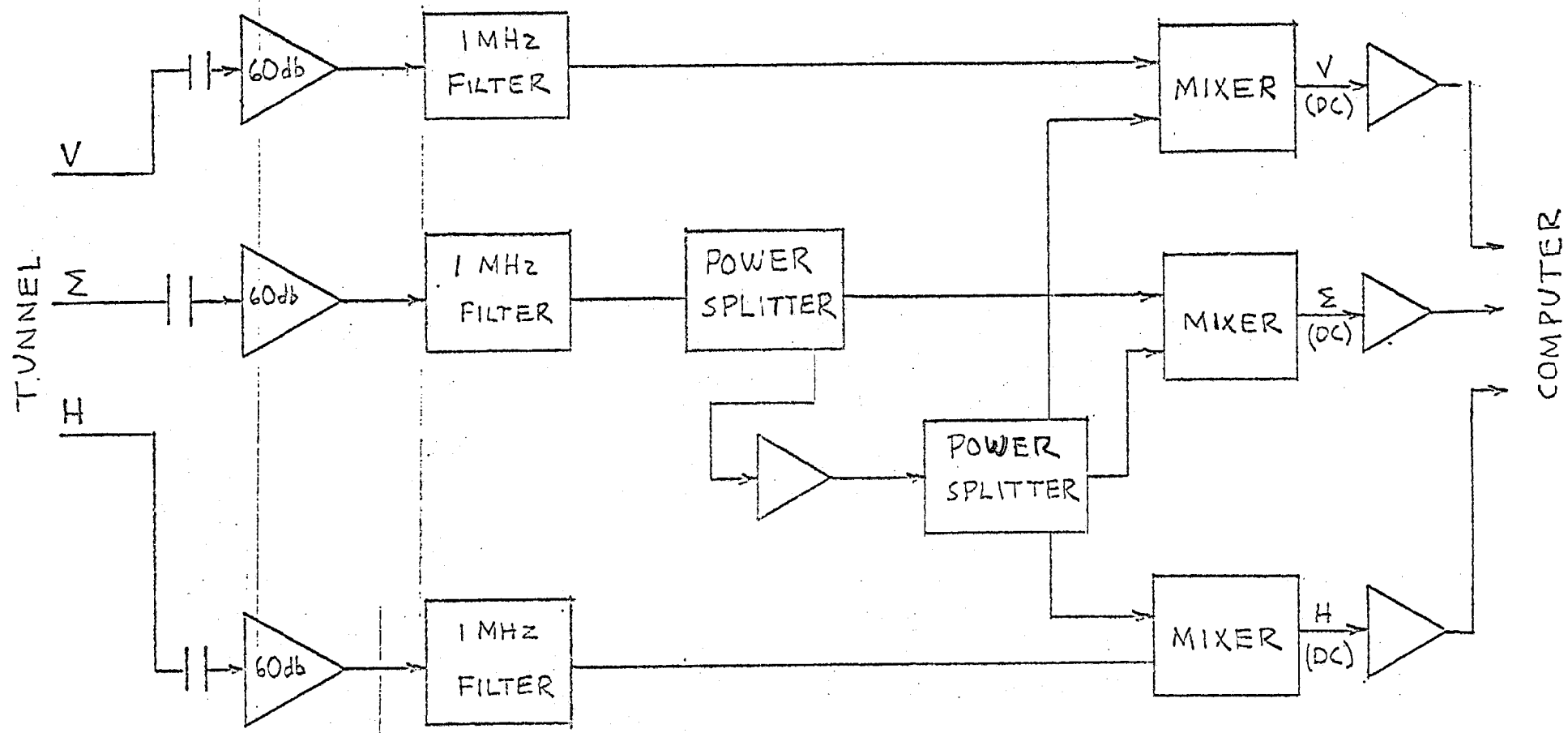


FIGURE G-3 BEAM POSITION MONITOR ELECTRONICS

H. Radio-Frequency Acceleration System

1. Introduction

The proton beam in the booster synchrotron is accelerated by 16 ferrite-tuned cavity resonators. Each cavity is driven by a 100 kW rf power amplifier which receives its dc power from a series tube modulator. Figure H-1 is a schematic diagram showing the major components of the acceleration system. The major parameters of the system are listed in Table H-I.

The 16 cavities are grouped in pairs. Each pair is mounted on a girder in one of the 6-m long straight sections in the booster magnet lattice as shown in Fig. A-1. The rf power amplifiers and the ferrite tuners are mounted on the rf cavities in the tunnel. The low level rf components, the tuner bias supplies, the modulators for the power amplifiers, and the control circuits are located in the equipment galleries above. The 25-kV dc power supplies for the anodes of the rf power tubes are located outdoors in the utility yards.

The final frequency at 8 GeV is approximately 52.8 MHz and is precisely matched to the rf frequency of the main synchrotron in order to permit synchronous transfer of the booster beam bunches into the main ring rf buckets. This final frequency is the 84th harmonic of the revolution frequency of the 8-GeV beam around the 75.5-m radius booster ring. The frequency at injection into the booster, when $v/c = 0.57$, is 30.3 MHz. During acceleration, the frequency must follow the change in velocity of the protons. An approximate rf frequency program is generated by a function generator.

Corrections to the frequency program are made by a slow feedback loop which keeps the beam at the correct radial position in the aperture and by a fast feedback loop which damps the phase oscillations. As the rf frequency changes, the cavities are tuned to resonance by varying the current in bus bars which link ferrite rings in the tuners.

The rf voltage program during the acceleration cycle of the booster has two phases. The first is the beam capture phase. The 200-MeV beam from the linac debunches completely in approximately one revolution. Adiabatic capture of the beam is then accomplished by turning on the voltage in 16 steps, one for each cavity. In about 150 μ sec, the voltage steps from zero to a final value of 100 kV per turn. At the end of this phase, the beam has been captured with negligible dilution in a stable phase area ("bucket") whose momentum width is about twice that of the beam from the linac.^{H1} The reason for a stepwise turn-on rather than a linear rf rise is that the rapid step rise crosses the multipactoring voltage range of the cavity quickly, preventing the buildup of a secondary electron cascade.

The second is the acceleration phase of the voltage program. This phase lasts 33 msec (1/30 second). Under conditions of constant bucket area and sinusoidal energy gain variation, the necessary voltage rises to a maximum of 810 kV per turn just before the middle of the acceleration period and drops monotonically to a lower value at the end. The time variations of the voltage and other acceleration parameters are shown in Figure H-2. The voltage program is

based on an injected momentum spread $\Delta p/p$ from the linac of $\pm 0.8 \times 10^{-3}$. (During the present operation the momentum spread is not this small. Therefore, some improvement in beam can be expected if, for example, a linac beam debuncher were operating.)

At design intensity, the average beam current at 8 GeV is 0.39 A, corresponding to 3.8×10^{12} protons circulating in the booster. To minimize phase and amplitude fluctuations of the cavity accelerating fields under beam loading, a wide-band feedback loop is planned.^{H2} This feedback loop is not installed at the present time.

2. RF Cavities

Figure H-3 is a cut-away drawing of a booster rf cavity with a power amplifier and three ferrite tuners mounted on it. The cavity contains a drift tube whose electrical length is 140° . There is an accelerating gap at each end. The drift tube is a tapered copper structure with a 2-1/4" i.d. beam pipe in the center. An alumina insulator near each end of the drift tube provides a vacuum-tight rf window. Only the beam pipe inside the drift tube and the accelerating gaps at the ends of the cavity are under vacuum. The central part of the cavity and the tuners are at atmospheric pressure. The rf parameters of the cavities are listed in Table H-II, and the power requirements at various times in the cycle are shown in Figure H-4.

3. Ferrite Tuners

Three tuners are attached to each cavity. The tuners are coaxial transmission line structures with shorted ends. The

center conductor of each tuner is connected to the center of the drift tube in the accelerating cavity, and the tuners are part of the resonating structure. There are 28 toroidal ferrite cores mounted in the rf field between the inner and outer conductor of the tuner.^{H3} Ten-turn bias windings (not shown in Figure H-3) pass through the center conductor of each tuner and link the ferrite cores. The reactance of the tuners and, consequently, the resonant frequency of the cavity structure are controlled by varying the current through the bias windings. The relationship between the bias current and the resonant frequency is shown in Figure H-5. Other parameters of the tuners are listed in Table H-II.

The tuner bias current for each cavity is supplied by a thyristor rectifier circuit. A computer controlled core memory curve generator produces two waveforms for controlling the thyristor firing and a shunt transistor bank regulator.^{H4} Each waveform is used to program the resonant frequency of eight of the cavities. Differences between individual cavities and differences between the programmed resonant frequency and the rf drive frequency are corrected by a feedback loop for each cavity which strives to minimize the phase difference between the rf drive and the cavity fields.

4. RF Power Amplifiers

The 100-kW rf power amplifier is mounted on top the cavity resonator as shown in Figure H-3. The anode circuit of the 100-kW power tube is an integral part of the resonant structure. The rf connection from the anode of the PA to the drift tube in the cavity was made through twelve 250 pF 30-kV blocking capacitors. Heating

caused by parasitic modes in the array of 12 blocking capacitors limited the booster operation to an average rate of 1 cycle/sec. In order to operate the booster for 13 cycles every main-ring cycle, these blocking capacitors have been replaced with a single 1000 pF, distributed blocking capacitor with alumina dielectric. The B^+ lead comes through the field-free region inside the inner conductor of a tuner and up through the inside of the drift tube to the anode of the power tube. A cross-section of the amplifier is shown in Figure H-6.

The 100-kW rf output is achieved with a cascode power stage using an Eimac Y567 (4CW100,000E) tetrode.^{H5} The driver section of the cascode stage consists of 14 Eimac 4CW800F tetrodes connected **in parallel**. To provide a suitable frequency response in the range from 30 to 53 MHz, a lossy powdered iron inductor has been inserted between the two halves of the cascode stage. The 2-watt input to the power amplifier is amplified to 100 watts by a 6-tube distributed amplifier which drives the cascode stage. The gain of the power amplifier is flat over the operating band from 30 to 53 MHz.

Since the accelerating voltage and the cavity input impedance vary over the booster cycle, the power output of the amplifier is programmed. The anode voltage of the output power tube in each amplifier is controlled by a 25-kV series tube modulator using a Y567. The rf current gain of the cascode stage is varied by modulating the current through the 14 cascode driver tubes. A waveform for all the dc anode voltages and a waveform for the cascode bias of all the amplifiers are generated by the core memory curve generator.

Two 30-kV rectifiers operating directly off the 13.8 kV power line supply the dc voltage to the modulators. Each rectifier unit supplies 8 modulators.

5. Booster Low-Level RF System

The low-level rf system (LLRF) provides the correct phase relation between the circulating beam bunches and the accelerating cavity gap voltage. This phase angle is continuously adjusted to maintain the required rate of energy gain. The frequency program to achieve this is shown in Figure H-7.

The 2-watt signal from the low-level system has a constant amplitude throughout the cycle. It is split two ways, one signal going to the West Gallery and one signal to the East Gallery. There the signals are each split eight ways and then amplified to provide 2 watts of drive for each of the 16 power amplifiers in the tunnel. The fan-out system provides the proper phase shift between the low-level system and each of the power amplifiers.

In the LLRF, the frequency source is a voltage controlled oscillator (VCO). It is programmed to an approximation of the ideal frequency with a digital waveform generator--Figure H-8. Values of f and the times at which they start are stored in a digital memory. When the memory cycle is initiated, the values are read out at the appropriate times and converted to a voltage level to form an approximation to the f curve of Figure H-9. This curve is integrated by a precision integrator in which the initial condition or starting frequency (f_0) is set through the digital control system. The integrator remains clamped except during the acceleration cycle when it provides the appropriate

bias to the VCO to generate a first-order approximation of the desired frequency. A second input to the VCO permits fine tuning of the frequency by the beam feedback loops.

A second frequency program generated by the VCO sweeps 10 MHz above the frequency used for acceleration. It is used as the "local oscillator" in both radial and phase-measuring systems which employ the superheterodyne principle to maintain the high signal-to-noise ratio inherent in a swept narrow band detector. Both output channels are amplified to produce an output of 2W \pm 1dB into 50 ohms.

Two coaxial beam current transformers are used to measure the beam-cavity phase. These transformers use ten Ceramic Magnetics NM-60 ferrite rings to achieve a bandwidth of 4 kHz to 300 MHz and a sensitivity of 4 mV/mA.

The position transformers used for beam steering are a ferrite picture frame configuration with one coaxial turn on each side. Currents through both turns are compared both in phase and differentially with commercial current transformers to provide signals proportional to current and current times position on 50 Ω output. The beam current output (Σ) has a sensitivity of 5 mV/mA and the differential output (Δ) is 10% of the sum per cm. The output is independent of vertical position over the useful aperture of the machine.

In the phase-measuring system both the rf signal representing the gap voltage and the output from the beam current transformers are mixed with the 40-63 MHz "local oscillator" output from the

VCO to produce two 10 MHz outputs which have amplitudes proportional to the swept inputs and maintain the same phase relationship as their swept counterparts. Both voltages are limited to provide constant amplitude signals whose phase difference is proportional to the beam-cavity phase. A dc voltage proportional to this phase difference is produced by a conventional 4-diode phase detector. The system provides a linear measure of phase from 0 to π to within $\pm 2^\circ$ and is insensitive to beam current changes.

The measurement of radial position requires the accurate measurements of the rf voltages from the position transformer and the normalization of those measurements. Signal detection is carried out in much the same way as in the phase measurement with only a few variations (see Figure H-10). As before, both swept inputs (Σ and Δ) are converted to 10 MHz signals. The Σ is split into two channels, one of which is limited to serve as a reference which drives two 4-diode mixers as synchronous detectors. This configuration provides linear and polarity-sensitive detection for the Σ and Δ inputs. An implicit analog divider provides the required $V_{\Delta x} = \Delta/\Sigma$. The system has a sensitivity of 1 V/cm and provides reliable information to better than 1 mm. Position read-out remains independent of intensity over a 30-1 range of beam current. Sensitivity is reduced at higher currents by means of external attenuators.

In the beam-control system, only one dc coupled loop is used--radial position (see Figure H-11). A high-pass filter with a cutoff of 300 Hz in the phase loop removes the dc component of ϕ_s .

This is done to make the position independent of cavity voltage except for variations within the passband of the phase loop. In this form the loop serves to damp coherent phase motion (even through transition). The dc component of ϕ_s is established by radial feedback only. The beam can be steered during the acceleration cycle by comparing the position voltage to that of a model produced by the digital, stored-program waveform generator. The error between actual position and the model shifts the frequency to bring ϕ_s to the value required to maintain the desired radius. Loop gains are programmed throughout the acceleration cycle by the stored-program function generator. The sign of the radial position error is changed at transition.

6. Synchronization with the Main Ring

When the beam is transferred from the booster to the main ring, the rf beam bunches from the booster are captured in empty stationary rf buckets in the main ring.^{H6} To synchronize the two rf systems, the main ring rf signal is transmitted to the phase lock unit in the booster low-level rf system. The phase lock circuit monitors the instantaneous phase difference between the main ring rf signal and the rf beam bunches in the booster. The booster frequency program is tuned to make the booster frequency equal to the main ring frequency about 1 msec before extraction.

As the booster frequency approaches the main ring frequency, the gain of the booster radial position feedback loop is programmed to 0, and the phase lock circuit is enabled. The phase-lock circuit

generates a model signal whose initial value is proportional to the phase difference at the time phase lock is initiated. Before transfer, the model signal decays to 0 in a predetermined way. The difference between the model signal and the actual phase difference provides an error signal which is used to reduce the phase difference to 0 by adjusting the booster frequency. This process produces a constant relative phase difference between the booster beam and the main ring buckets from cycle to cycle of the booster. A phase shifter in the line from the main ring to the booster is adjusted to center the beam bunches in the main ring buckets.

The main ring rf frequency is fixed at 52.813 MHz while successive batches of beam from the booster are transferred to the main ring. The revolution frequency of the beam circulating in the main ring must be equal to the rf frequency divided by 1113 to keep the beam centered in the stationary rf buckets. The correct revolution frequency is maintained by feeding a signal from the main ring radial position detector back to the main ring magnet regulator and trimming the magnetic field to hold the correct radial position.

The longitudinal phase space is matched with a main ring rf voltage of 1500 kV and a booster rf voltage at transfer of 305 kV.^{H7} However, with the booster rf voltage this low, beam is sometimes lost from the buckets during the phase locking process, and the system is usually operated with higher rf voltages in the booster at extraction.

Transfer of the beam from successive 15-Hz booster cycles must be timed in such a way that the beam is stacked end to end around the circumference of the main ring. During the stacking process, the beam circulating in the main ring is held in stationary rf buckets. To keep track of the beam injected into the main ring on previous cycles, a marker pulse is generated every 1113 cycles of the main ring rf accelerating voltage. This pulse marks the time of successive revolutions of the beam circulating around the main ring since 1113 is the harmonic number of the main ring.

The booster extraction system and the main ring injection system are triggered by the first revolution marker pulse after a pulse from the booster timing system indicates that the booster beam has reached the extraction energy. Thus, the booster extraction time jitters from cycle to cycle by up to 21 μ sec, the time of one revolution of the beam around the main ring.

After each transfer of beam to the main ring, the marker is delayed 1.6 μ sec, the time of one revolution around the booster. Thus, injection of beam from the next booster cycle starts just after beam from the previous cycle passes through the main ring inflector. Since the main ring rf voltage is turned on before transfer of the first booster batch, the revolution marker initiates the transfer of the first batch in the same way as the later ones.

References

- H1. J.A. MacLachlan, NAL Report TM-303 (1971).
- H2. Q.A. Kerns and W.S. Flood, IEEE Transactions on Nuclear Science, Vol. NS-12, No. 3, p. 58 (1965).
- H3. Q.A. Kerns and B.R. Sandburg, IEEE Transactions on Nuclear Science, Vol. NS-18, No. 3, p. 244 (1971).
- H4. M. Birk, R. Ducar, Q. Kerns, and G. Tool, IEEE Trans. on Nuclear Science, Vol. NS-18, No. 3, p. 427 (1971).
- H5. Q.A. Kerns and H.W. Miller, IEEE Transactions on Nuclear Science, Vol. NS-18, No. 3, p. 246 (1971).
- H6. J.A. Dinkel, J.E. Griffin, E.L. Hubbard, R.E. Peters, and L.C. Teng, Proc. 1973 Particle Accelerator Conf., San Francisco.
- H7. L.C. Teng, NAL Report TM-281 (1971).

Table H-I

PARAMETERS OF INJECTOR-SYNCHROTRON ACCELERATING STRUCTURE

Total Number of Cavities	16
Cavity Length	2.4 m
Total Length of Accelerating Structure	38.4 m
Total Peak Power Delivered to Beam	265 kW
Total Peak Ferrite Losses	830 kW
Total Weight of Ferrite	6,720 lb.
Injection Frequency	30.067 MHz
Ejection Frequency	52.812 MHz
Harmonic Number h	84 (1113 in Main Ring)

Table H-II

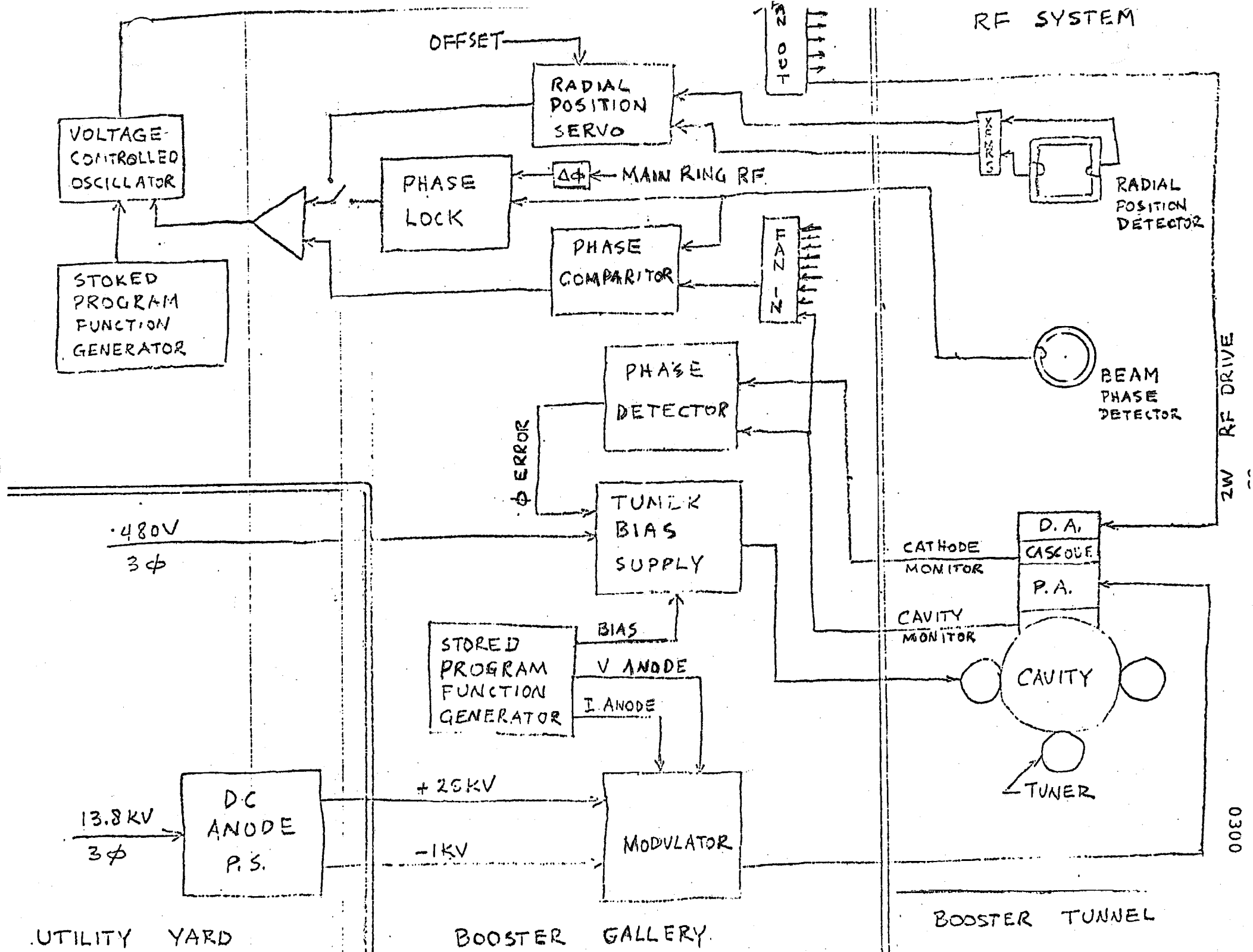
INDIVIDUAL INJECTOR-SYNCHROTRON CAVITY PARAMETERS

Ferrite Tuners--Total for 3 tuners/cavity

Ferrite Density	5 gm/cm ³
Ferrite Weight for 3 tuners	420 lbs.
Weight of 1 Tuner, complete	590 lbs.
Resistance of Bias Circuit at dc, 23°C	3.8 milliohms at cavity
Maximum H	30 kA/m
Minimum H	4.5 kA/m
Ferrite μ_{Δ} Injection	7.2
Ferrite μ_{Δ} Ejection	1.5

RF Parameters

Cavity Peak Voltage (across 2 gaps/cavity)	54 kV
Axial Field Strength in Gap	0.36 mV/m
Cavity RF Current (at current maximum)	1300 A
Cavity Z_0 (tapers from 80 Ω at a gap to 20 Ω at center)	60 Ω
H_{rf} (at location of ferrite)	850 A/m
RF Stored Energy/Cavity at Maximum Voltage	0.03 J



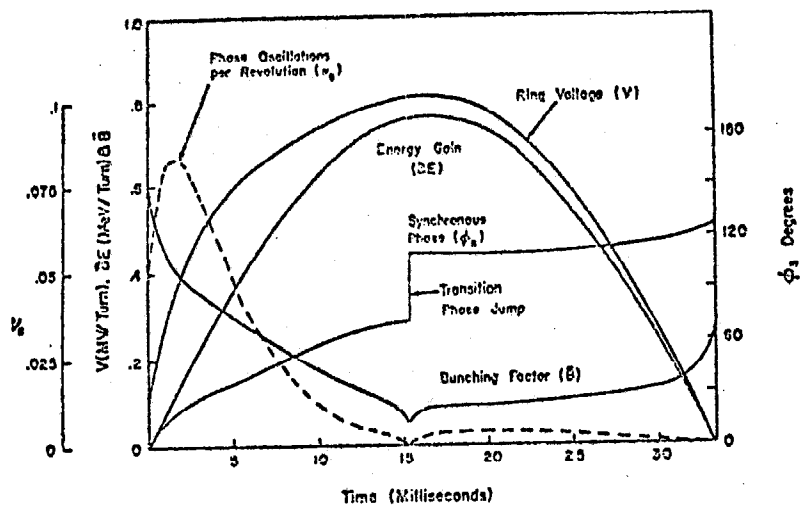


Figure H-2 Booster-Synchrotron RF Acceleration Parameters

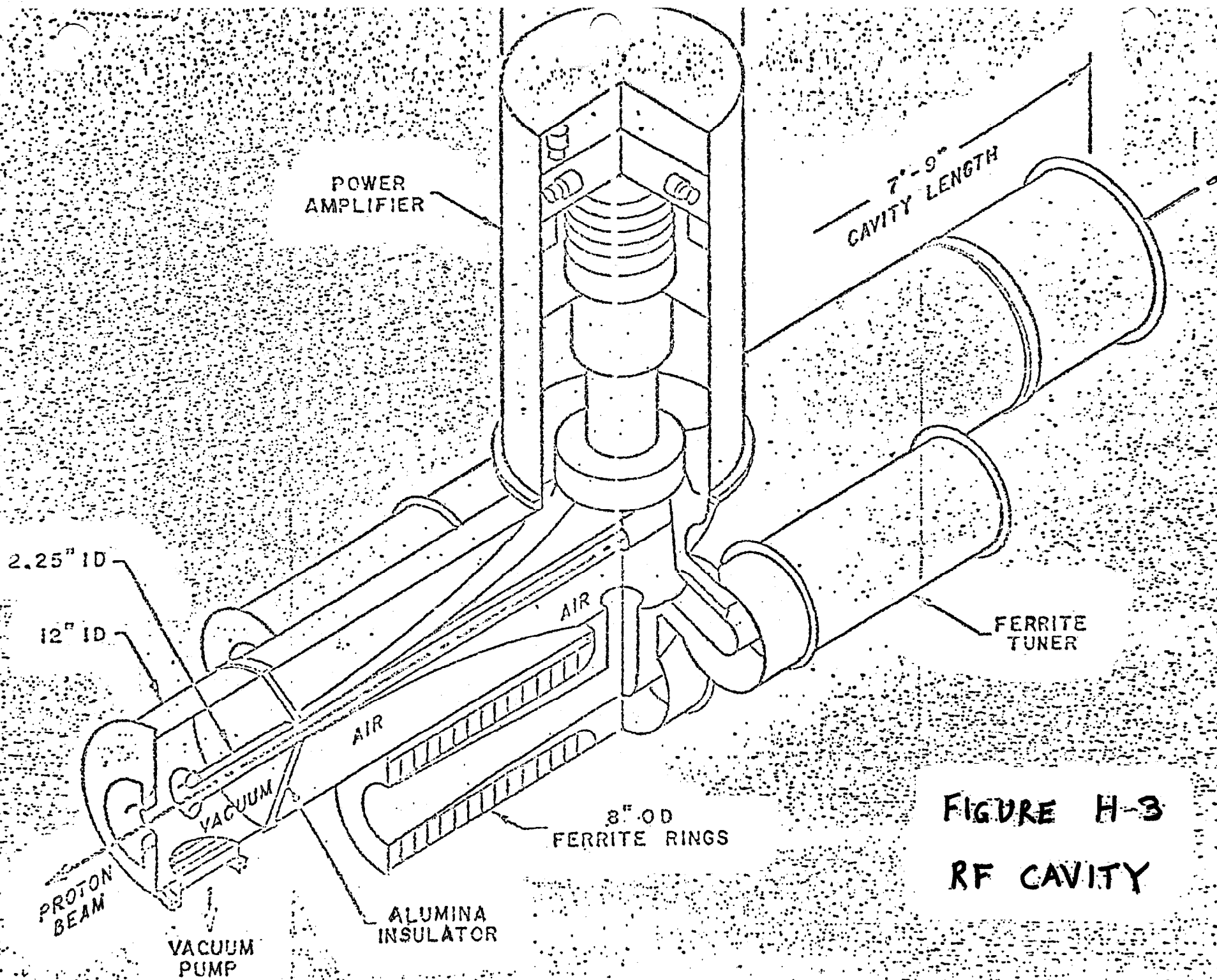


FIGURE H-3
RF CAVITY

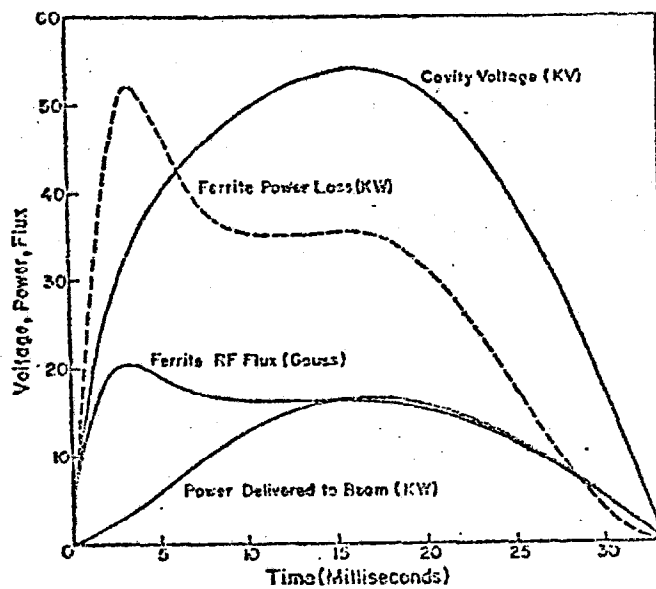


Figure H-4 Booster-Synchrotron RF Power
(For One Module)

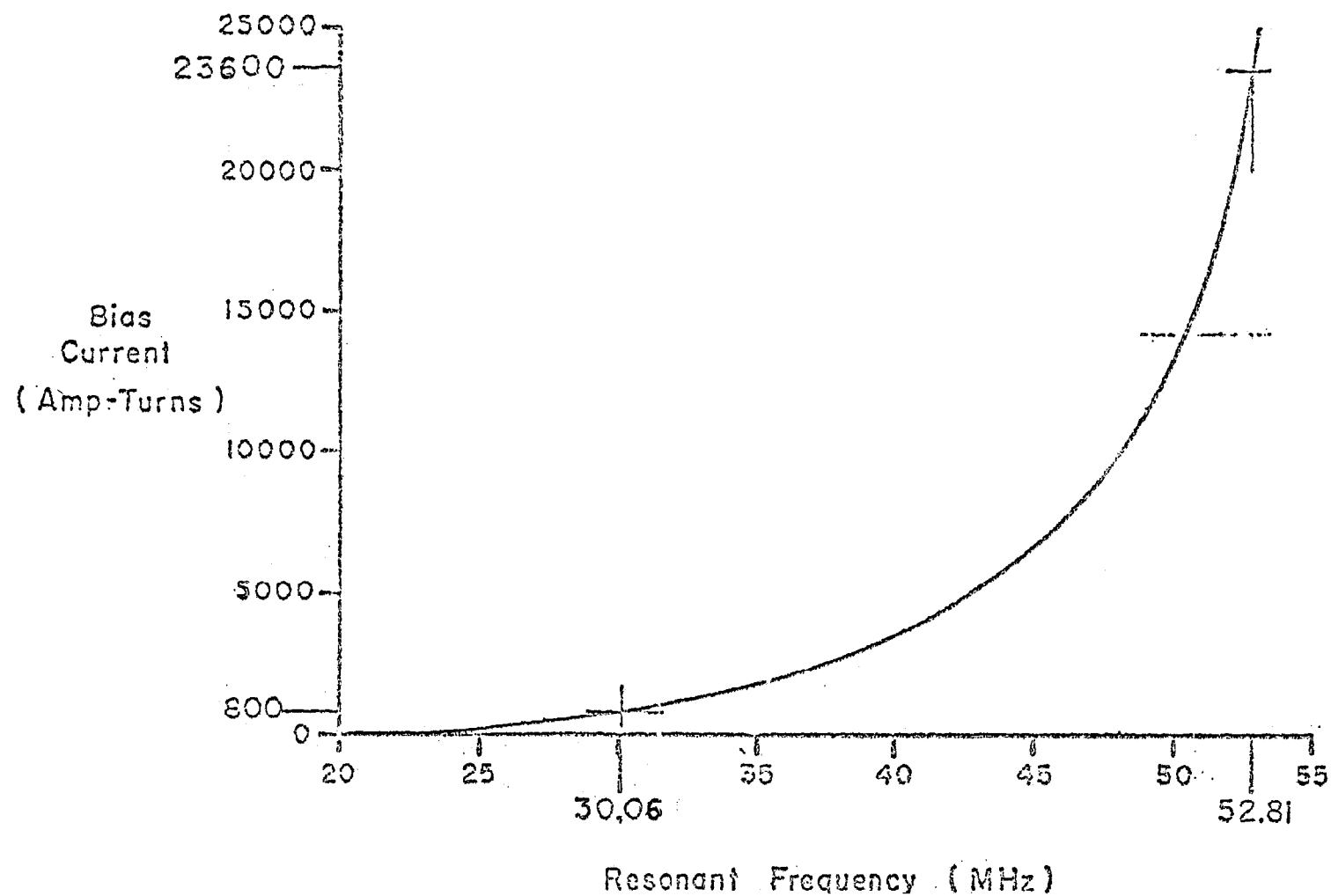


Fig. H-5

BOOST. CAVITY TUNING CHARACTERISTIC

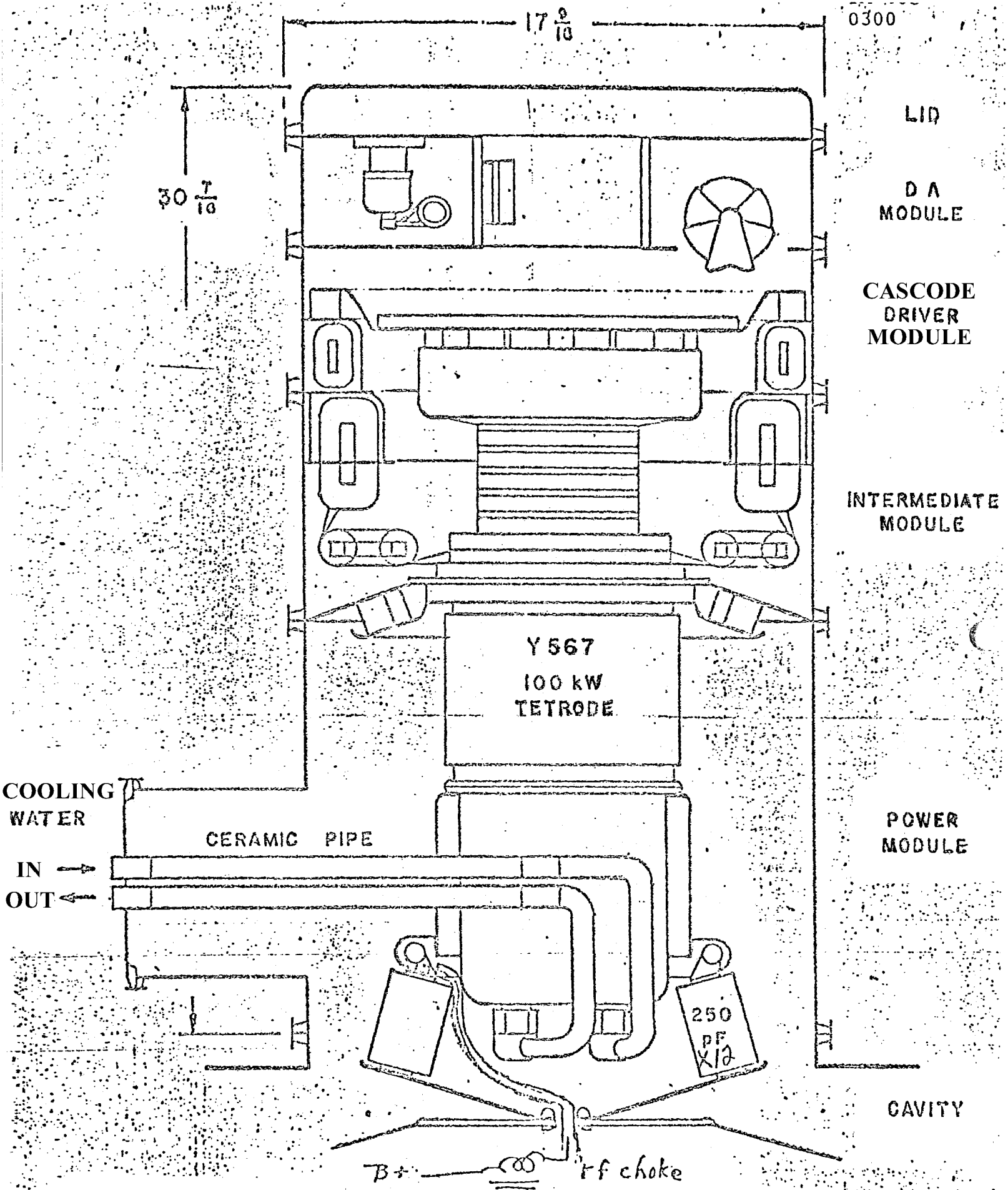


FIG. H-6 CASCODE POWER AMPLIFIER

BOOSTER RF FREQUENCY (MHZ)

30

35

40

45

50

55

TIME (MSEC)

0

5

10

15

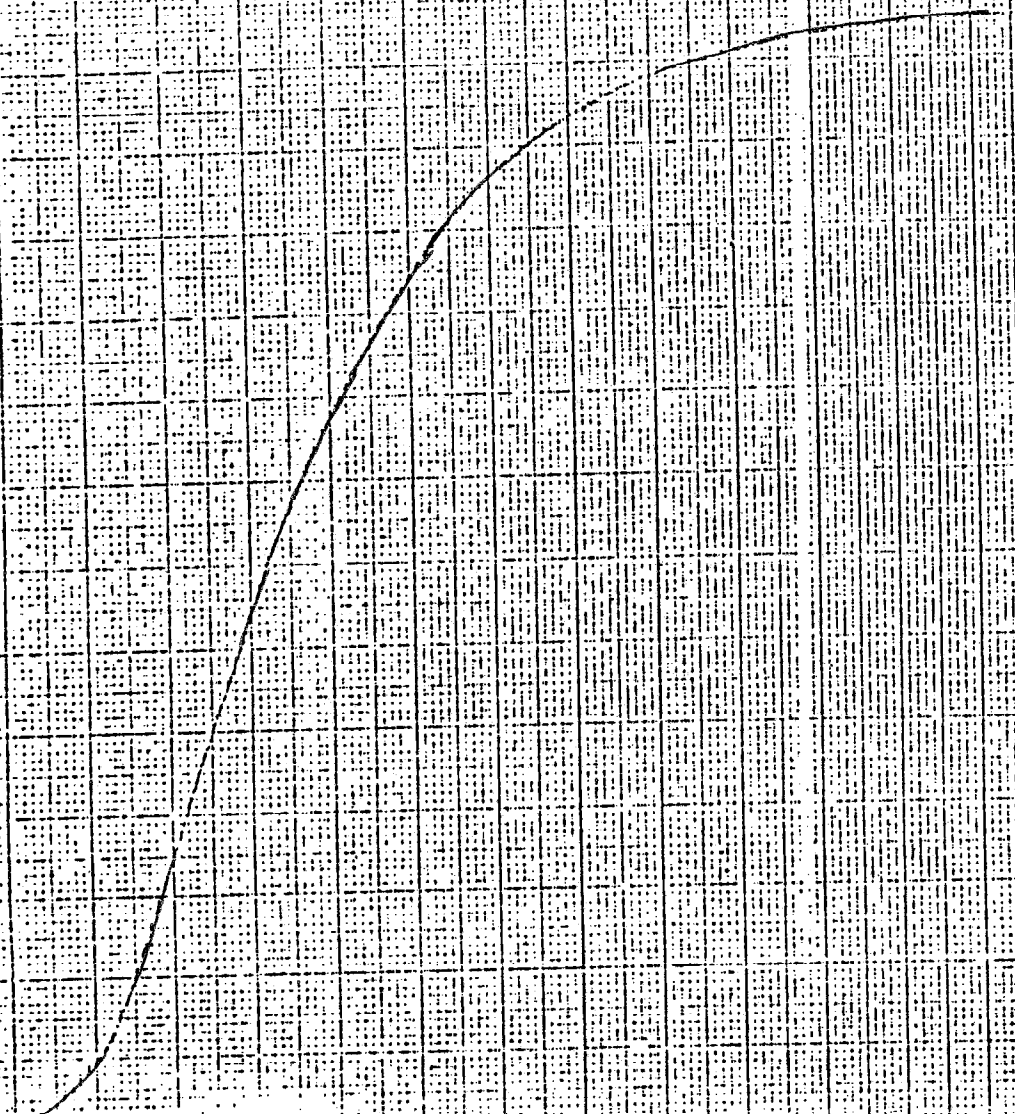
20

25

30

35

FIG H-7



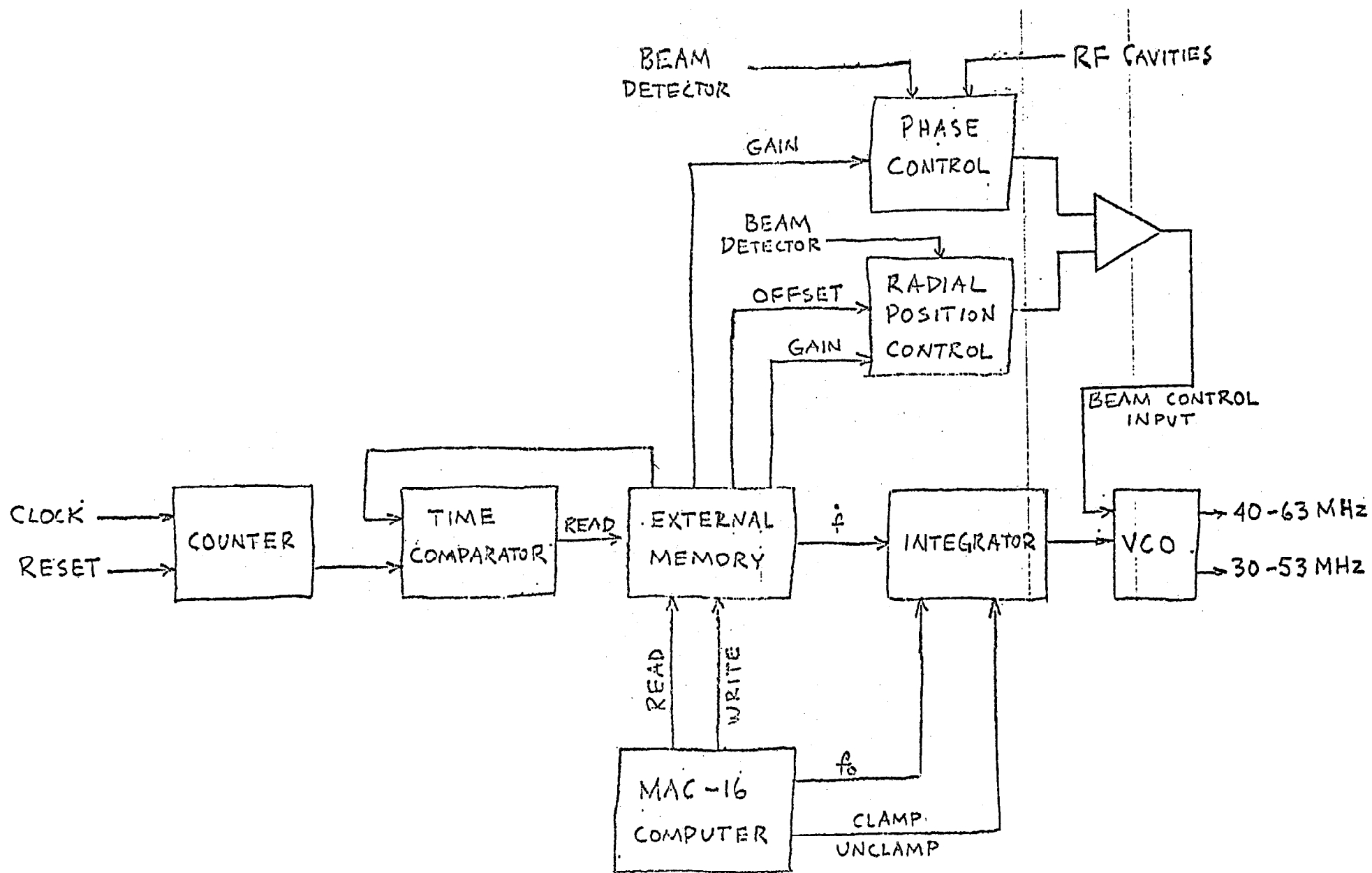
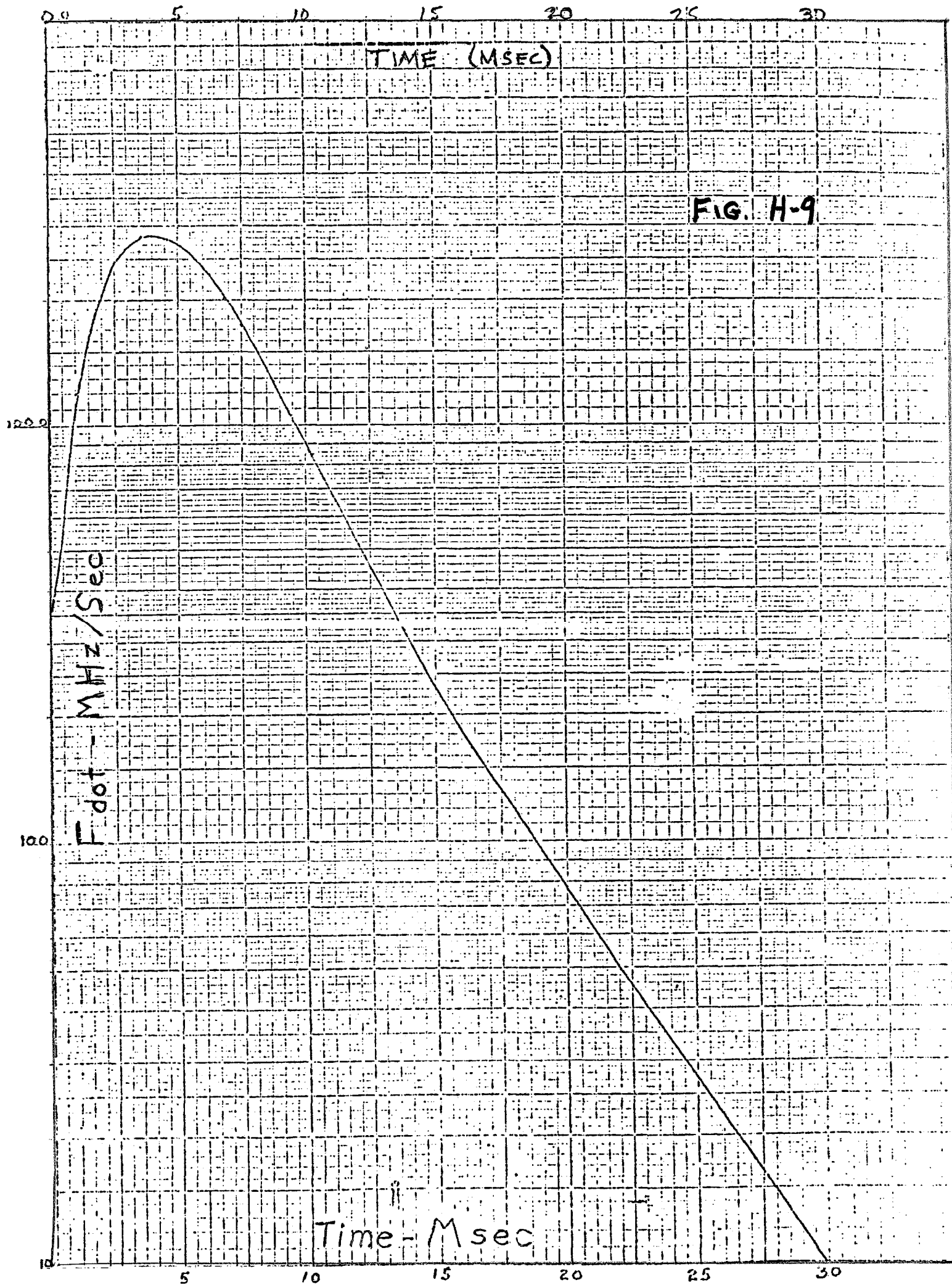


FIGURE H-8

STORED - PROGRAM WAVEFORM GENERATOR,

FOR

BOOSTER LOW LEVEL RF SYSTEM



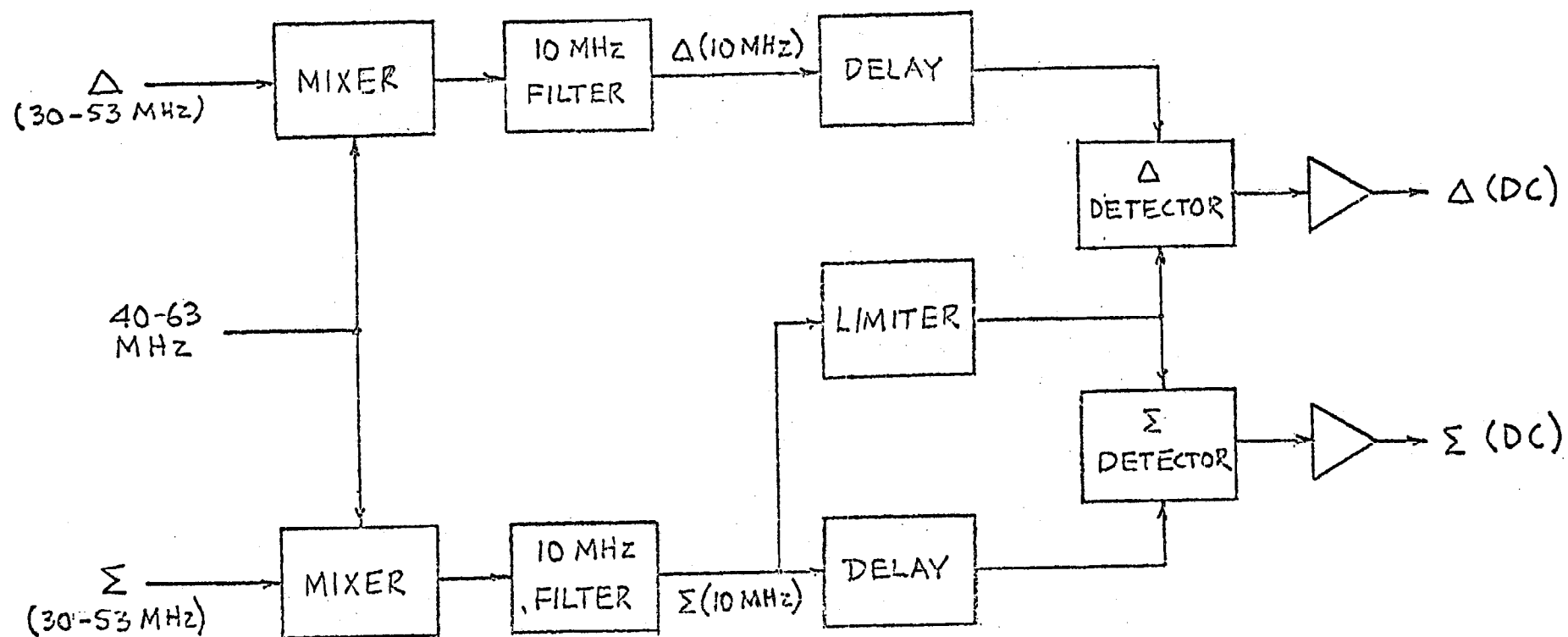


FIGURE H-10
LLRF RADIAL POSITION DETECTOR

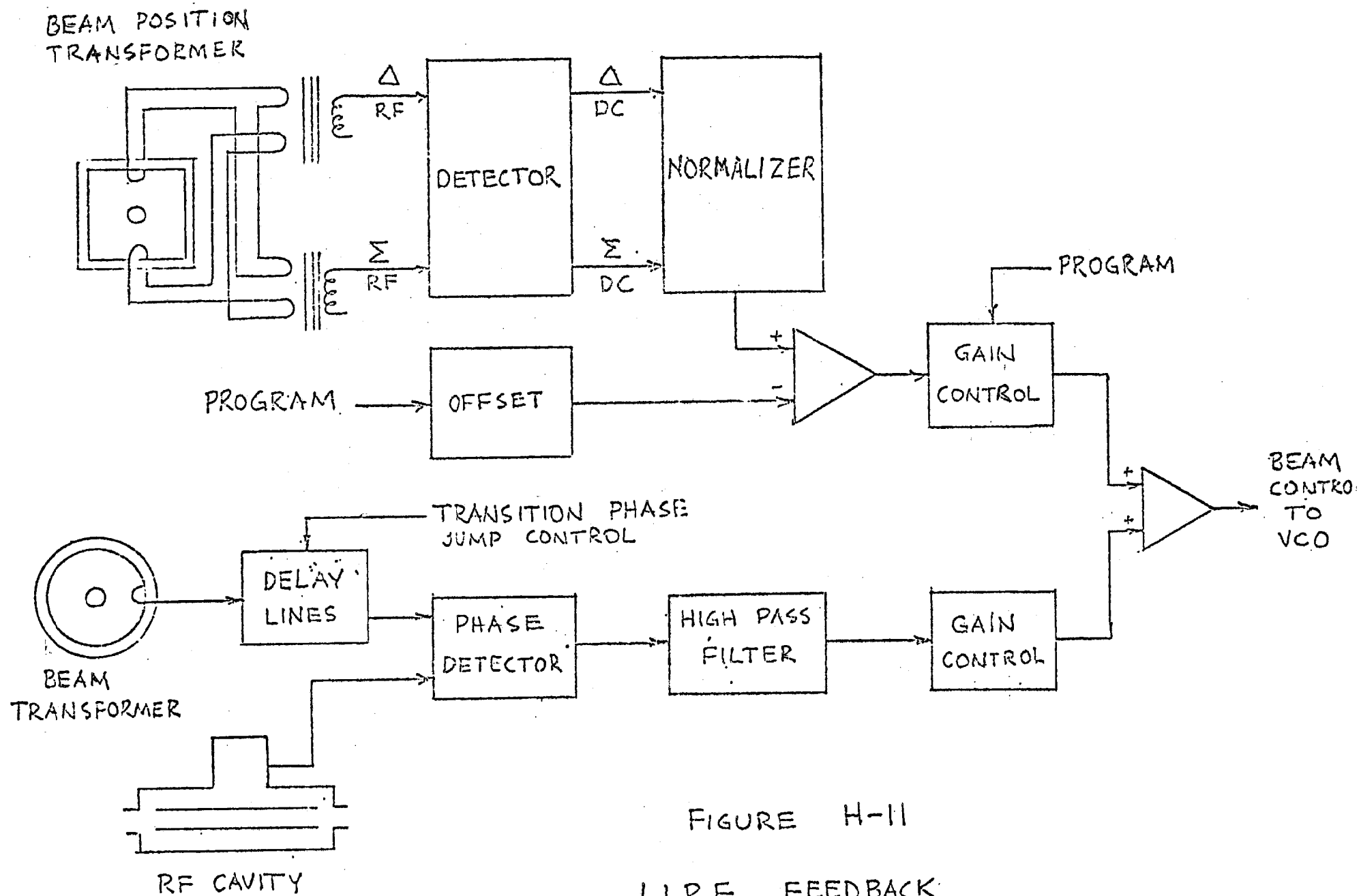


FIGURE H-11

LLRF FEEDBACK
SYSTEM

I. 200-MeV Beam Transfer System

1. Introduction

The 203-MeV proton beam from the linac can be steered into either of two beam lines.¹¹ One beam line leads to the system for measuring the emittance and the momentum spread of the linac beam. The other beam line transports the beam from the linac to the inflector of the booster synchrotron. A layout of the area occupied by the two systems is shown in Figure I-1.

The beam line leading to the equipment for analyzing the linac beam proceeds straight ahead from the end of the linac to a 40° spectrometer magnet. The momentum spread is determined by bending the beam with the 40° magnet and measuring the beam profile at the image. The beam used for emittance measurements proceeds in a straight line through a hole in the yoke of the spectrometer magnet. The emittance is determined by three beam profile measurements along this line. Beam dumps are located at the ends of both the emittance and momentum analysis systems. An enlarged view of the area used for analysis of the linac beam is shown in Figure I-2.

The beam to be injected into the booster synchrotron is bent immediately after leaving the linac by a pulsed electrostatic deflector and a septum magnet. The beam leaves the linac analysis area and proceeds to the booster tunnel, which is at a lower level, through a narrow duct 40 feet long. With this arrangement, installation and maintenance work can be done in the booster tunnel while the linac is operating and the beam is stopped in one of the beam dumps located at the end of the analysis area. The beam proceeds

along the booster tunnel near the outside wall for 70 feet before being injected into the synchrotron. Provision is made for either single turn or multiturn injection into the booster.

2. Chopper

Most of the deflection which separates the beam line going to the booster from the beam line going straight ahead to the linac analysis area is produced by a 9.7° septum magnet. The beam is switched from one side of the 0.2-inch thick septum to the other by a pulsed electrostatic kicker located just after the last cavity of the linac.

To reduce the voltage required on the plates of the kicker in order to switch the beam from one side of the septum to the other, the beam is focused in the horizontal phase plane to a 0.5-cm wide waist at the leading edge of the septum. Since there is room for only one quadrupole magnet between the last cavity of the linac and the septum, this focusing must be done with quadrupole magnets inside the drift tubes of the linac. Therefore, independent adjustment of the strengths of the last four quadrupoles in the linac has been provided. The position of the septum is adjusted remotely so that the 0.5-cm wide beam skims past the outside edge of the septum when the kicker voltage is off. The focusing and steering of the beam at the leading edge of the septum are monitored with the beam profile detector W-1.

The pulsed electrostatic kicker is designed to select the segment of the linac beam pulse with the best quality and send it to the booster synchrotron while the remainder of the linac beam pulse goes into one of the beam dumps at the end of the

linac analysis area. The length of the beam segment selected can be adjusted from 1 μ sec to 100 μ sec. For the nominal 4-turn injection planned for the booster, an 11- μ sec segment will be sent to the booster. Shorter pulses are available for booster tune-up and diagnostic work.

The chopper kicker consists of two 56-1/8-inch long plates separated by 1 inch. Both plates are charged to 75 kV in between linac pulses. The leading part of the linac pulse goes straight ahead to a beam dump beyond the linac analysis area. To deflect the beam to the booster, one plate is crobared with a thyatron in 100 nsec. At the end of the booster injection interval, the other plate is crobared, and the remainder of the beam goes to the beam dump.

The 3-kG field in the septum magnet is produced by a 10,000 A current pulse in a single turn coil. The 3/16-inch thick septum is welded to the laminated poles, and the current is confined to the septum by the insulation between the laminations.¹² The magnet itself is electrically insulated from the vacuum box, and the return conductor is insulated from the laminations. The radius of curvature of the septum and the stack of laminations is larger than the radius of curvature of the beam in the magnet to allow the clearance to increase toward the output end of the magnet. The laminations are normal to the beam at the input end, but there is 8.8° edge angle focusing at the output end. The fringing field at the input end was reduced to 0.2% by extending the coil and steel beyond the connection between the septum and the inner

conductor. The current pulse is a half sine wave which is 416 μ sec long. The parameters of the magnet are listed in Table I-I.

3. Linac Beam Analysis System

Emittance Measurement. To avoid dispersion, the emittance measurements are made in the straight-ahead beam line. The beam is focused to a waist inside the straight-through pipe in the yoke of the momentum analysis magnet by quadrupole magnets Q2 and Q3. The emittance of the beam is determined by measurements of the beam profile at three locations. Since the central measurement is made near a waist, a favorable condition for an accurate emittance determination is obtained.^{I3}

The beam profiles are measured by intercepting a small fraction of the beam on a 0.001-inch diameter wire which is stepped across the beam aperture.^{I4} The wire is moved in steps, one step in each interval between beam pulses. Thus, several beam pulses are required to obtain one complete beam profile, and the beam properties must be stable from pulse to pulse. The wire profile scanners labeled W-2, W-3, and W-4 in Figure I-2 are used for the emittance measurements. The values of the beam current intercepted by the wires are stored in the linac control computer. The emittance is calculated by the computer and displayed on the linac control console.^{I5}

Momentum Analysis. The 40° spectrometer magnet was built to measure the energy spread in the beam from the linac. It has also proved useful for monitoring in the mean energy of the beam. An

accurate absolute calibration has not been attempted.

The pole faces of the spectrometer magnet are flat and parallel to each other. The ends of the poles were shimmed to make $\int (B/\rho) ds$ along beam trajectories constant to within 0.05% inside the good field width of 10 cm. Vertical focusing is provided by quadrupole Q1.

The small horizontal waist at the entrance to the chopper septum magnet serves as the object for the spectrometer. The width of the beam at the object point is monitored with the wire profile scanner W-1. Instead of defining the emittance with slits in the customary way, it is measured with the profile detectors in the straight-through beam line. This eliminates the problem of residual radioactivity on the slits. The momentum spread is determined by measuring the width of the beam at the image plane of the spectrometer with the wire profile detector M. The quadrupoles Q2 and Q3 are turned off during the measurements. The dispersion at the image plane is 3 mm per 0.1% in $\Delta p/p$, and the calculated resolution is 0.1% for the design linac emittance of 8π mm-mrad. In practice, the emittance is seldom measured, and an emittance of zero is used in reducing the momentum spread measurements.

Beam Dumps. The beam dumps are buried in the dirt outside the room used for analysis of the linac beam. They are re-entrant steel castings approximately 3 feet in diameter. The beam enters through a hole along the axis. It is stopped on one side wall of the hole, which slopes at an angle of 3° with respect to the beam direction in order to spread out the area that the beam hits.

The steel castings serve as the vacuum chambers for the dumps which are open into the beam pipes in the analysis system. They provide fast neutron shielding and shielding for the residual radioactivity. Slow neutron shielding is provided by a layer of concrete about 1-1/2 feet thick which was cast in place around the steel casting. Additional shielding is provided by earth fill over the top and sides of the beam dumps.

The heat generated inside the dumps is conducted through the steel and concrete to the earth where it is dissipated. It is estimated that the 15-ton, 9-ft. long steel casting for the beam dump at the end of the momentum analysis line will dissipate from 3 to 10 kW. The steel casting for the dump at the end of the emittance line is only 6 feet long, and the dissipation is expected to be in the range of 0.3 to 1 kW. The maximum temperature rise during a beam pulse is expected to be less than 10° C provided the beam diameter is at least 4 cm.

4. Transport to the Booster

In order to make the beam line to the booster achromatic, the bend which separates this beam line from the linac analysis line was divided into two parts. The chopper kicker and septum magnet are the first part of the bend and the 5.9° horizontal bending magnet makes the second part. Momentum recombination is done with Q6. Vertical focusing for this part of the system is provided by Q1.

Since this arrangement does not provide any means of adjusting the acceptance of the transport line, the emittance of the linac

must be matched to the acceptance of the transport line by tuning the quadrupoles in the linac. In practice, it has proved difficult to achieve and maintain the required matching while simultaneously keeping the narrow waist required at the septum magnet. More satisfactory operation has been obtained by abandoning the achromatic conditions and tuning Q1 and Q6 to improve the emittance matching.

As shown in the elevation view in the lower part of Figure I-1, two 12.8° vertical bending magnets produce the vertical translation required to get the beam from the linac level down to the level of the booster synchrotron. Quadrupoles Q9 to Q12 are used to make the vertical translation achromatic and to provide focusing in this part of the beam line. The quadrupole magnets Q7 and Q8 are used for matching between the bending system in the linac analysis area and the vertical translation.

To increase the drift distance available for debunching the beam goes along the outer wall of the booster tunnel for 18 m before being bent across the tunnel to the inflector. The total drift distance from the linac to a debuncher located just ahead of Q16 would be 45 m.

The beam is injected from the outside of the closed orbit by a 0.7° electrostatic inflector. The inflection bend is increased to 9° by a septum magnet. The quadrupole magnets Q20, Q21 and Q22 together with the inflection bend and the 24.6° bending magnet at the outside of the tunnel form a system which can be tuned either to be achromatic or to give dispersion matching. The quadrupole magnets Q13 to Q19 are used to match the beam to the transverse

acceptance of the booster and to provide focusing in the long drift space. The parameters of the magnets in the transport system are listed in Table I-II.

The beam intensity is monitored at several points along the transport system with current transformers. Multiwire beam profile monitors at eight locations along the transport line are used to check the steering and focusing conditions. Air core trim magnets similar to the dipole correction magnets in the booster ring are used to correct steering errors.

5. Space Charge Effects

The detailed design calculations for the transport system have been done with the SLAC computer program Transport and do not take space charge effects into account.^{I6} Estimates for 100 mA beam currents indicated that transverse space charge forces will increase the beam size by a factor of approximately $4/3$ if the low intensity tuning of the system is not changed. Space charge will also affect the achromatic properties of the system.

A version of Transport which includes the effects of space charge is now available.^{I7} It indicates that space charge effects are small for the 20 mA linac beams now in use. At higher intensities it provides a guide to retuning the transport line to compensate for space charge. It should be possible to reduce the transverse dimensions of a high intensity beam by increasing the strength of the quadrupoles.

Calculations for a 100-mA beam bunched at 200 MHz indicated that the width in phase of the bunches will increase from a nominal value of approximately $\pm 8^\circ$ at the end of the linac to approximately $\pm 20^\circ$ after a 50-m drift. At the same time, the momentum spread increases by a factor of two from the nominal value of 0.1% at the end of the linac.¹⁸

The longitudinal spreading of the rf bunches helps to reduce space charge effects in the booster synchrotron. However, the increase in momentum spread increases the rf voltage required in the synchrotron accelerating cavities in order to trap the beam. For this reason, the design of the transport system includes provision for the future installation of a debuncher to reduce the momentum spread. The calculated phase width of the bunches and the dependence of the energy deviation on phase indicate that a conventional first harmonic debuncher should be satisfactory. Space charge forces will change the momentum spread very little as the beam drifts beyond 50 m.

6. Injection into the Booster

Inflection. Figure I-3 is a layout of the injection area in the booster.¹⁹ The beam is injected 2 feet downstream from the center of the 6-m long straight section. The final inflection is an 0.7° dc electrostatic deflector with an 0.002 inch Ta wire septum. It bends the incoming beam parallel to the closed orbit in the booster. The septum is located 1-1/8 inch outside the closed orbit. Here the half width of the circulating beam is 0.93 inch. Therefore, it should be possible to control the closed orbit

so that none of the circulating beam hits the septum. The septum of the electrostatic inflector is made as thin as possible to minimize the radial phase space obscured by it during multiturn injection. The inflector deflects the incoming beam far enough that it clears the 0.20 inch septum in the magnet upstream from it. The 3 kG, pulsed septum magnet bends the incoming beam 8.3° so that it misses the synchrotron magnet at the upstream end of the injection straight section. The septum magnet is identical to the one used in the chopper (Table I-I). However, it is oriented with the fringe field shielding at the output end where the circulating beam skims close to the septum.

Multiturn Injection. For multiturn injection, the closed orbit is displaced outward by two pairs of bump magnets. One pair is located at each end of the injection straight section. At the start of injection the orbit displacement is $1\frac{1}{8}$ inches, and the closed orbit is at the same radius as the inflector septum. As injection proceeds, the displacement decays at a rate of half a beam width per turn, and the radial position of the injected beam with respect to the closed orbit increases. The first particles injected have a coherent betatron oscillation amplitude equal to half the width of the beam. The betatron amplitude increases as injection proceeds until the horizontal acceptance of the booster is filled. Three to four turns of a beam with the nominal linac emittance of 9π mm-mrad fit into the nominal 90π mm-mrad acceptance of the booster magnets. It should be possible to inject 2 to $2\frac{1}{2}$ turns into a radial acceptance area of 54π mm-mrad.

Losses from beam hitting the inflector septum after one turn around the booster are reduced by lowering the horizontal betatron frequency ν_x as close to $6-1/2$ as is permitted by the half integral stopband. At present, ν_x is shifted to 6.55 during injection with the dc quadrupole correction magnets.

Each pair of bump magnets is constructed as a unit with a single one-turn coil exciting both magnets of the pair. By feeding the coil in the center, equal and opposite fields are produced in the two magnets. The parameters of the bump magnets are listed in Table I-III. Injection starts at 2.75 kG, halfway down the decay of the 20,000-A half sine wave current pulse applied to each magnet.

Much weaker bump magnets could be used if they were placed $1/4$ betatron wave length from the inflector. However, the long straight sections on the upstream side are filled with rf cavities, and part of the injection orbit would be outside the "good field width" of the booster magnets.

Single Turn Injection. The same electrostatic inflector and septum magnet are used for single-turn injection, but the closed orbit bump is not used. The incoming beam enters the first period of the booster magnet displaced outward from the closed orbit and parallel to it. It crosses the central orbit a quarter of a betatron wavelength downstream in the next 6-m long straight section. Here the beam is bent 7 mrad by a fast kicker magnet to point it along the closed orbit. After beam has been injected for the 2.8- μ sec period of one revolution around the booster, the kicker magnet is turned off in 50 nsec. This magnet consists of two

80-gauss, 44-inch long, delay-line type magnet sections identical to those used for extracting the beam from the booster.

With the inflector in design location, $1\frac{1}{8}$ inches from the central orbit, the center of the incoming beam goes within $\frac{1}{8}$ inches of the edge of the good magnetic field region in the first F magnet in the booster ring, and some of it is scraped off on the beam pipe in the mid-F straight section. During the early operation of the booster, the inflector was moved inward to a location 0.825 inch outside the central orbit. The half width of the beam is 0.36 inch at this point.

References

- I1. E.L. Hubbard, W.C. Martin, G. Michelassi, R.E. Peters, and M.F. Shea, Proc. 1970 Proton Linear Accelerator Conf., NAL, p. 1095.
- I2. H. Edwards, E.L. Hubbard, R. Juhala, International Symposium on Magnet Technology, Brookhaven Natl. Lab. (1972).
- I3. C. Metzger, CERN Report CERN/SI/Int. DL/69-10 (1969).
- I4. R.W. Goodwin, E.R. Gray, G.M. Lee and M.F. Shea, Proc. 1970 Proton Linear Accelerator Conf., NAL, p. 107 (1970).
- I5. E.R. Gray, IEEE Transactions on Nuclear Sci. Vol. NS-18, No. 3, p. 941 (1971).
- I6. K.L. Brown and S.K. Howry, Report SLAC-91 (1970).
- I7. F.J. Sacherer and T.R. Sherwood, IEEE Trans. on Nuclear Sci., Vol. NS-18, No. 3, p. 1066 (1971).
- I8. L. Smith, NAL Physics Note FN-146 (1968).
- I9. R. Billinge, E.L. Hubbard, R. Juhala and R.W. Oram, IEEE Trans. on Nuclear Sci., Vol. NS-18, No. 3, p. 979 (1971).

Table I-I

Parameters
Pulsed Septum Magnets

Effective bending length	40.95 inches
Cap	1-1/2 inches
Width of aperture	2 inches
Lamination thickness	0.014 inch
Septum thickness	3/16 inch
Width of half sine wave current pulse	416 μ sec
Inductance	1.7 μ H
Radius of curvature of septum	351 inches

	<u>Chopper</u>	<u>Inflector</u>
	(S1)	(S2)
Bend Angle	8.8°	8.3°
Peak current	9600 A	9100 A
Peak voltage	123	116 V
Peak Mag field	3.17 kG	3.00 kG

Table I-II

A. Parameters of Bending Magnets in 200-MeV Transport System

Label	Bend Angle deg.	Eff. Length cm	Gap (Inside Vacuum Chamber) inch	Magnetic Field kG	Voltage	Current A
MH1	5.9	49.5	2	4.5	10	37
MV1 MV2	12.3	38.0	2-1/2	12.6	67	240
MH2	25.8	56.7	1-5/8	16.3	27	260

B. Parameters of Quadrupole Magnets

Aperture	3-1/4 inch
Effective Length	30 cm
Maximum Current	50 A
Magnetic Field Gradient	17.9 gauss/cm/A

Table I-III
Parameters
Multiturn Injection Bump Magnets

Length	18 inches
Gap	2.46 inch
Width of Aperture	
Spacing between Magnets in one pair	1-1/8 inch
Peak magnetic field	4.0 kG
Width of half sine wave pulse	47 μ sec
Peak current	20,000 A
Inductance	.75 μ H
Magnetic field for 1-1/8" orbit displacement	2.75 kG
Bend angle for 1-1/8" orbit displacement	59 mrad
Lamination thickness	0.004 inch

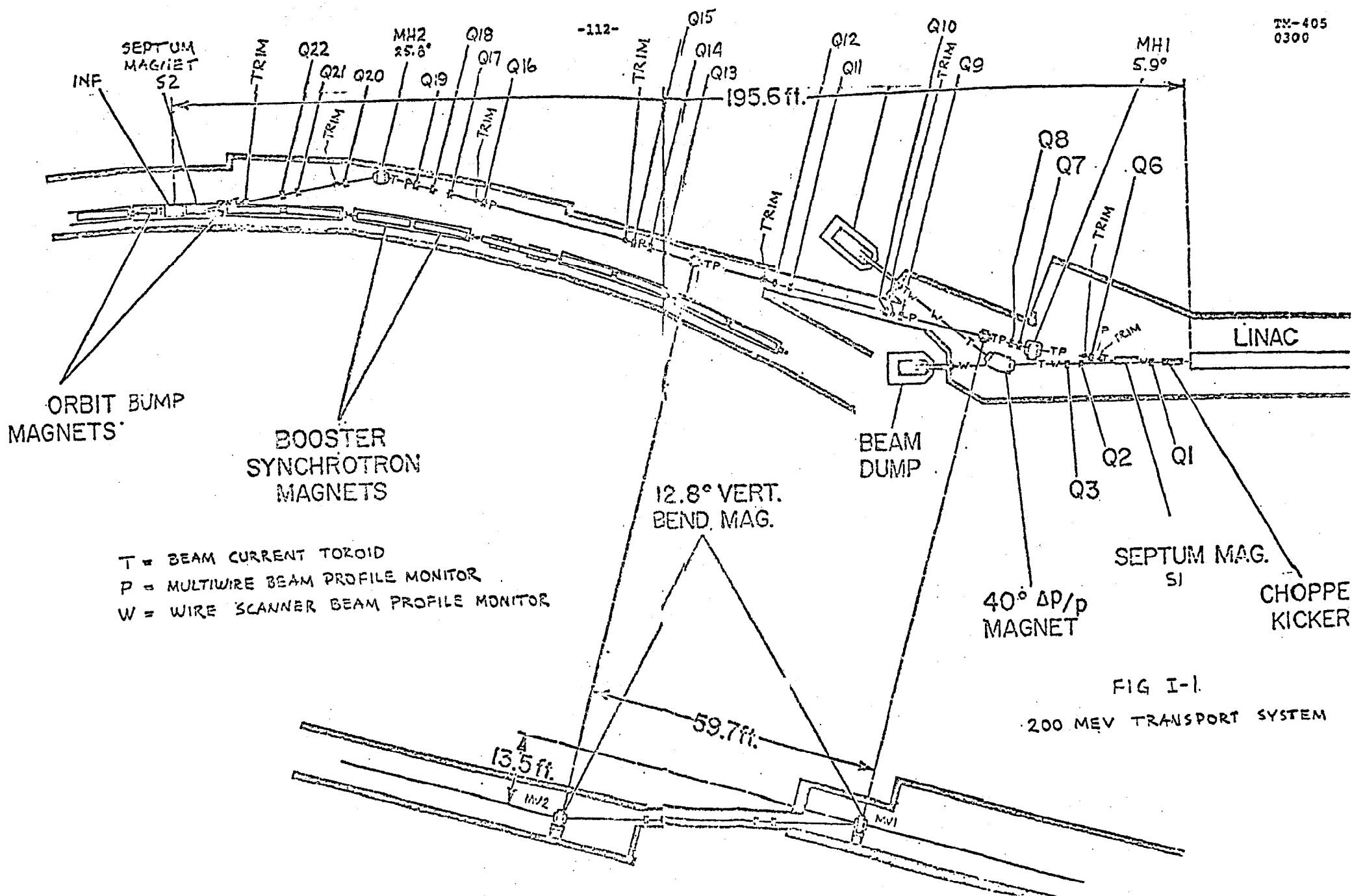
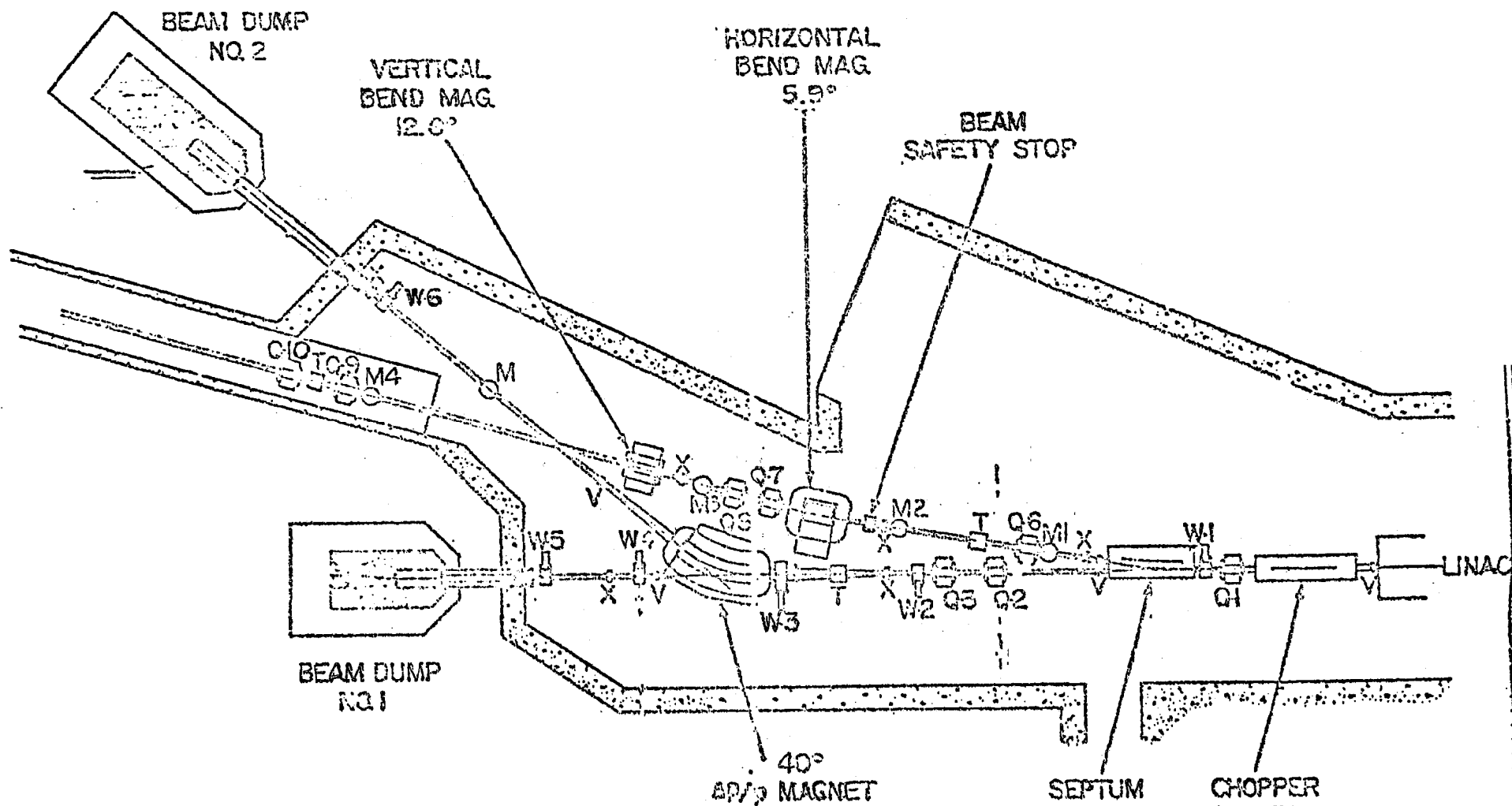


FIG I-1.
200 MEV TRANSPORT SYSTEM



V = VACUUM VALVE

Q = QUADRUPOLE MAGNET

X = BEAM CURRENT TRANSFORMER

W = WIRE SCANNER BEAM PROFILE DETECTOR

T = TRIM STEERING MAGNETS

M = BEAM PROFILE DETECTOR
(MULTIWIRE TYPE)

FIG I-2

LINAC BEAM ANALYSIS SYSTEM

NO.	DESCRIPTION	QUANTITY	REMARKS
1	BEAM DUMP NO. 1	1	
2	BEAM DUMP NO. 2	1	
3	VERTICAL BEND MAG	1	
4	HORIZONTAL BEND MAG	1	
5	40° MAGNET	1	
6	SEPTUM MAGNET	1	
7	CHOPPER KICKER	1	
8	W1	1	
9	W2	1	
10	W3	1	
11	W4	1	
12	W5	1	
13	W6	1	
14	Q1	1	
15	Q2	1	
16	Q3	1	
17	Q4	1	
18	Q5	1	
19	Q6	1	
20	Q7	1	
21	M1	1	
22	M2	1	
23	M3	1	
24	M4	1	
25	X	1	
26	V	1	
27	T	1	
28	LINAC	1	

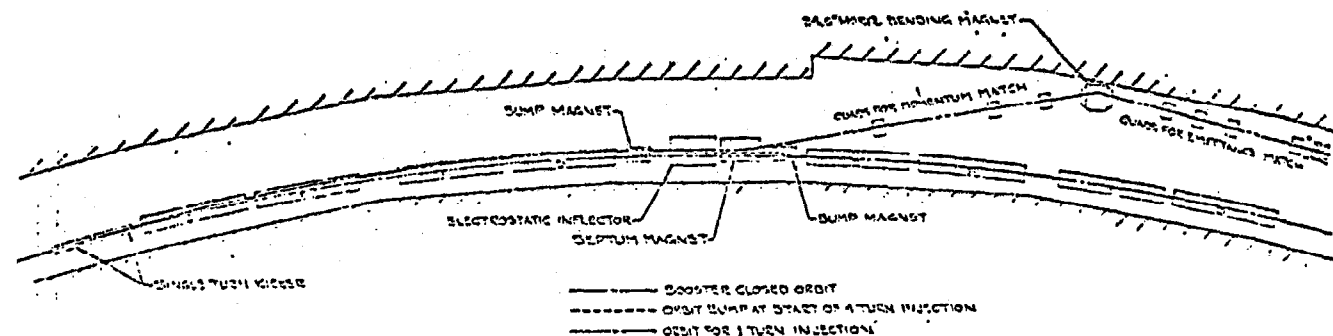


Fig. I-3 Layout of Booster Injection System

J. Extraction

The beam is extracted vertically from the booster with a full aperture fast kicker magnet located in one of the 8-m long straight sections and a pulsed septum magnetic in the next 6-m straight section.^{J1} Smaller deflecting fields are required for vertical extraction than for horizontal extraction because of the magnet geometry and the large vertical betatron amplitude function in the 6-m long straight sections. The displacement of the beam is very near its maximum at the septum since the vertical betatron phase shift is 93° from the center of the kicker magnet to the lip of the septum. A 1.1 mrad kick is required to produce the 23-mm vertical displacement needed to clear the septum.

The fast kicker magnet is divided into four sections each 44 inches long. Each section is a 50-ohm transmission line-type magnet and is terminated with a 50-ohm load. The vacuum chamber is a ceramic tube with a nominal inside diameter of 2-1/4 inches.^{J2} The current pulse is produced by discharging a 70-kV pulse line into each section with a deuterium thyratron switch. The parameters of a section of kicker magnet are given in Table J-I.

The rise time of the field is 25 nsec, which is greater than the time between rf beam bunches at 8 GeV. Thus, one beam bunch passes through the magnet while its field is rising. This bunch receives only part of the required deflection and hits the extraction septum. To reduce the residual radioactivity on the septum, it is planned to kick out one bunch of beam at low energy and synchronize the firing of the kicker with passage of the empty bucket through it.

The extraction septum magnet deflects the beam vertically 44 mrad, which is sufficient for the beam to clear the downstream booster magnet. A cross section of the septum magnet is shown in Figure J-1, and the parameters of the magnet are listed in Table J-II. The magnetic core is made of 4-mil tape wound silicon steel. The gap was machined after the core was mounted in the aluminum shell and impregnated with epoxy. A vertical bending magnet of similar construction is used to bend the beam horizontally again after it is clear of the booster. The two magnets are powered in series with a 460 μ sec, half sine wave current pulse from a capacitor discharge-type power supply.^{J3}

Since the septum hangs down inside the magnet aperture at the point in the lattice where β_y has its maximum value, it reduces the vertical acceptance of the booster. To use all of the remaining aperture for injection, the closed orbit is bumped downward at this point with the dc dipole correcting magnets. With the septum 15 mm above center, the vertical acceptance is 23π mm-mrad, and there is sufficient aperture in the septum magnet to extract a beam with the corresponding emittance after the beam size has been reduced by acceleration to 8 GeV.

References

- J1. A.W. Maschke and L.W. Oleksiuk, IEEE Trans. on Nuclear Sci. Vol. NS-18, No. 3, p. 989 (1971).
- J2. E.B. Tilles, J.D. McCarthy, and R.F. Nissen, IEEE Trans. on Nuclear Sci., Vol. NS-18, No. 3, p. 1020 (1971).
- J3. A.T. Visser and R.F. Nissen, IEEE Trans. on Nuclear Sci., Vol. NS-18, No. 3, p. 991 (1971).

Table J-I

Parameters of One Section of Fast Kicker Magnet

Length of section	44 inches
Maximum magnetic field	90 gauss
Characteristic impedance	50 ohms
Rise time	25 μ sec
Aperture of ceramic vacuum chamber	
nominal	2-1/4 inch dia
minimum clear	2 inch
Maximum pulse line voltage	75 kV
Maximum pulse current	700 A
Switch (EEV thyatron)	Type CX1168

Table J-II
Extraction Septum Magnet Parameters

Magnet length	60 inches
Gap	1.1 inch x 1.1 inch
Peak magnetic field	8.8 kG
Septum thickness	
Copper	0.060 inch
Iron shield	0.030 inch
Fringe field	3 gauss
Peak Current	20,000 A
Capacitor bank voltage	1250 V
Width of half sine wave pulse	460 μ sec
Inductance	1.9 μ H

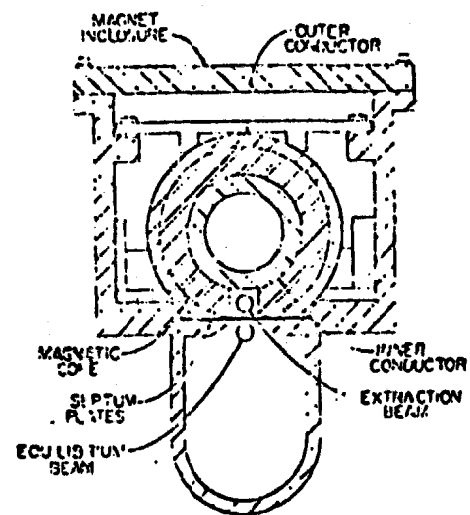


Fig. J1 Pulsed Extraction Septum Magnet

K. Staff

The following members of the professional staff made significant contributions to the design and construction of the booster: F. Ascolese, E.J. Barsotti, R. Billinge, F.F. Cilyo, J.R. Clarke, R.E. Daniels, J.A. Dinkel, A.R. Donaldson, R.J. Ducar, H.T. Edwards, J.E. Griffin, J.H. Grimson, W.B. Hanson, E.F. Higgins, E.L. Hubbard, R. Juhala, O.A. Kerns, L.A. Klaisner, G.M. Lee, A.W. Maschke, M. May, J.D. McCarthy, G. Michelassi, H.W. Miller, R.F. Nissen, R.W. Oram, U. Patel, R.E. Peters, P.J. Reardon, C.H. Rode, J. Ryk, J.R. Sauer, M.F. Shea, S.C. Snowdon, J.M. Stephenson, G.S. Tool, A. Van Steenberghe, A.T. Visser, J.T. Walton, R.R. Wilson and R.A. Winje.